United States
Department of
Agriculture

Forest Service

Forest
Products
Laboratory

Research
Paper

FPL–RP–635

JMFA 2—A Graphically Interactive Java Program That Fits Microfibril Angle X-ray Diffraction Data

Steve P. Verrill
David E. Kretschmann
Victoria L. Herian

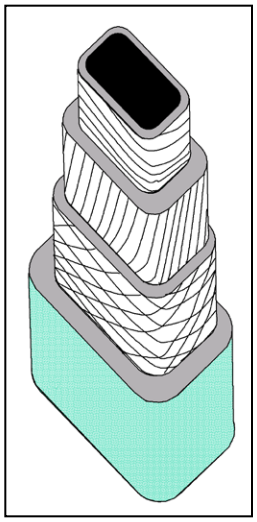

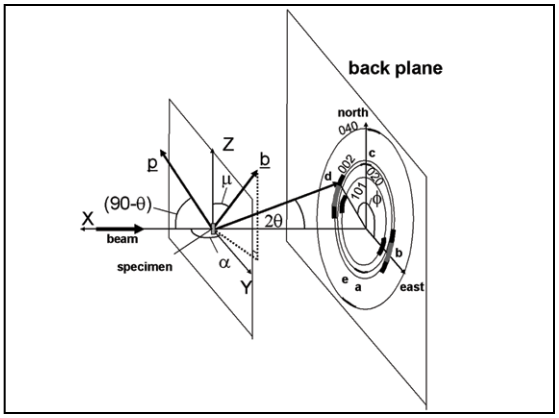

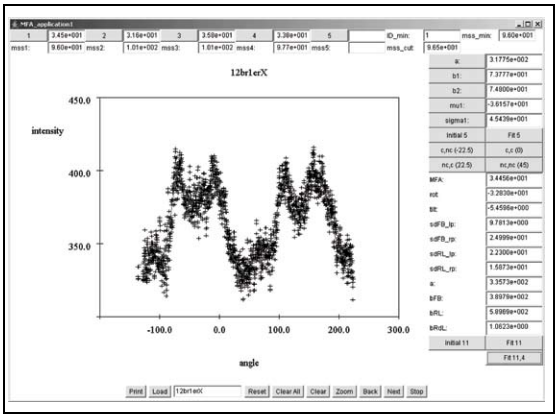

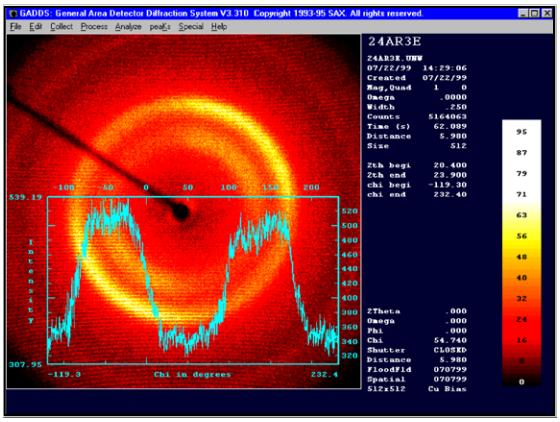

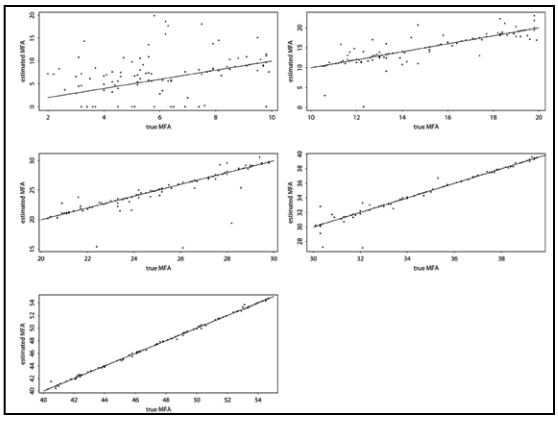

Abstract

X-ray diffraction techniques have the potential to decrease the time required to determine microfibril angles dramatically. In this paper, we discuss the latest version of a curve-fitting toll that permits us to reduce the time required to evaluate MFA X-ray diffraction patterns. Further, because this tool reflects the underlying physics more accurately than existing tools, we expect it to yield more accurate estimates of MFA.

Keywords: microfibril angle, X-ray diffraction, Java, interactive graphics, mechanical properties of wood, forest monitoring

Contents

Introduction 1
Physical Theory and Our Program 3
MFA as a Function of the Eight Spot Locations 7
Problems with Our Current Approach 8
Summary 9
Acknowledgment 10
References 10
Appendix A — An Extension to Cave's Equation 11
Appendix B — The Effects of a Change in Tilt Sign or of Rotation Sign on the Pattern of Eight Spots 16
Appendix C — The Applet and the Application 18

July 2006

Verrill, Steve P.; Kretschmann, David E.; Herian, Victoria L. JMFA2—A Graphically Interactive Java Program That Fits Microfibril Angle X-ray Diffraction Data. Research Paper FPL-RP-635. Madison, WI: U.S. Department of Agriculture, Forest Service, Forest Products Laboratory. 69 p.

A limited number of free copies of this publication are available to the public from the Forest Products Laboratory, One Gifford Pinchot Drive, Madison, WI 53726–2398. This publication is also available online at www.fpl.fs.fed.us. Laboratory publications are sent to hundreds of libraries in the United States and elsewhere.

The Forest Products Laboratory is maintained in cooperation with the University of Wisconsin.

The use of trade or firm names in this publication is for reader information and does not imply endorsement by the United States Department of Agriculture (USDA) of any product or service.

The USDA prohibits discrimination in all its programs and activities on the basis of race, color, national origin, age, disability, and where applicable, sex, marital status, familial status, parental status, religion, sexual orientation, genetic information, political beliefs, reprisal, or because all or a part of an individual's income is derived from any public assistance program. (Not all prohibited bases apply to all programs.) Persons with disabilities who require alternative means for communication of program information (Braille, large print, audiotape, etc.) should contact USDA's TARGET Center at (202) 720–2600 (voice and TDD). To file a complaint of discrimination, write to USDA, Director, Office of Civil Rights, 1400 Independence Avenue, S.W., Washington, D.C. 20250–9410, or call (800) 795–3272 (voice) or (202) 720–6382 (TDD). USDA is an equal opportunity provider and employer.

JMFA 2 — A Graphically Interactive Java Program That Fits Microfibril Angle X-ray Diffraction Data

Steve P. Verrill, Mathematical Statistician
David E. Kretschmann, Research General Engineer
Victoria L. Herian, Statistician
Forest Products Laboratory, Madison, Wisconsin

1 Introduction

X-ray diffraction techniques have the potential to decrease the time required to determine microfibril angles dramatically. This decrease will permit us to gain a better understanding of the relationships between microfibril angle (MFA) and the mechanical properties of wood, which will in turn permit us to do a better job of managing the changing wood resource. In this paper, we discuss the latest version of a curve-fitting tool that permits us to reduce the time required to evaluate MFA X-ray diffraction patterns. Further, because this tool reflects the underlying physics more accurately than existing tools, we expect it to yield more accurate estimates of MFA.

1.1 Background

Much of our future timber supply is expected to come from improved softwood and hardwood trees grown on managed plantations or from small-diameter timber removed during forest management operations. This short-rotation resource will contain higher proportions of juvenile wood than the present resource.

Boone and Chudnoff (1972) raised early concerns about the quality of plantation-grown material. Their research was conducted on 8-year-old plantation Caribbean pine (*Pinus caribaea* Morelet) from Puerto Rico. In their study of small clear specimens, specific gravity, bending stiffness, and strength values were reduced by more than 50% from the published values for virgin timber of the same species. At about the same time, research conducted at North Carolina State University on clear wood of loblolly pine (*Pinus taeda* L.) demonstrated that the problem was juvenile wood, not plantation wood (Pearson and Gilmore 1971). This research demonstrated that juvenile wood has substantially lower mechanical property values than does mature wood, which generally accounts for the inferior properties of short rotation plantation wood compared with those of long rotation timber.

One can respond to these reductions in properties by attempting to improve silvicultural practices. Improved silvicultural practices require improved tools for monitoring stand quality. Microfibril angle measurements hold promise as one such tool.

1.2 Importance of Microfibril Angle

Wood cells are made up of multiple layers: a primary layer, P, and three secondary layers, S1, S2, and S3 (Fig. 1). The secondary layers consist of helically arranged cellulose microfibrils oriented toward the long axis of the tracheid. The thickest of the secondary layers is the S2 layer, and its

properties strongly influence the properties of the wood fiber. Microfibril angle is measured as the angular deviation from the vertical of the microfibrils in the S2 layer.

Orientations of microfibrils in the S2 layer of juvenile wood tracheids vary widely both within and among trees of a species. In loblolly pine, for example, the MFA in mature wood is small, averaging about 5 to 10 degrees. In juvenile loblolly, MFA is large; it averages 25 to 35 degrees, is often as high as 50 degrees in the annual rings next to the pith, and decreases outward in the juvenile core (Megraw 1986, Bendtsen and Senft 1986). The decrease in MFA often continues well beyond the juvenile core. For example, Ying and others (1994) found that MFAs in tracheids of fast-grown loblolly pines decreased from 33 degrees at age 1 to 23 degrees at age 10 to 17 degrees at age 22. Bendtsen and Senft (1986) reported that MFAs had not yet attained stable values in 30-year-old loblolly pines.

Researchers conclude that the MFA of the S2 layer of the woody cell wall is a critical factor in the mechanical behavior of wood (Megraw 1986). Orientation of the S2 MFA has a significant influence on the tensile strength, stiffness, and shrinkage of wood.

Data from Bendtsen and Senft (1986), based on a 30-year-old loblolly pine plantation, suggest that differences in strength properties between juvenile and mature wood cannot be accounted for solely by differences in specific gravity. Their data also suggest that the volume of earlywood and the high MFAs of earlywood tracheids in early juvenile wood growth rings might be far more important. Cave and Walker (1994) concluded that MFA plays a major role in the pronounced decrease in stiffness (modulus of elasticity) for juvenile wood in fast-grown radiata pine and that MFA is a factor that can be used as a selection tool in plantation management.

A strong relationship exists between MFA and longitudinal shrinkage. In tests on juvenile wood of radiata pine (*Pinus radiata* D. Don), Harris and Meylan (1965) showed that longitudinal shrinkage increased sharply while tangential shrinkage decreased at MFAs greater than 25 degrees. Longitudinal shrinkage was low at MFAs below 25 degrees, whereas tangential shrinkage increased as MFAs fell below 15 degrees. Ying and others (1994) showed that MFAs of 25 degrees or greater corresponded to the outer boundary of the 10-year juvenile core in loblolly pine. Modeling suggests that the relative thickness of the P, S1, and S3 layers contributes significantly to the variability of longitudinal shrinkage (Cave 1976).

Given that our future timber supply is expected to come from shorter rotation forests, definitive information is needed on the influence of MFA on lumber properties so that selection and utilization methods can be adjusted accordingly.

1.3 Methods of Measuring MFA

The traditional methods for determining the MFA of the S2 layer have been based on the orientation of cross-field pit apertures (Dadswell and Nicholls 1959, 1960; Donaldson 1991), the enhancement of checks or the maximum extinction position using polarizing light (Echols 1955, Foracs 1961), the use of fluorescence light microscopy to enhance checks (Marts 1955), and the orientation of iodine crystals that form in induced checks (Senft and Bendtsen 1985). Much of the current literature has been developed using these techniques, but these methods are slow and tedious.

X-ray diffraction techniques have also been used to determine MFA (Cave 1966, Harris and Meylan 1965, Meylan 1967). Recently, Evans and others (1996), Cave and Robinson (1998), Kretschmann and others (1998), and Lichtenegger and others (1998) have done work to refine X-ray diffraction as a much more rapid technique for measuring MFA. This technique uses the diffraction pattern created by the interaction of X-rays with wood tissue to determine MFA (Fig. 2). A group of fibers is irradiated perpendicular to the fiber length by a narrow, monochromatic X-ray beam. A diffraction pattern is produced by the crystalline cellulose structure of the fibers and is recorded

on film or by an electronic detector. This pattern consists of a series of arcs that are spaced apart by a number of well-defined concentric circles. See the back plane of Figure 2. (In Fig. 2, locations a, b, c, d, and e on the back plane yield the intensities plotted at angles −90, 0, 90, 180, and 270 degrees in Figs. 33–36.) The diameters of the concentric circles are indications of the spacing and locations of the crystalline planes within the cellulose crystalline fibrils.

In this paper, we discuss a new version of a graphically interactive Java program that yields rapid analyses of microfibril X-ray diffraction patterns. See Verrill, Kretschmann, and Herian (2001) for a discussion of the first version of this program. In addition to leading to speedy analyses, this program makes use of an improved model of the underlying physics that should yield more accurate MFA estimates.

2 Physical Theory and Our Program

Cave (1966) derived an equation that relates the locations of the spots of high X-ray intensity on the back plane of the X-ray apparatus to the Bragg angle associated with the X-rays, the rotation of the wood cell, and the MFA. This equation applies to cells with square cross sections. (In the appendix to Verrill, Kretschmann, and Herian (2001) we worked through a derivation of Cave's equation. We also described a method for finding analytic solutions to the equation.) Figure 2 illustrates the relevant geometry. The equation is

$$\tan(\theta)\cos(\alpha) + \sin(\alpha)\cos(\phi) + \cot(\mu)\sin(\phi) = 0 \tag{1}$$

where θ is the Bragg angle (11.35 degrees for X-rays of wavelength 1.54 angstroms), μ is the MFA, α is 90 degrees plus the rotation of the "front" face of the wood cell beyond perpendicular to the incoming beam, and ϕ is the angle (measured counterclockwise) from the east of the spot on the "2θ circle" on the back plane. $\alpha = 90$ degrees if the front face is perpendicular to the incoming beam (Fig. 3).

In the current paper, we extend this model to one in which the wood cell can be tilted as well as rotated. We denote the tilt by η. The relevant geometry is illustrated in Figure 4. In Appendix A we derive the four equations corresponding to the four faces of the cell. For reasonable tilts and microfibril angles, these equations yield two spots for each face of the cell.

In Figure 5 we plot a generic circle that corresponds to the 002 circle on the back plane of Figure 2 and the circles in Figures 6 through 18 and 20 through 32. On this generic circle we have labeled the cardinal directions and have illustrated the relationship between the ϕ angle and these directions.

In Figures 6 through 18 we plot the locations of the eight spots for a tilt of 0 degrees and rotations of 0, 10, 20, 22.5, 30, 40, 45, 50, 60, 67.5, 70, 80, and 90 degrees. In Figure 19 we plot bright spot locations versus cell rotation for an MFA of 30 degrees and a tilt of 0 degrees. This plot provides an alternative view of the 30-degree MFA material in Figures 6 though 18.

In Figures 20 through 32 we plot the locations of the eight spots for a tilt of 15 degrees and rotations of 0, 10, 20, 22.5, 30, 40, 45, 50, 60, 67.5, 70, 80, and 90 degrees.

In Appendix B we describe the effects of a change in tilt sign or of rotation sign on the pattern of 8 spots.

We claim that, for practical purposes, distinct μ, η, α triplets lead to distinct collections of eight spots. Thus given the locations of the eight spots, we can estimate the MFA μ (as well as the cell tilt and cell rotation). Our justification of this claim is provided in Section 3.

2.1 Cave's 1966 Approach

Cave (1966) argued that for the case of a 0-degree rotation and 0-degree tilt (Fig. 6), the outer edges of the two main intensity profiles (Fig. 33) would be due primarily to a broadening of the four points associated with the front and back faces of the wood cells. For a 0-degree rotation, a 0-degree tilt, and MFA μ, these spots can be shown (via Eq. (1)) to lie at angles $-\mu$, μ, $180-\mu$, and $180+\mu$ (where these angles are measured counterclockwise from the east in Fig. 6). Consider the broadened bright spot at angular location $-\mu$. If it is broadened in a Gaussian fashion, and if the contributions of the other bright spots to the left edge of the first profile in Figure 33 can be neglected, then the left edge of the first profile in Figure 33 is given by

$$\text{intensity}(\phi) = a + b \times \exp(-(\phi - (-\mu))^2/(2\sigma^2))$$

where ϕ is the angle and σ is the broadening factor. The left point of inflection of this left profile can be shown to lie at $-\mu-\sigma$, and the line that is tangent to the profile at the inflection point can be shown to intersect the background level (intensity $= a$) at angle $-\mu-2\sigma$. Similarly, if only the bright spot at $+\mu$ contributes to the intensity at the right edge of the left profile in Figure 33, the line that is tangent to the left profile at its right point of inflection intersects the background level at angle $\mu+2\sigma$.

For practical reasons, Meylan (1967) had previously recommended that

$$T \equiv (\text{right intersection point} - \text{left intersection point})/2$$

be used as an indirect measure of MFA. By his argument, Cave established that

$$T \approx (\mu + 2\sigma - (-\mu - 2\sigma))/2 = \mu + 2\sigma. \tag{2}$$

He further argued that there were empirical reasons to believe that

$$\sigma \approx \mu/3. \tag{3}$$

Equations (2) and (3) yield

$$\mu \approx 0.6T \tag{4}$$

where T is half the distance between the intercept of the tangent line to the right inflection point of a profile with the background and the intercept of the tangent line to the left inflection point of a profile with the background. For years, some version of Equation (4) has been used to analyze MFA X-ray diffraction profiles. (Evans (1999) developed an alternative approach.) Initially, tangent lines were drawn by hand. More recently, Stuart and Evans (1994) and Kretschmann and others (1998) automated the process by assuming that a left (or right) profile (Figures 33–36) could be fit by a single Gaussian (rather than by a combination of four Gaussians). Nonlinear least squares techniques were used to perform this fit, and then it was possible to calculate the T value from the left and right inflection points of the one fitted Gaussian. (This procedure will tend to yield tangent lines that are too shallow and thus MFA values that are too large.)

Cave's 1966 procedure will be appropriate if the following asumptions hold:

1. The intensity spots associated with the front and back faces are located at angles $-\mu$, μ, $180-\mu$, and $180+\mu$, where the angles of the bright spots on the back plane are measured in a counterclockwise direction from the east. (See Figs. 2 and 5.)

2. The left and right edges of a profile are only affected by a single one of the four spots associated with the profile.

3. We can approximate the point broadening σ with a function of μ (such as $\sigma \approx \mu/3$).

2.2 Limitations of the 1966 Procedure

As can be seen in Figures 6 through 18, as the front face is rotated away from a position perpendicular to the incoming beam, assumption 2 becomes invalid. For example, in Figure 9 one can see that for a rotation of 22.5 degrees, the left edge of the left profile in Figure 34 (due to the right half of the circle in Fig. 9) will be a combination of both the front face and left face spot broadenings. The right edge of the left profile in Figure 34 will be a combination of both the right face and back face broadenings.

Also, as the front face is rotated away from a position perpendicular to the incoming beam, assumption 1 becomes invalid. For example, from Equation (1) we can calculate that for the right half circle on the back plane, the location of the front face spot in the 30 MFA degree circle in Figure 10 (30-degree rotation) is 23.59 (rather than 30) degrees clockwise from the east. The location of the back face spot is 23.59 (rather than 30) degrees counterclockwise from the east.

2.3 An Improved Approach

In our program, we avoid Cave's 1966 assumptions by taking advantage of the relationship between the eight point profiles and the μ, η, α triplet to estimate μ on the basis of the profiles. In particular, we perform an 11 parameter nonlinear least squares, in which we find a linear combination of *all* eight Gaussians that best fits the observed X-ray intensity profile. Such an approach would not have been feasible in 1966. It has only become feasible with the massive increases in computing power of the last 40 years.

The 11 parameters of the nonlinear least squares model are as follows:

- μ, the MFA
- *rot*, the rotation of the wood cell counterclockwise about the original z axis (after the tilt) (Fig. 3)
- *tilt*, the tilt of the vertical in the wood cell down toward the incoming X-ray beam (before a rotation of the wood cell about the z axis) (Fig. 4)
- *sdFB_lp*, the standard deviation (broadening factor) associated with the spots on the right of the back plane (contributing to the left profile in the plot) due to the front and back faces of the wood cell
- *sdFB_rp*, the standard deviation (broadening factor) associated with the spots on the left of the back plane (contributing to the right profile in the plot) due to the front and back faces of the wood cell
- *sdRL_lp*, the standard deviation (broadening factor) associated with the spots on the right of the back plane (contributing to the left profile in the plot) due to the right and left faces of the wood cell
- *sdRL_rp*, the standard deviation (broadening factor) associated with the spots on the left of the back plane (contributing to the right profile in the plot) due to the right and left faces of the wood cell
- a, the background X-ray intensity
- *bFB*, additional intensity caused by the spots associated with the front and back faces of the wood cell

- bRL, additional intensity caused by the spots associated with the right and left faces of the wood cell
- $bRdL$, the ratio of the intensity on the left half circle of the back plane to the intensity on the right half circle (the ratio of the right to the left profiles on the plot presented to the user of the program)

As currently written, the program constrains the MFA estimate to lie between -75 and 75 degrees, the tilt estimate to lie between -50 and 50 degrees, the rotation estimate to lie between -90 and 90 degrees, the standard deviation estimates to lie between 0.001 and 24.999 degrees, the estimates of bFB and bRL to lie between 1 and 9999, and the estimate of $bRdL$ to lie between 0.001 and 19.999.

The a parameter is an artifact of the data collection process. The b (intensity) and s (broadening) parameters have some physical meaning, but they also contain ad hoc elements in our current implementation. We know of no physical reason why the intensity of the left half profile should differ from the intensity of the right half. However, we do see this in data so we provided for it via the $bRdL$ parameter. Because the front and back faces are parallel, we expect them to yield equal contributions to the X-ray intensity. Hence the bFB parameter. Similarly, the right and left faces are parallel and share the bRL parameter. In the low-tilt case (see Figs. 6 through 18) the front and back hot spots are in symmetric positions on the right of the back plane and in different symmetric positions on the left of the back plane. Hence the distinct $sdFB\_lp$ and $sdFB\_rp$ values. Similarly, the right and left hot spots are in symmetric positions on the right of the back plane and in different symmetric positions on the left of the back plane. Hence the distinct $sdRL\_lp$ and $sdRL\_rp$ values. When tilt becomes significant these symmetries are partially lost, especially for high MFA values (see Figs. 20–32), and our broadening model could presumably be improved.

2.4 Predicted Intensity

Let ϕ_1 be the location of the X-ray bright spot that is due to the front face and that lies in the right half of the back plane (and is thus associated with the left profile in Figs. 33–36). (See Appendix A for equations that permit us to calculate the ϕs. The ϕs will depend on the values of the μ, η, α triplets.) Let ϕ_2 be the location of the X-ray bright spot that is due to the front face and that lies in the left half of the back plane (and is thus associated with the right profile in Figs. 33–36).

Let ϕ_3 be the location of the X-ray bright spot that is due to the right face and that lies in the right half of the back plane. Let ϕ_4 be the location of the X-ray bright spot that is due to the right face and that lies in the left half of the back plane.

Let ϕ_5 be the location of the X-ray bright spot that is due to the back face and that lies in the right half of the back plane. Let ϕ_6 be the location of the X-ray bright spot that is due to the back face and that lies in the left half of the back plane.

Let ϕ_7 be the location of the X-ray bright spot that is due to the left face and that lies in the right half of the back plane. Let ϕ_8 be the location of the X-ray bright spot that is due to the left face and that lies in the left half of the back plane.

(In the program the ϕs are adjusted to $\phi - (90 - \text{minimum location})$ where the minimum location depends upon the set-up of the X-ray apparatus, should be known by the user, and is provided by the user in the start-up box. See Section 10.1.2, and Figs. 37 and 39.)

Define

$$\begin{aligned} a_1(x) &\equiv (x-\phi_1)^2/(2 \times sdFB\_lp^2) \\ a_2(x) &\equiv (x-\phi_2)^2/(2 \times sdFB\_rp^2) \end{aligned}$$

$$
\begin{aligned}
a_3(x) &\equiv (x-\phi_3)^2/(2\times sdRL\_lp^2)\\
a_4(x) &\equiv (x-\phi_4)^2/(2\times sdRL\_rp^2)\\
a_5(x) &\equiv (x-\phi_5)^2/(2\times sdFB\_lp^2)\\
a_6(x) &\equiv (x-\phi_6)^2/(2\times sdFB\_rp^2)\\
a_7(x) &\equiv (x-\phi_7)^2/(2\times sdRL\_lp^2)\\
a_8(x) &\equiv (x-\phi_8)^2/(2\times sdRL\_rp^2)
\end{aligned}
$$

The predicted intensity at angle x that is fit via the nonlinear least squares program to the observed intensity is

$$
\begin{aligned}
\text{predicted}(x) = {} & a + bFB \times (\exp(-a_1(x))/sdFB\_lp + bRdL \times \exp(-a_2(x))/sdFB\_rp \\
& + \exp(-a_5(x))/sdFB\_lp + bRdL \times \exp(-a_6(x))/sdFB\_rp) \\
& + bRL \times (\exp(-a_3(x))/sdRL\_lp + bRdL \times \exp(-a_4(x))/sdRL\_rp \\
& + \exp(-a_7(x))/sdRL\_lp + bRdL \times \exp(-a_8(x))/sdRL\_rp)
\end{aligned} \tag{5}
$$

The nonlinear least squares program returns as an estimate of the MFA, μ, the value that minimizes the sum (over the angles at which intensity was measured) of the squared differences between the observed intensity and the intensity predicted from Equation (5).

Two versions of the program have been developed, an "applet" version and an "application" version. The applet version can be run via a browser over the Web. The application version can be downloaded and run completely on the user's own machine. In Appendix C, we discuss the applet, the application, and their use in detail.

3 MFA as a Function of the Eight Spot Locations

We claim that, for practical purposes, given a profile caused by the broadening of eight X-ray bright spots, there is a unique MFA that could have caused the profile. In this section we provide our justification for this claim. Before doing so, however, we note that there *are* situations in which distinct MFAs lead to essentially the same collection of bright spots. In this case our program cannot work perfectly. An example of such a situation is the following. Both the MFA, tilt, rotation triplets 73.5, 0, 22.5 and 75.9, 0, 4.96 lead to bright spots at angles 67.7, 74.9, 103.2, and 150.2 and their negations. If we see these bright spots (or the profiles due to these bright spots) in an X-ray back plane pattern, we cannot know whether they were due to an MFA of 73.5 or to an MFA of 75.9. However, MFAs this high are extreme and the difference between 73.5 and 75.9 is not of practical importance. In the sections below we argue that for reasonable MFAs our approach leads to good estimates.

3.1 Grid Search

We first wanted to establish in a rough manner that clearly distinct MFAs do not lead to identical bright spots. We did this by calculating the bright spot locations for $112 \times 180 \times 81 = 1,632,960$ cases — MFA varying from 0.5 to 56 in steps of 0.5 (112 values), rotation varying from 0.5 to 90 in steps of 0.5 (180 values), and tilt varying from -20 to 20 in steps of 0.5 (81 values). We then checked whether there were any pairs of MFA/tilt/rotation triplets in which the MFAs differed by more than 2 degrees, but spot location i for triplet 1 differed by less than 0.1 degree from spot location i for triplet 2 for $i = 1, 2, \ldots, 8$. There were no such pairs. However, this is merely suggestive. First, it is certainly conceivable that there are off-grid triplets for which MFAs differ by

more than 2 degrees, but bright spot locations do not differ by more than 0.1 degree. Second, it is certainly conceivable that there are on-grid triplets for which MFAs differ by more than 2 degrees, but bright spot locations do not differ by more than 0.11 (say) degree. Finally, even if there were no triplets among all possible triplets for which MFAs differed by more than 2 degrees, but bright spots were within 0.1 degree of each other, it is conceivable that the noise associated with real data could confuse our algorithm and lead to highly erroneous MFA estimates. We investigated this possibility via a simulation study which we discuss in the next subsection.

3.2 Simulation Study

We used the X-ray diffraction model expressed in Equations 15–19 of Appendix A to generate 5 data sets of 100 X-ray intensity profiles (the program that generated these data sets can be found at `http://www1.fpl.fs.fed.us/mfa_simul.html`). To produce the five data sets, we randomly uniformly generated MFAs on the five intervals [2,10], [10,20], [20,30], [30,40], and [40,55]. For all five data sets, the rotations were randomly uniformly generated on the interval $[-45,45]$. The tilts were randomly uniformly generated on the interval $[-15,15]$. The *sdFB_rp* broadening standard deviations were randomly uniformly generated on the interval [5,20]. (The *sdFB_rp*, *sdFB_lp*, *sdRL_rp*, *sdRL_lp*, *bFB*, *bRL*, and *bRdL* parameters are defined in Section 2.3). The *sdFB_lp* broadening standard deviations were randomly uniformly generated on the interval [*sdFB_rp* $-$ 5, *sdFB_rp* $+$5]. The *sdRL_rp* broadening standard deviations were randomly uniformly generated on the interval [5,20]. The *sdRL_lp* broadening standard deviations were randomly uniformly generated on the interval [*sdRL_rp* $-$5, *sdRL_rp* $+$5]. The base intensity was 300. The *bFB* and *bRL* intensity multipliers were independently randomly uniformly generated on the interval [500,2000]. The *bRdL* intensity multiplier was randomly uniformly generated on [0.6,1.4]. Random $N(0, 10^2)$ noise was added to the intensity values generated by the broadened X-ray hot spots. All of the intervals and the noise level were based on values that we have seen in fits to actual data.

After the data sets were generated, we fit them with our program. In Figure 43, we present histograms of the estimated MFA minus generating MFA value for the five data sets. The mean absolute deviations (in degrees) between estimated and generating MFA for the data sets were 3.1, 1.1, 0.6, 0.2, and 0.1. Thus we do a fairly poor job of estimating MFA when the true MFA falls below 10 degrees (although in this case 100% of the estimates were below 20 degrees, 94% below 15 degrees, and 80% below 10 degrees). However we do a great job of estimating higher MFAs. This result is further illustrated in Figure 44 where we plot estimated MFA versus generating MFA.

The source of the comparatively poor performance in the small MFA case becomes clear when we examine Figures 6 through 18 and 20 through 32. For small MFAs, the bright spots are tightly clustered, and peak broadening and noise in the intensity data will make a proper identification of the distinct peaks relatively difficult. Some improvement in performance can be achieved by increasing the X-ray exposure time, which will increase the signal to noise ratio in the intensity data.

In Figure 45, we plot smoothers through plots of absolute errors versus generating rotation. It appears that rotations near to 45 degrees lead to better results than rotations near 0 degrees. This makes sense when we note that rotations near to 45 degrees lead to more distinctive features in the data (see, for example, Figs. 33–36). This has led us to develop a protocol in which specimens are rotated so that their front faces are 45 degrees from the incoming X-ray beam.

4 Problems with Our Current Approach

Here we discuss six limitations of our current approach.

1. As noted at the end of Section 2.3, an improved physical model might include eight distinct broadening parameters. We have found that, given our current technology, a Java program that includes eight broadening parameters is too slow.

2. Cells frequently have hexagonal rather than rectangular cross-sections. Again, given our current technology, a version of our Java program that accounts for hexagonal cross-sections is too slow.

3. There are more complex tilt combinations possible (for example, a tilted cell on a tilted spindle), but we have found in these complex cases that distinct combinations of angles can lead to the same pattern of eight spots on the back plane. Also, angles become non-unique if we permit the center value to be a parameter rather than a pre-determined (and fixed) value. Thus in complex cases, rotation angles are not uniquely determined.

4. If, for example, the rotation angle equals zero and MFA + tilt $>$ 90 $-$ Bragg angle (this difference equals 78.65 degrees in our case), there will be no diffraction from the left face and our current computer program will fail. This will only occur if we have a large MFA and a large tilt.

5. It appears (see the last paragraph of Section 3.2) that the program does a better job of fitting specimens that have been rotated 45 degrees from directly perpendicular to the incoming X-ray beam. It is possible that further improvements in the MFA estimate could be produced if two separate X-ray patterns were produced for each specimen—for example, one at a nominal rotation of 0 degrees and one at a nominal rotation of 45 degrees. The two patterns would be fit simultaneously.

6. We sometimes see small intensity peaks 90 degrees from the main peaks. Currently, we do not attempt to model these peaks. We believe that they might be due to radial rays in the wood specimens.

The first two problems will be resolved as computer speeds increase. The third problem is inherent in the approach but will not present a serious problem if the X-ray equipment is properly aligned. The fourth through sixth problems can be resolved by further program development.

5 Summary

The changing nature of the nation's timber supply requires improved silvicultural practices, which in turn require improved tools for monitoring stand quality. Measurements of MFA hold promise as stand quality predictors, and X-ray diffraction techniques appear to represent a practical method for quickly estimating MFAs for large numbers of wood cells. In this report, we have discussed a graphically interactive Java computer program that permits a user to obtain measurements of MFA rapidly from X-ray diffraction patterns. Because this program is based on a more complete physics model than earlier programs, we expect that it will yield more accurate MFA estimates. Preliminary comparisons of the new program's MFA estimates with microscopy based estimates are encouraging. A complete evaluation of the accuracy of the program's estimates will appear in a subsequent paper.

The current version of the program can be run as an applet over the World Wide Web, or it can be downloaded and run as an application on a user's own machine. Both the applet and the application can be accessed at `http://www1.fpl.fs.fed.us/mfa0.html`. We are continuing to evaluate and improve this computer program.

6 Acknowledgment

We thank Dr. Ian Cave for valuable discussions in which he shared his insight into new approaches to the analysis of MFA X-ray diffraction data.

7 References

Bendtsen, B.A.; and Senft, J. 1986. Mechanical and anatomical properties in individual growth rings of plantation-grown eastern cottonwood and loblolly pine. Wood and Fiber Science 18(1): 23-38.

Boone, R.S.; Chudnoff, M. 1972. Compression wood formation and other characteristics of plantation-grown Pinus caribaea. Rio Piedros, Puerto Rico: USDA For. Serv. Res. Pap. ITF-13, Institute of Tropical Forestry.

Cave, I.D. 1966. X-ray measurement of microfibril angle. Forest Products Journal 16(10): 37-42.

Cave, I.D. 1976. Modeling the structure of the softwood cell wall for computation of mechanical properties. Wood Science and Technology 10: 19-28.

Cave, I.D.; Robinson, W. 1998. Measuring microfibril angle distribution in the cell wall by means of X-ray diffraction. In: Microfibril Angle in Wood. Butterfield, B. G., ed. International Association of Wood Anatomists. University of Canterbury, New Zealand: 94-107.

Cave, I.D.; Walker, J.C.F. 1994. Stiffness of wood in fast-grown plantation softwoods. Forest Products Journal 44(5): 43-48.

Dadswell, H.E.; Nicholls, J.W.P. 1959. Assessment of wood qualities for tree breeding. I. In *Pinus elliottii* var. *elliottii* from Queensland. Queensland, Australia: Division of Forest Products Technology Paper No. 4.

Dadswell, H.E; Nicholls, J.W.P. 1960. Some aspects of wood anatomy in relation to pulping quality and to tree breeding. Appita Journal 13(5): 161-172.

Donaldson, L.A. 1991. The use of pit apertures as windows to measure microfibril angle in chemical pulp fibres. Wood and Fiber Science 23(2): 290-295.

Echols, R.M. 1955. Linear relation of fibrillar angle to tracheid length, and genetic control of tracheid length in slash pine. Tropical Woods 102: 11-22.

Evans, R.E. 1999. A Variance approach to the X-ray diffractometric estimation of microfibril angle in wood. Appita Journal 52(4): 283-289,294.

Evans, R.; Stuart, S.A.; van der Touw, J. 1996. Microfibril angle scanning of increment cores by X-ray diffractometry. In: Proceedings, Appita General Conference, May 6-10, 1996, Auckland, New Zealand: 879-882.

Foracs, O. L. 1961. Structural weaknesses in softwood pulp tracheids. Tappi 44: 112-119.

Harris, J.M.; Meylan, B.A. 1965. The influence of microfibril angle on longitudinal and tangential shrinkage in *Pinus radiata*. Holzforschung 19(5): 144-153.

Kretschmann, D.E.; Alden, H.A.; Verrill, S. 1998. Variations of microfibril angle in loblolly pine: comparison of iodine crystallization and X-ray diffraction techniques. In: Microfibril Angle in Wood, Butterfield, B. G., ed. International Association of Wood Anatomists. University of Canterbury, New Zealand: 157-176.

Lichtenegger, H.; Reiterer, A.; Tschegg, S.; Fratzl, P. 1998. Determination of spiral angles of elementary fibrils in the wood cell wall: comparison of small angle X-ray scattering and wide angle X-ray diffraction. In: Microfibril Angle in Wood. Butterfield, B. G., ed. International Association of Wood Anatomists. University of Canterbury, New Zealand: pages 157-176.

Marts, R. O. 1955. Fluorescence microscopy for measuring fibril angles in pine tracheids. Stain Technology 30(5): 243-248.

Megraw, R.A. 1986. Wood quality factors in loblolly pine: the influence of tree age, position in the tree, and cultural practice on wood specific gravity, fiber length and fibril angle. TAPPI Press: 1-88.

Meylan, B. A. 1967. Measurement of microfibril angle by X-ray diffraction. Forest Products Journal 17(5): 51-58.

Pearson, R.G.; Gilmore, R.C. 1971. Characterization of the strength of juvenile wood of loblolly pine. Forest Products Journal 21(1): 23-30.

Senft, J.F.; Bendtsen, B.A. 1985. Measuring micofibrillar angles using light microscopy. Wood and Fiber Science 17(4): 564-567.

Stuart, S.; Evans R. 1994. X-ray diffraction estimation of the microfibril angle variation in eucalypt wood. Appita Journal 48(3): 197-200.

Verrill, S.P.; Kretschmann, D.E.; Herian, V.L. 2001. JMFA–A graphically interactive Java program that fits microfibril angle X-ray diffraction data. Res. Note FPL-RN-0283. Madison, WI: U.S. Department of Agriculture, Forest Service, Forest Products Laboratory. 44 p.

Ying, L.; Kretschmann, D.E.; Bendtsen, B.A. 1994. Longitudinal shrinkage in fast-grown loblolly pine plantation wood. Forest Products Journal 44(1): 58-62

8 Appendix A — An Extension to Cave's Equation

Cave (1966) derived an equation for the locations of the spots of high X-ray intensity on the back plane of the X-ray apparatus. This equation applies to cells with square cross sections. It does not account for cell tilt. See the appendix to Verrill, Kretschmann, and Herian (2001) for a detailed derivation of Cave's equation. In this appendix we extend Cave's analysis to the case in which the cell can be tilted.

8.1 Microfibril Directions

To derive the four equations (one for each of the cell's four sides) we first need the microfibril angle directions. Let θ denote the Bragg angle (11.35 degrees for light of wavelength 1.54 angstroms), μ denote the microfibril angle, η denote the tilt of the vertical axis in the wood cell down toward the positive x axis, α equal 90 degrees plus the counterclockwise rotation of the cell around the original z axis (after the tilt), and ϕ equal the angle (measured counterclockwise from the east) of the bright spot on the "2θ circle" on the back plane. See Figures 2–4.

8.1.1 "Front" Face

Before tilt and rotation, the direction of a microfibril on the front face is

$$\begin{pmatrix} 0 \\ \sin(\mu) \\ \cos(\mu) \end{pmatrix}$$

After a tilt of the top of the cell down toward the positive x axis, the direction becomes

$$\begin{pmatrix} \cos(\mu)\sin(\eta) \\ \sin(\mu) \\ \cos(\mu)\cos(\eta) \end{pmatrix}$$

Now, the mathematical tranformation that corresponds to a physical rotation through angle rot of the cell about the original z axis is the matrix

$$\begin{pmatrix} \cos(-\text{rot}) & \sin(-\text{rot}) & 0 \\ -\sin(-\text{rot}) & \cos(-\text{rot}) & 0 \\ 0 & 0 & 1 \end{pmatrix}$$

which equals

$$\begin{pmatrix} \sin(\alpha) & \cos(\alpha) & 0 \\ -\cos(\alpha) & \sin(\alpha) & 0 \\ 0 & 0 & 1 \end{pmatrix}$$

where $\alpha = \pi/2 + \text{rot}$.

Thus the direction of the microfibril angle after tilt and rotation is

$$\mathbf{b} = \begin{pmatrix} \sin(\alpha) & \cos(\alpha) & 0 \\ -\cos(\alpha) & \sin(\alpha) & 0 \\ 0 & 0 & 1 \end{pmatrix} \begin{pmatrix} \cos(\mu)\sin(\eta) \\ \sin(\mu) \\ \cos(\mu)\cos(\eta) \end{pmatrix} = \begin{pmatrix} \sin(\alpha)\cos(\mu)\sin(\eta) + \cos(\alpha)\sin(\mu) \\ -\cos(\alpha)\cos(\mu)\sin(\eta) + \sin(\alpha)\sin(\mu) \\ \cos(\mu)\cos(\eta) \end{pmatrix} \tag{6}$$

8.1.2 "Right" Face

Before tilt and rotation, the direction of a microfibril on the right face is

$$\begin{pmatrix} -\sin(\mu) \\ 0 \\ \cos(\mu) \end{pmatrix}$$

After a tilt of the top of the cell down toward the positive x axis, the direction becomes

$$\begin{pmatrix} -\sin(\mu-\eta) \\ 0 \\ \cos(\mu-\eta) \end{pmatrix}$$

The direction of the microfibril angle after tilt and rotation is thus

$$\mathbf{b} = \begin{pmatrix} -\sin(\alpha)\sin(\mu-\eta) \\ \cos(\alpha)\sin(\mu-\eta) \\ \cos(\mu-\eta) \end{pmatrix} \tag{7}$$

8.1.3 "Back" Face

Before tilt and rotation, the direction of a microfibril on the back face is

$$\begin{pmatrix} 0 \\ -\sin(\mu) \\ \cos(\mu) \end{pmatrix}$$

After a tilt of the top of the cell down toward the positive x axis, the direction becomes

$$\begin{pmatrix} \cos(\mu)\sin(\eta) \\ -\sin(\mu) \\ \cos(\mu)\cos(\eta) \end{pmatrix}$$

The direction of the microfibril angle after tilt and rotation is thus

$$\mathbf{b} = \begin{pmatrix} \sin(\alpha)\cos(\mu)\sin(\eta) - \cos(\alpha)\sin(\mu) \\ -\cos(\alpha)\cos(\mu)\sin(\eta) - \sin(\alpha)\sin(\mu) \\ \cos(\mu)\cos(\eta) \end{pmatrix} \tag{8}$$

8.1.4 "Left" Face

Before tilt and rotation, the direction of a microfibril on the left face is

$$\begin{pmatrix} \sin(\mu) \\ 0 \\ \cos(\mu) \end{pmatrix}$$

After a tilt of the top of the cell down toward the positive x axis, the direction becomes

$$\begin{pmatrix} \sin(\mu+\eta) \\ 0 \\ \cos(\mu+\eta) \end{pmatrix}$$

The direction of the microfibril angle after tilt and rotation is thus

$$\mathbf{b} = \begin{pmatrix} \sin(\alpha)\sin(\mu+\eta) \\ -\cos(\alpha)\sin(\mu+\eta) \\ \cos(\mu+\eta) \end{pmatrix} \tag{9}$$

8.2 The Four Equations

There are two conditions that a 002 reflecting plane must meet to reflect a beam coming in along the x axis. First, $\mathbf{b}$ is in the 002 crystallographic planes of the cellulose crystals associated with the microfibrils so the normal, $\mathbf{p}$, to the 002 plane that succeeds in reflecting the beam must be perpendicular to $\mathbf{b}$. Second (the Bragg condition), the normal to the 002 reflecting plane must make a $90 - \theta$ angle to the x axis, where θ is the Bragg angle for the X-ray wavelength being used. Given these two conditions, we want to be able to determine the location at which the reflected beam intersects the back plane of the X-ray apparatus.

The second condition gives us

$$p_1 = \begin{pmatrix} 1 \\ 0 \\ 0 \end{pmatrix} \cdot \mathbf{p} = \cos(90 - \theta) = \sin(\theta). \tag{10}$$

We also have

$$p_1^2 + p_2^2 + p_3^2 = 1. \tag{11}$$

Making use of Equations (10) and (11), we obtain

$$p_2^2 + p_3^2 = \cos^2(\theta). \tag{12}$$

The first condition and result (10) give us

$$\begin{pmatrix} \sin(\theta) \\ p_2 \\ p_3 \end{pmatrix} \cdot \mathbf{b} = 0 \tag{13}$$

Thus the solutions for (p_2, p_3) will be the 0, 1, or 2 points represented by the intersection of line (13) with circle (12). Circle (12) has radius $\cos(\theta)$ and a point on circle (12) has form $(\cos(\phi)\cos(\theta), \sin(\phi)\cos(\theta))$ for some angle ϕ. That is,

$$\begin{aligned} p_2 &= \cos(\phi)\cos(\theta) \\ p_3 &= \sin(\phi)\cos(\theta) \end{aligned} \tag{14}$$

From Equations (13) and (14) and results (6)–(9), after dividing by $\cos(\theta)$, we obtain four versions of the following equation

$$d_1 + d_2 \times \cos(\phi) + d_3 \times \sin(\phi) = 0 \tag{15}$$

(In the next section we relate the ϕ in Equations (14) and (15) to the angle (counterclockwise from the east) of the bright spot on the back plane.)

For the **front**, we have

$$\begin{aligned} d_1 &= (\sin(\alpha)\cos(\mu)\sin(\eta) + \cos(\alpha)\sin(\mu))\tan(\theta) \\ d_2 &= -\cos(\alpha)\cos(\mu)\sin(\eta) + \sin(\alpha)\sin(\mu) \\ d_3 &= \cos(\mu)\cos(\eta) \end{aligned} \tag{16}$$

For the **right**, we have

$$\begin{aligned} d_1 &= -\sin(\alpha)\sin(\mu - \eta)\tan(\theta) \\ d_2 &= \cos(\alpha)\sin(\mu - \eta) \\ d_3 &= \cos(\mu - \eta) \end{aligned} \tag{17}$$

For the **back**, we have

$$\begin{aligned} d_1 &= (\sin(\alpha)\cos(\mu)\sin(\eta) - \cos(\alpha)\sin(\mu))\tan(\theta) \\ d_2 &= -\cos(\alpha)\cos(\mu)\sin(\eta) - \sin(\alpha)\sin(\mu) \\ d_3 &= \cos(\mu)\cos(\eta) \end{aligned} \tag{18}$$

For the **left**, we have

$$\begin{aligned} d_1 &= \sin(\alpha)\sin(\mu + \eta)\tan(\theta) \\ d_2 &= -\cos(\alpha)\sin(\mu + \eta) \\ d_3 &= \cos(\mu + \eta) \end{aligned} \tag{19}$$

Now in each of the four cases we can use Equation (15) to solve for ϕ. For $\phi \in [0, \pi]$, (15) yields

$$d_1 + d_2 x = -d_3 \sqrt{1 - x^2} \tag{20}$$

for $x = \cos(\phi)$. Squaring both sides and collecting terms, we obtain the quadratic equation

$$d_1^2 - d_3^2 + 2 d_1 d_2 x + (d_2^2 + d_3^2) x^2 = 0$$

We then find the $\phi \in [0, \pi]$ for which $\cos(\phi) = x_{\text{sol}}$ where x_{sol} is a solution to the quadratic equation. Of course, for this to yield a ϕ there must be a solution to the quadratic equation and this solution must lie in [−1,1].

For $\phi \in [-\pi, 0]$, (15) yields

$$d_1 + d_2 x = d_3 \sqrt{1 - x^2} \tag{21}$$

and the resulting quadratic equation is unchanged. In our computer program we check the (at most) two solutions for the $\phi \in [0, \pi]$ case against Equation (20) and the (at most) two solutions for the $\phi \in [-\pi, 0]$ case against Equation (21). If the total number of solutions is not exactly two (as it should be given the physics for "reasonable" MFAs and tilts), then the program reports non-convergence.

8.3 Relation between ϕ and the Angle (Counterclockwise from the East) of the Bright Spot on the Back Plane

Let us now consider the issue of where the reflected beam intersects the back plane. We know that the beam comes in along the x axis and reflects off a plane whose normal is given by (14). Consider now a canonical situation in which a beam reflects off a plane with normal (0,0,1) (the z axis). In this case the direction vector of the reflected beam is the same as the direction vector of the incident beam except that the sign of the z coordinate is reversed.

To make use of this result, we first find the transform that takes the $\mathbf{p}$ vector to the z vector. This requires a rotation of $90 - \phi$ degrees of the z axis towards the y axis (to bring the z axis in line with the projection of $\mathbf{p}$ onto the y, z plane), followed by a rotation of θ degrees of the z axis towards the x axis (to bring the z axis into line with $\mathbf{p}$). These two rotations can be represented by the transform

$$T \equiv \begin{pmatrix} \cos(\theta) & 0 & -\sin(\theta) \\ 0 & 1 & 0 \\ \sin(\theta) & 0 & \cos(\theta) \end{pmatrix} \begin{pmatrix} 1 & 0 & 0 \\ 0 & \sin(\phi) & -\cos(\phi) \\ 0 & \cos(\phi) & \sin(\phi) \end{pmatrix}$$

One can check that

$$T(\mathbf{p}) = T \cdot \begin{pmatrix} \sin(\theta) \\ \cos(\phi)\cos(\theta) \\ \sin(\phi)\cos(\theta) \end{pmatrix} = \begin{pmatrix} 0 \\ 0 \\ 1 \end{pmatrix}$$

Now in the original coordinate system, the X-ray incident direction is

$$\begin{pmatrix} -1 \\ 0 \\ 0 \end{pmatrix}$$

In the coordinate system in which the $\mathbf{p}$ vector has been transformed to the z vector, this incident direction becomes

$$T \cdot \begin{pmatrix} -1 \\ 0 \\ 0 \end{pmatrix} = \begin{pmatrix} -\cos(\theta) \\ 0 \\ -\sin(\theta) \end{pmatrix}$$

so the beam reflects off in the

$$\begin{pmatrix} -\cos(\theta) \\ 0 \\ \sin(\theta) \end{pmatrix}$$

direction. Transformed back into the original coordinate system, this direction vector is

$$\begin{pmatrix} 1 & 0 & 0 \\ 0 & \sin(\phi) & -\cos(\phi) \\ 0 & \cos(\phi) & \sin(\phi) \end{pmatrix}^{-1} \begin{pmatrix} \cos(\theta) & 0 & -\sin(\theta) \\ 0 & 1 & 0 \\ \sin(\theta) & 0 & \cos(\theta) \end{pmatrix}^{-1} \begin{pmatrix} -\cos(\theta) \\ 0 \\ \sin(\theta) \end{pmatrix}$$

$$= \begin{pmatrix} -\cos(2\theta) \\ \cos(\phi)\sin(2\theta) \\ \sin(\phi)\sin(2\theta) \end{pmatrix}$$

We extend a beam in this direction to its intersection with a back plane that is perpendicular to the x axis and x_0 units behind the specimen by multiplying by a factor of $x_0/\cos(2\theta)$. Thus the beam intersects the back plane at the point

$$\begin{pmatrix} -x_0 \\ \cos(\phi)\sin(2\theta)x_0/(\cos(2\theta)) \\ \sin(\phi)\sin(2\theta)x_0/(\cos(2\theta)) \end{pmatrix} = \begin{pmatrix} -x_0 \\ \cos(\phi)\tan(2\theta)x_0 \\ \sin(\phi)\tan(2\theta)x_0 \end{pmatrix}$$

Looking face on at the back plane, this is the point that is on the circle of radius $\tan(2\theta)x_0$ (the "2θ circle") and ϕ degrees in a counterclockwise direction from the y axis. So the ϕ that is a solution to (14) is also the angle (counterclockwise from the east) of the point of maximum X-ray intensity.

9 Appendix B — The Effects of a Change in Tilt Sign or of Rotation Sign on the Pattern of Eight Spots

9.1 Change in Tilt Sign

The effect of a change in tilt sign can be seen by a comparison of Figures 24 and 41. In both cases the cell rotation angle is 30 degrees. However, in Figure 24 the cell tilt is 15 degrees whereas in Figure 41, the cell tilt is -15 degrees. The result is that hot spot locations are reflected across the horizontal west to east line (see Figure 5). Also front, back IDs are exchanged, and right, left IDs are exchanged.

This effect is embodied in the following four claims.

Claim 1

If ϕ is a solution for a front hot spot under tilt η, then $-\phi$ is a solution for a back hot spot under tilt $-\eta$.

Claim 2

If ϕ is a solution for a back hot spot under tilt η, then $-\phi$ is a solution for a front hot spot under tilt $-\eta$.

Claim 3

If ϕ is a solution for a right hot spot under tilt η, then $-\phi$ is a solution for a left hot spot under tilt $-\eta$.

Claim 4

If ϕ is a solution for a left hot spot under tilt η, then $-\phi$ is a solution for a right hot spot under tilt $-\eta$.

Equations 15–19 can be used in a straightforward manner to establish these claims. Here, for the purposes of illustration, we establish Claim 1.

From Equations 15 and 16 we have (recall that $\alpha = \pi/2 + \text{rot}$ so $\cos(\alpha) = -\sin(\text{rot})$ and $\sin(\alpha) = \cos(\text{rot})$)

$$\begin{aligned} 0 &= (\cos(\text{rot})\cos(\mu)\sin(\eta) - \sin(\text{rot})\sin(\mu))\tan(\theta) \\ &+ (\sin(\text{rot})\cos(\mu)\sin(\eta) + \cos(\text{rot})\sin(\mu))\cos(\phi) \\ &+ \cos(\mu)\cos(\eta)\sin(\phi) \end{aligned}$$

Multiplying this equation by -1 we obtain

$$\begin{aligned} 0 &= (-\cos(\text{rot})\cos(\mu)\sin(\eta) + \sin(\text{rot})\sin(\mu))\tan(\theta) \\ &+ (-\sin(\text{rot})\cos(\mu)\sin(\eta) - \cos(\text{rot})\sin(\mu))\cos(\phi) \\ &- \cos(\mu)\cos(\eta)\sin(\phi) \end{aligned}$$

or

$$\begin{aligned} 0 &= (\cos(\text{rot})\cos(\mu)\sin(-\eta) + \sin(\text{rot})\sin(\mu))\tan(\theta) \\ &+ (\sin(\text{rot})\cos(\mu)\sin(-\eta) - \cos(\text{rot})\sin(\mu))\cos(-\phi) \\ &+ \cos(\mu)\cos(-\eta)\sin(-\phi) \end{aligned}$$

which is what we needed to establish.

9.2 Change in Rotation Sign

The effect of a change in rotation sign can be seen by a comparison of Figures 24 and 42. In both cases the cell tilt angle is 15 degrees. However, in Figure 24 the cell rotation is 30 degrees whereas in Figure 42 the cell rotation is -30 degrees. The result is that hot spot locations are reflected across the vertical south to north line (see Fig. 5). Also front, back IDs are exchanged. Right, left IDs remain unchanged.

This effect is embodied in the following four claims.

Claim 1

If $\pi/2 - \beta$ is a solution for a front hot spot under rotation rot, then $\pi/2 + \beta$ is a solution for a back hot spot under rotation $-$rot.

Claim 2

If $\pi/2 - \beta$ is a solution for a back hot spot under rotation rot, then $\pi/2 + \beta$ is a solution for a front hot spot under rotation $-$rot.

Claim 3

If $\pi/2 - \beta$ is a solution for a right hot spot under rotation rot, then $\pi/2 + \beta$ is a solution for a right hot spot under rotation $-$rot.

Claim 4

If $\pi/2 - \beta$ is a solution for a left hot spot under rotation rot, then $\pi/2 + \beta$ is a solution for a left hot spot under rotation $-$rot.

Equations 15–19 can be used in a straightforward manner to establish these claims. Here, for the purposes of illustration, we establish Claim 1.

From Equations 15 and 16 we have

$$\begin{aligned} 0 &= (\cos(\text{rot})\cos(\mu)\sin(\eta) - \sin(\text{rot})\sin(\mu))\tan(\theta) \\ &+ (\sin(\text{rot})\cos(\mu)\sin(\eta) + \cos(\text{rot})\sin(\mu))\cos(\pi/2 - \beta) \\ &+ \cos(\mu)\cos(\eta)\sin(\pi/2 - \beta) \end{aligned}$$

or

$$\begin{aligned} 0 &= (\cos(\text{rot})\cos(\mu)\sin(\eta) - \sin(\text{rot})\sin(\mu))\tan(\theta) \\ &+ (-\sin(\text{rot})\cos(\mu)\sin(\eta) - \cos(\text{rot})\sin(\mu))(-\cos(\pi/2 - \beta)) \\ &+ \cos(\mu)\cos(\eta)\sin(\pi/2 - \beta) \end{aligned}$$

or

$$\begin{aligned} 0 &= (\cos(-\text{rot})\cos(\mu)\sin(\eta) + \sin(-\text{rot})\sin(\mu))\tan(\theta) \\ &+ (\sin(-\text{rot})\cos(\mu)\sin(\eta) - \cos(-\text{rot})\sin(\mu))\cos(\pi/2 + \beta) \\ &+ \cos(\mu)\cos(\eta)\sin(\pi/2 + \beta) \end{aligned}$$

which is what we needed to establish.

10 Appendix C — The Applet and the Application

10.1 The Applet

10.1.1 Getting data to and from the applet

Currently, the Java applet expects data in the following form: The data file should be an ASCII text file, not a proprietary word processing or spreadsheet document. Text files can be produced by proprietary word processing or spread sheet programs. On personal computers they tend to have extensions such as ".txt" or ".prn".

The text file should begin with a data set's name. The name *cannot contain spaces.* Next, the text file should contain two columns of X-ray diffraction pattern data. The first column should contain angle values (for example, −180 to 180 or 0 to 360), and the second column should contain the corresponding intensity values. The angles in the first column must be increasing but they do not have to be increasing in constant increments. At the end of this angle/intensity data set, a new data set can be placed. Again, it must begin with a line that contains only the data set name. Here is an excerpt from the beginning of the `mfa_demo_input` file that is the default applet data file. A user can run the applet on this data file by going to `http://www1.fpl.fs.fed.us/mfa.html`.

```
03ar1erX
-0.1364E+03          0.3084E+03
-0.1363E+03          0.3084E+03
-0.1362E+03          0.3125E+03
-0.1361E+03          0.3144E+03
-0.1360E+03          0.3144E+03
.
```

.
.
0.2232E+03 0.3016E+03
0.2233E+03 0.3026E+03
0.2234E+03 0.3084E+03
0.2235E+03 0.3084E+03
0.2236E+03 0.3084E+03
12br1erX
-0.1364E+03 0.3259E+03
-0.1363E+03 0.3259E+03
-0.1362E+03 0.3275E+03
-0.1361E+03 0.3343E+03
-0.1360E+03 0.3343E+03
.
.
.

A version of data set 03ar1erX that has been cleaned by removal of a glitch is plotted in Figure 38. A cleaned version of data set 12br1erX is plotted in Figure 40.

Currently, the applet can handle at most 100 data sets in the data file. Also, each data set can contain at most 3,700 observations (for a possible total of 370,000 angle/intensity pairs in the data file). If the reader wishes to use this applet and either of these restrictions presents a problem, please contact Steve Verrill at the USDA Forest Service Forest Products Laboratory (`sverrill@fs.fed.us` or 608-231-9375).

We describe below how to obtain a Java application version of this applet that can be run locally on your machine with access to your file system. It can read the data file directly from your file system and write the results files directly to your file system. However, for quite good security reasons, Java applets cannot read from or write to your file system. Thus, if you do not want to download and install the application version of this applet but do want to run it on your data, you must anonymous ftp the data file to `www1.fpl.fs.fed.us` and put it in the pub/data directory. (Anonymous ftp directions can be found at `http://www1.fpl.fs.fed.us/anonftp0.html`.) Then, after you start the applet, replace "mfa_demo_input" in the first applet window with the name of your data file and "mfa_demo_output" in the first applet window with the prefix that you want for your output files. These names *must be unique to you* to avoid intermixing your results with those of another user.

10.1.2 First applet window

When a user goes to `http://www1.fpl.fs.fed.us/mfa.html`, the applet is started and the user is presented with a small window (Fig. 37) that contains the data file and results file prefix input boxes mentioned in the previous section. The window also contains a text field in which the user must specify the Bragg angle associated with their experimental setup. In addition, the window contains a text field in which the user specifies the location in degrees of the minimum intensity between the left and right profiles of their data. (This fixed location depends on the experimental set-up and should be known by the user.) After the four text fields are filled, the user clicks the **Go** button and the main applet window pops up. (Fig. 38.) This may take a number of seconds if the data set is large.

10.1.3 Main applet window

After the main applet window pops up, a user should maximize it to ensure that all text fields are displayed.

As described in the heuristic justification section, the program performs an 11 parameter nonlinear least squares fit to estimate the MFA. To perform such a fit, we need reasonable initial estimates of the parameters. We obtain these by first performing a simpler six parameter nonlinear least squares fit. *This fit must be completed before an 11 parameter fit is attempted.*

The predicted intensity in this case is given by

$$\begin{aligned} \text{predicted}(x) &= a + b_1 \times \exp(-(x-\mu_1)^2/(2\sigma_1^2)) \\ &\quad + b_2 \times \exp(-(x-(\mu_1+180))^2/(2\sigma_2^2)) \end{aligned}$$

where the parameters are a, b_1, b_2, μ_1, σ_1, and σ_2. (We have produced some confusing notation here. In the theoretical discussion we have used μ to denote the MFA. Here we are using μ_1 to denote the center of a peak.) In other words, we model the complete profile as a double Gaussian in which the two peaks may have different heights and widths. Initial estimates for this six parameter fit are obtained automatically by clicking the **Initial 6** button in the right panel (Fig. 38). The resulting initial intensity curve appears as a blue line overlaying the data. If this initial curve is even *roughly* reasonable, then a user can obtain a good six parameter fit by clicking the **Fit 6** button in the right panel. The resulting six parameter fit appears as a green curve overlaying the data. The corresponding fitted a, b_1, b_2, μ_1, and σ_1 values appear in the boxes in the right panel next to these names, and the resulting initial estimates for the 11 parameters in the more complicated model appear next to their names in the right panel.

Occasionally, the initial curve for the six parameter fit is not a reasonable starting point for the nonlinear least squares program. A user quickly learns to identify such situations from the appearance of the blue overlay. In this case the user must provide improved initial estimates. This can be done in two ways. The user can type initial estimates into the text fields next to the **a**, **b1**, **b2**, **mu1**, and **sigma1** buttons or the user can use the mouse to identify good initial values:

- To use the mouse to identify an initial a value, click the **a** button. A horizontal blue line will appear at the height corresponding to the current a value. Now click the mouse on the plot at a height that is approximately even with the plot's baseline. The first horizontal blue line will be replaced with a new one that corresponds to the height selected by the mouse click. This new a value will also appear in the text field next to the **a** button. In addition, the old initial fit overlay will be replaced by a new (cyan) overlay based on the new initial parameter values.

- To use the mouse to identify an initial b_1 value, click the **b1** button. A horizontal blue line will appear at the height corresponding to the current $a + b_1$ value. Now click the mouse on the plot at a height that is approximately even with the *leftmost* main peak's maximum. The first horizontal blue line will be replaced with a new one that corresponds to the height selected by the mouse click. The new b_1 value (calculated as click height minus the a value) will also appear in the text field next to the **b1** button. In addition, the old initial fit overlay will be replaced by a new (cyan) overlay based on the new initial parameter values.

- To use the mouse to identify an initial b_2 value, click the **b2** button. A horizontal blue line will appear at the height corresponding to the current $a + b_2$ value. Now click the mouse on the plot at a height that is approximately even with the *rightmost* main peak's maximum. The first horizontal blue line will be replaced with a new one that corresponds to the height

selected by the mouse click. The new b_2 value (calculated as click height minus the a value) will also appear in the text field next to the **b2** button. In addition, the old initial fit overlay will be replaced by a new (cyan) overlay based on the new initial parameter values.

- To use the mouse to identify an initial μ_1 value, click the **mu1** button. A vertical blue line will appear at the x value corresponding to the current μ_1 value. Now click the mouse on the plot at a x value that is approximately at the midpoint of the *leftmost* main peak. The first vertical blue line will be replaced with a new one that corresponds to the x value selected by the mouse click. The new μ_1 value will also appear in the text field next to the **mu1** button. In addition, the old initial fit overlay will be replaced by a new (cyan) overlay based on the new initial parameter values.

- To use the mouse to identify an initial σ_1 value (which is used for both σ_1 and σ_2), click the **sigma1** button. A vertical blue line will appear at the x value corresponding to the current μ_1 value. A second vertical blue line will appear at the x value corresponding to $\mu_1 + \sigma_1$. Now click the mouse on the plot at a x value that is approximately equal to an improved $\mu_1 + \sigma_1$ estimate. (Ideally, this should be at a point at which the curve is at about 60% of its maximum height. However, the initial σ_1 value does not have to be very close at all to the correct value for the subsequent nonlinear least squares to succeed.) The second vertical blue line will be replaced with a new one that corresponds to the x value selected by the mouse click. The new σ_1 value (calculated as the click x value minus μ_1) will also appear in the text field next to the **sigma1** button. In addition, the old initial fit overlay will be replaced by a new (cyan) overlay based on the new initial parameter values.

After a user is satisfied with a new initial fit overlay (one set of button clicks should be sufficient), they can proceed with a fit of the two single peaks model by clicking the **Fit 6** button. The result of a nonlinear least squares fit of this model will appear as a green overlay (replacing the blue or cyan initial conditions overlay).

The initial estimates for the 11 parameter fit are obtained as follows:

- $\boldsymbol{\mu}$ The initial estimate of the MFA is $0.8 \times 0.6 \times (\sigma_1 + \sigma_2)$. This is approximately equal to $0.8 \times 0.6 \times T$ where the T value is that of Stuart and Evans (1994). (When we approximate the left profile by a *single* Gaussian, we obtain $T =$ (right intersection point $-$ left intersection point)$/2 = (\mu_1 + 2\sigma_1 - (\mu_1 - 2\sigma_1))/2 = 2\sigma_1$. Similarly, fitting a single Gaussian to the right profile, we obtain $T = 2\sigma_2$. Averaging, we obtain $T \approx \sigma_1 + \sigma_2$.) The 0.6 multiplier appears in Cave (1966). The 0.8 value is an ad hoc multiplier that we have found leads to initial MFA estimates that are more in accord with microscopy-based estimates.

- **rot** The initial wood cell rotation estimate is 0 degrees. However, see the descriptions of the **c,c**; **nc,c**; **c,nc**; and **nc,nc** buttons given later in this section.

- **tilt** The initial wood cell tilt estimate is 0 degrees.

- **sds** The initial estimate of all four *sd* values is 10 degrees. Our fits of hundreds of X-ray profiles suggest that *sd* values between 5 and 20 degrees are typical. (Given that the MFAs from our fits vary from 0 degrees to 55 degrees [approximately], this is very roughly in accord with Cave's onservation that $\sigma \approx$ MFA$/3$.)

- **a** The initial a value is the estimated a from the six parameter fit.

- **bFB** and **bRL** The initial bFB and bRL values are $4 \times b_1$ where b_1 is the estimated b_1 from the six parameter fit.

- **bRdL** The initial $bRdL$ value is b_2/b_1.

Any of these "automatic" initial estimates can be altered by typing in the box next to the relevant name. The curve based on these initial estimates can be viewed by clicking on the **Initial 11** button in the right panel. The initial curve then appears as an orange overlay on the data.

Before proceeding with an 11 parameter fit, we need to consider the possibility that the initial estimate of the rotation of the wood cells should not be 0 degrees. As noted in the section on the heuristic justification for our approach, if the front faces of the wood cells in a specimen are not perpendicular to the X-ray beam, then the location of the eight bright spots will change. As we saw in Figure 33, if the front faces are perpendicular to the beam, the complete broadened profile should contain left and right profiles with central peaks. As we saw in Figure 34, if the front faces of the wood cells are rotated 22.5 degrees counterclockwise (looking down at the specimen from above), the complete profile should contain a left profile with two noncentral peaks and a right profile with a central peak (here we are assuming that tilt is 0). If a user sees this pattern, they could click the **nc,c** (this stands for noncentral, central) button on the right panel prior to performing the 11 parameter fit. As we saw in Figure 35, if the front faces of the wood cells are rotated 45 degrees counterclockwise, the complete profile should contain left and right profiles that each contain two noncentral peaks. If a user sees this pattern, they could click the **nc,nc** button on the right panel prior to performing the 11 parameter fit. Finally, as we saw in Figure 36, if the front faces of the wood cells are rotated 67.5 degrees counterclockwise (or -22.5 degrees clockwise), the complete profile should contain a left profile with a central peak and a right profile with two noncentral peaks. If a user sees this pattern, they could click the **c,nc** button on the right panel prior to performing the 11 parameter fit.

A user performs an 11 parameter fit by clicking on either the **Fit 11** button or the **Fit 11,4** button. If the **Fit 11** button is clicked, one nonlinear least squares fit is performed and the resulting predicted intensity values are plotted as a red overlay. In addition, a smoothed version of the data is plotted as a green line. The final parameter estimates are displayed in the "MFA," "rot," "tilt," "sdFB_lp," "sdFB_rp," "sdRL_lp," "sdRL_rp," "a," "bFB," "bRL," and "bRdL" text fields. The MFA estimate also appears in the panel at the top of the window. If the fit is the first 11 parameter fit of the data set, the MFA estimate appears next to the **1** button. If the fit is the second 11 parameter fit of the data set, the MFA estimate appears next to the **2** button. And so on. When more than one fit is performed, the ID of the fit that corresponds to a minimum mean sum of squares is placed in the box to the right of "ID_min" in the top panel. The corresponding minimum mean sum of squares is placed in the box to the right of "mss_min" in the top panel. Currently, the program permits at most five 11 parameter fits of a particular data set. (Of course one can always reload the data set to obtain additional fits. However, in general, this should not be necessary.) See below for a description of how results are saved to a file.

If the **Fit 11,4** button is clicked (this is our standard protocol), four fits are automatically performed. They differ only in the initial estimate of the rotation. The four fits use -22.5 degrees, 0 degrees, 22.5 degrees, and 45 degrees as the initial rotation estimates. If there are four or five empty fields at the top of the page, and the **Fit 11,4** button is clicked, the results from all four fits will appear at the top. If one to three fields are available at the top of the page, and the **Fit 11,4** button is clicked, only the best of the four fits will appear at the top.

10.1.4 Load, Reset, Clear All, Clear, and Zoom buttons

If a user never clicks the **Load** button, the data sets are simply presented in the order in which they appear in the data file. The **Load** button permits a user to load a particular one of the data

sets in the data file. The user must type the data set name (as it appears in the data file) into the text field next to the **Load** button and then click the **Load** button. After a file has been loaded via the **Load** button, the files are presented in the order in which they appear in the data file but beginning with the file just loaded.

The **Reset**, **Clear All**, **Clear**, and **Zoom** buttons can be used to remove "glitches" in the data.

- A user *excludes rectangular regions* of data by pushing a mouse button down at one corner of the rectangle, holding the button down while moving the pointer to the opposite corner of the rectangle, and then releasing the button. While a user is performing this movement, an animated red rectangle appears that outlines the current exclusion region. After the button is released, the outline of the rectangle turns black, and it can no longer be moved.

- If a user wants to see only the data that have not been excluded, the user should press the **Zoom** button. A sequence of zooms can be performed.

- Currently, the program does not permit a user to unzoom a single zoom. However, a user can reactivate all the data by pressing the **Reset** button at the bottom of the page. A user can see all of the inactivated rectangles by performing a fit and then by clicking the appropriate recall button at the top of the page.

- The data in an inactivated rectangle can be reactivated if the rectangle is "cleared." A user clears a rectangle by clicking a mouse button in it (all rectangles that contain this point will be cleared) and then clicking on the **Clear** button at the bottom of the page. All rectangles that are shown on the current page (in the current "zoom state") will be cleared if the user clicks the **Clear All** button at the bottom of the page.

10.1.5 Buttons 1, 2, 3, 4, and 5 in the top panel

As explained above, a user fits the active data by sequentially clicking the **Initial 6**, **Fit 6**, and **Fit 11** or **Fit 11,4** buttons in the right hand panel.

As we explained above, after an 11 parameter fit has been performed, an estimate of the MFA appears in the next available box at the top of the page. At any time prior to a click of the **Load**, **Back**, **Next**, or **Stop** buttons, this fit can be recalled by clicking the top panel button (buttons **1**–**5**) associated with the fit.

10.1.6 Writing results to files

The **Back** button loads the preceeding data set in the data file. The **Next** button loads the next data set in the data file. The **Stop** button ends the execution of the program. *If an 11 parameter fit has been performed*, then when the next **Load**, **Back**, **Next**, or **Stop** button is clicked, information is written to two results files. To a file titled xxx.ests (where xxx is the output prefix provided by the user in the startup box) in the pub/data anonymous ftp space on www1.fpl.fs.fed.us, the applet writes the ID and the 11 parameter estimates (including the MFA estimate) calculated from the *most recently displayed* 11 parameter fit. Thus, if the user wants to save results from the fit that yielded the lowest mean sum of squares, and it was not the most recent fit, they will have to first recall it by clicking on the button at the top of the page (from **1** to **5**) that corresponds to the fit. To a file titled xxx.inact (where xxx is the output prefix provided by the user in the startup box), the applet writes the ID, the number of inactivated rectangles associated with the *most recently displayed* fit, and the pairs of x, y values that define them. These files can be retrieved

via anonymous ftp from the pub/data directory of www1.fpl.fs.fed.us. (Anonymous ftp directions can be found at `http://www1.fpl.fs.fed.us/anonftp0.html`.)

10.2 The Application

The application differs from the applet in how it is accessed, in how the data set is read, and in how results are written.

The application expects data in the same form expected by the applet and has the same restrictions on data set size. The data can be located in any directory on your machine to which you have access.

You can download the Java application to have a version of the program that resides on your personal machine. The code is available in both compressed tar and zip forms.

The source code, class files, and associated documentation and data files for a **UNIX** (The Open Group, San Francisco, California) machine are included in the file `mfa.src.tar.Z`. You can install and run the program on your machine by following these instructions:

1. Go to `www1.fpl.fs.fed.us/mfa.src.tar.html` and click on the `mfa.src.tar.Z` link.

2. Once you click on this link, a box comes up asking where you want to save the file on your computer. Once you give it a path and file name and click OK, it will be written to that directory.

3. After you receive the file as (for example) `mfa.src.tar.Z`, you will have to uncompress the file with the command (for example) `uncompress mfa.src.tar.Z`, and then untar the resulting file with the command (for example) `tar xvf mfa.src.tar`. This should be done in a directory that lies in the CLASSPATH of your machine.

4. To start the application, type `java MFA_application`.

For more information, please read the README.html, copyright, and disclaimer files.

The source code, class files, and associated documentation and data files for a **Windows** (Microsoft Corporation, Redmond, Washington) machine are included in the file `mfa.src.98.exe`. You can install and run the program on your machine by following these instructions:

1. Go to `www1.fpl.fs.fed.us/mfa.src.98.zip.html` and click on the `mfa.src.98.exe` link.

2. Once you click on this link, a box comes up asking where you want to save the file on your computer. Save it in a directory such as `c:\mfa`.

3. Next, open a DOS window. Click the START button and go to PROGRAMS $--> $ ACCESSORIES $--> $ COMMAND PROMPT.

4. When the DOS window comes up, go to the directory in which `mfa.src.98.exe` has been saved (for example, `cd c:\mfa`).

5. Then, while in the directory, type **mfa.src.98.exe** and the archive will unpack itself. (Alternatively, in Windows Explorer you might be able to double click on the icon for mfa.src.98.exe and proceed from there.)

6. In the DOS window you then need to type `install.bat` to create the necessary subdirectories.

7. You can then run the application by typing `java MFA_application`.

Further information on both the applet and the application can be found at `http://www1.fpl.fs.fed.us/mfa0.html`.

After you have started the application on your computer, a start-up window appears (Fig. 39). It contains five text input fields and a **Go** button. In the first text field you need to place the name of the data file. If the data file does not lie in the directory in which you are running the Java application, you need to provide the *full* path name to the data file. Alternatively, you can use the associated **Browse** button to find the data file. After you click on the file in the browse window and then click on the open button in the browse window, the correct path to the file will appear in the text field.

A user needs to fill out the "MFA estimates file" text field (either directly or via the associated **Browse** button) to provide a file to which the fitted parameters (including the estimated microfibril angles) will be written.

A user needs to fill out the "Inactive rectangles file" text field (either directly or via the associated **Browse** button) to provide a file to which the application writes data set IDs, numbers of inactivated rectangles, and pairs of x, y values that define them.

The window also contains a text field in which the user must specify the Bragg angle associated with their experimental setup. Finally, the window contains a text field in which the user specifies the location in degrees of the minimum intensity between the left and right profiles of their data. (This fixed location depends on the experimental set-up and should be known by the user.) After the user has filled in the five text fields, they click on the **Go** button to bring up the main window.

The application has one feature not provided by the applet. It includes a **Print** button in the bottom panel of the main window (Fig. 40). Provided that one of the user's printers can handle PostScript (Adobe Systems, Inc., San Jose, California) output, this button permits the user to print the current image displayed in the plotting portion of the main window. Alternatively, the PostScript image of the plot can be written to a file (to be printed on someone else's PostScript-capable printer).

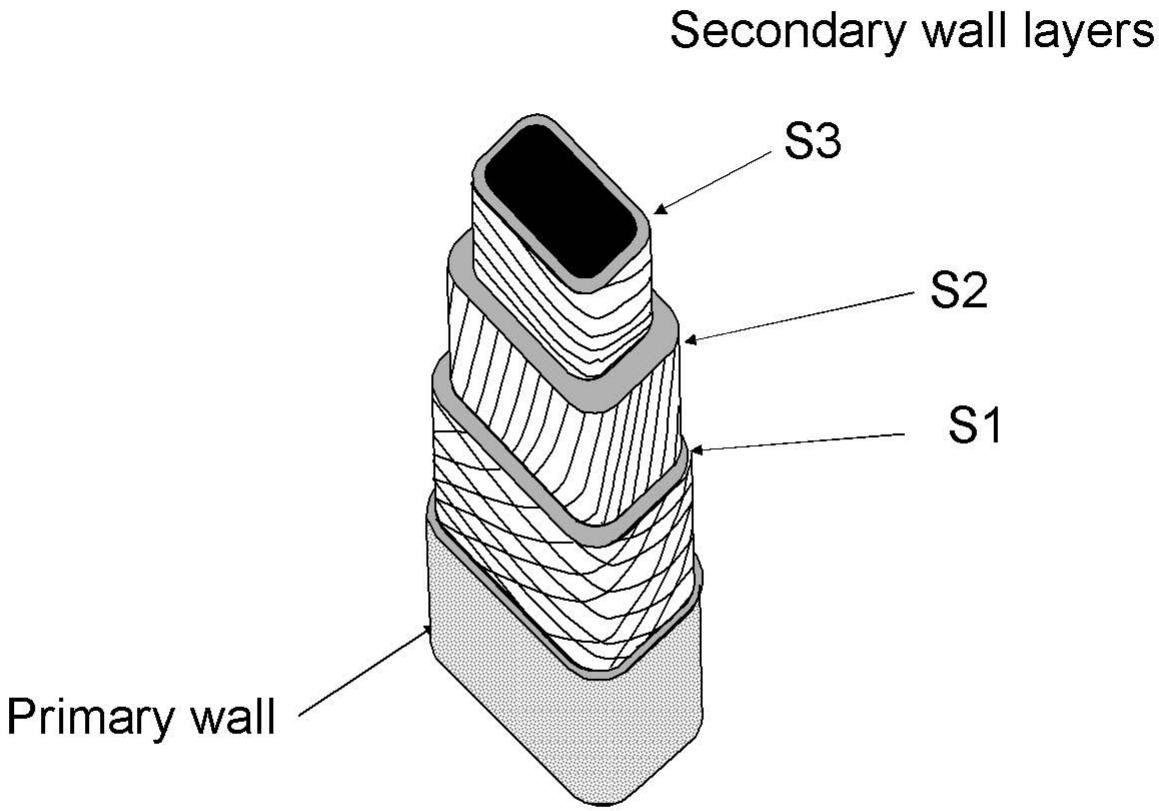

Figure 1: Wood cell structure

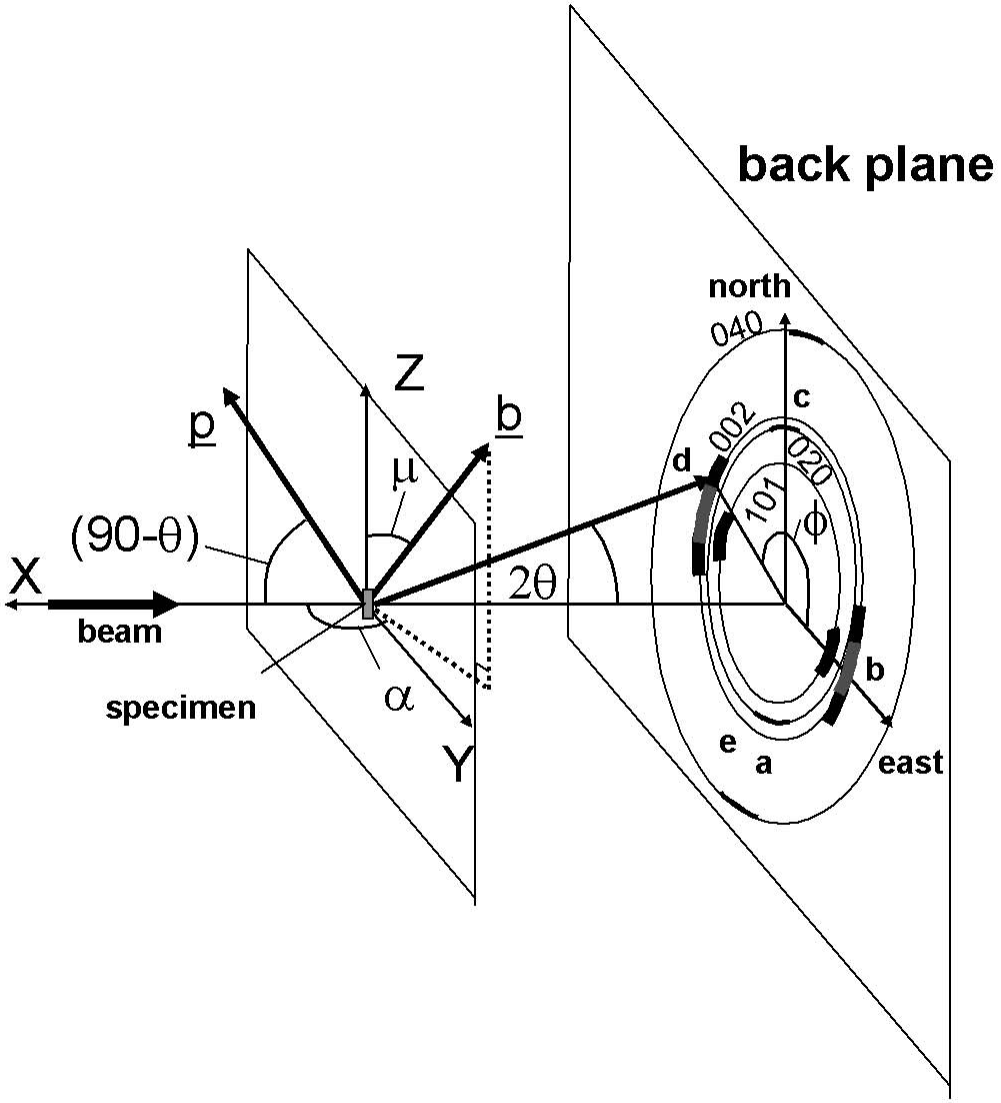

Figure 2: Geometry of the X-ray diffraction

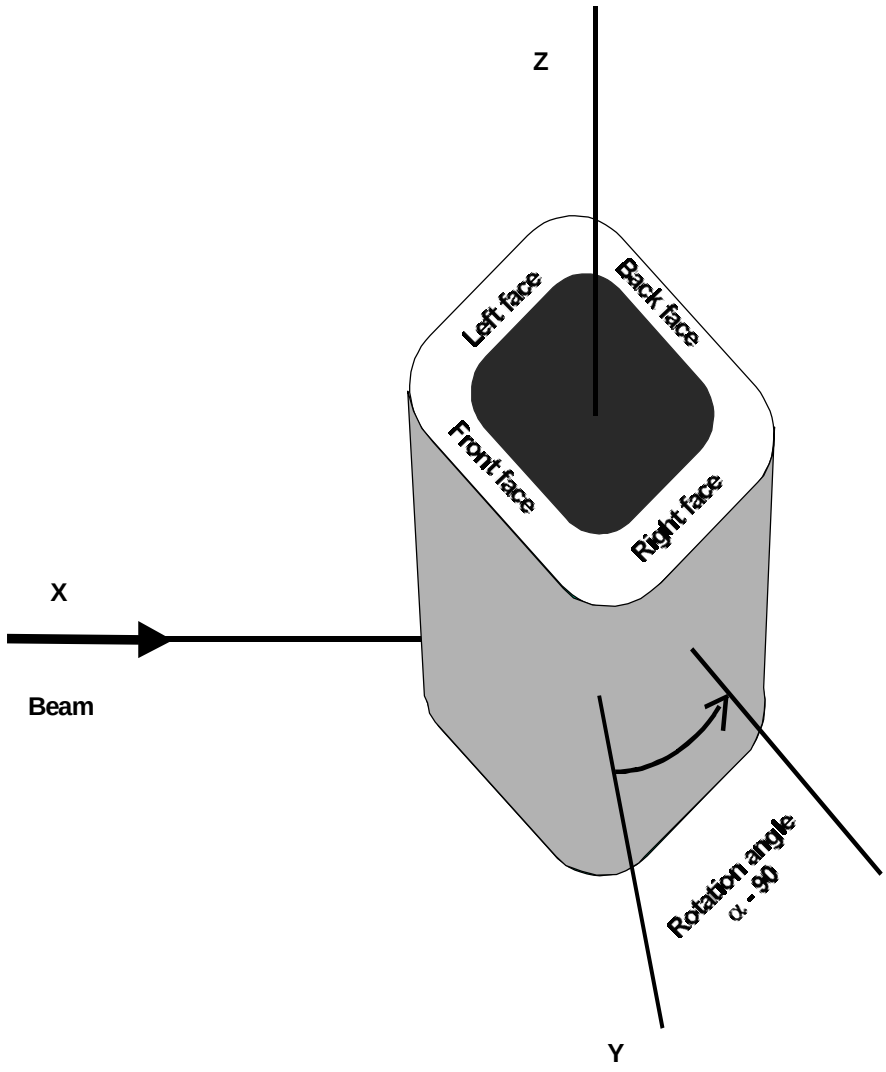

Figure 3: Wood cell rotation

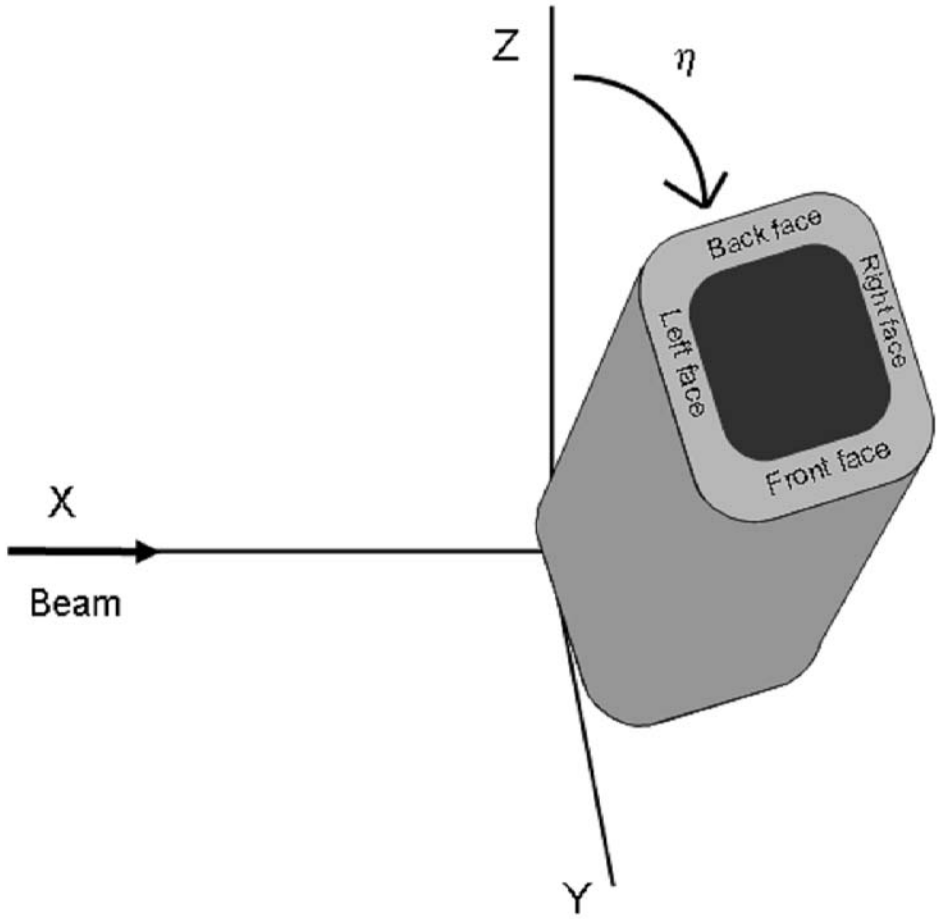

Figure 4: Wood cell tilt

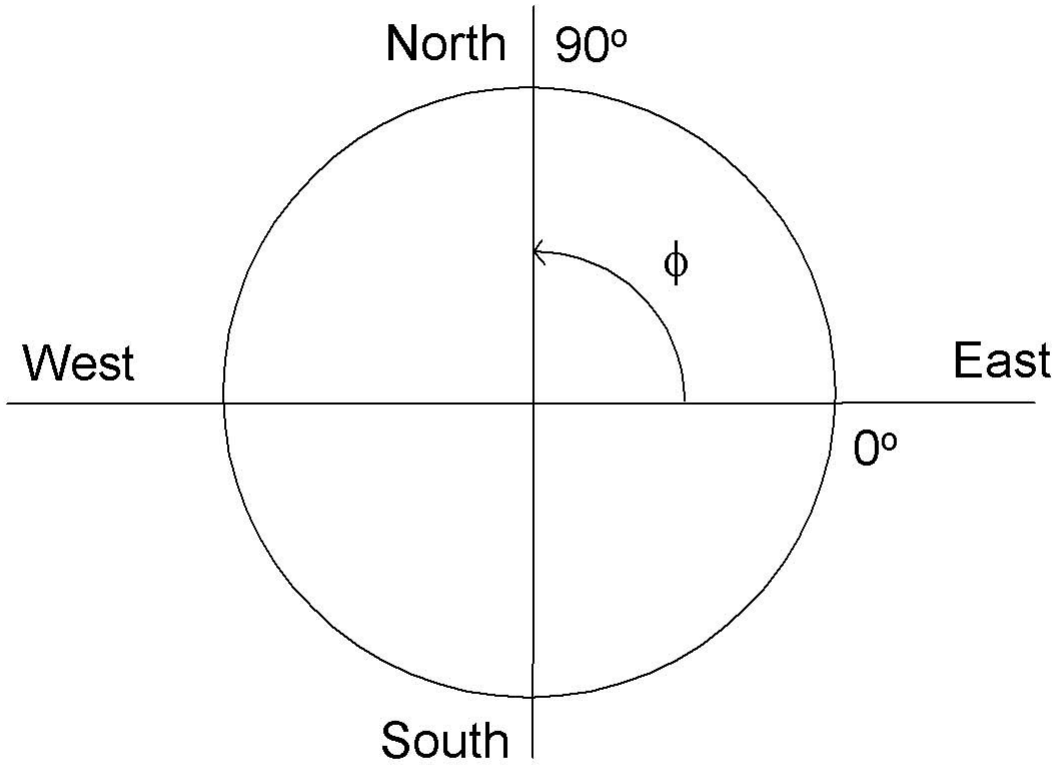

Figure 5: Back plane circle

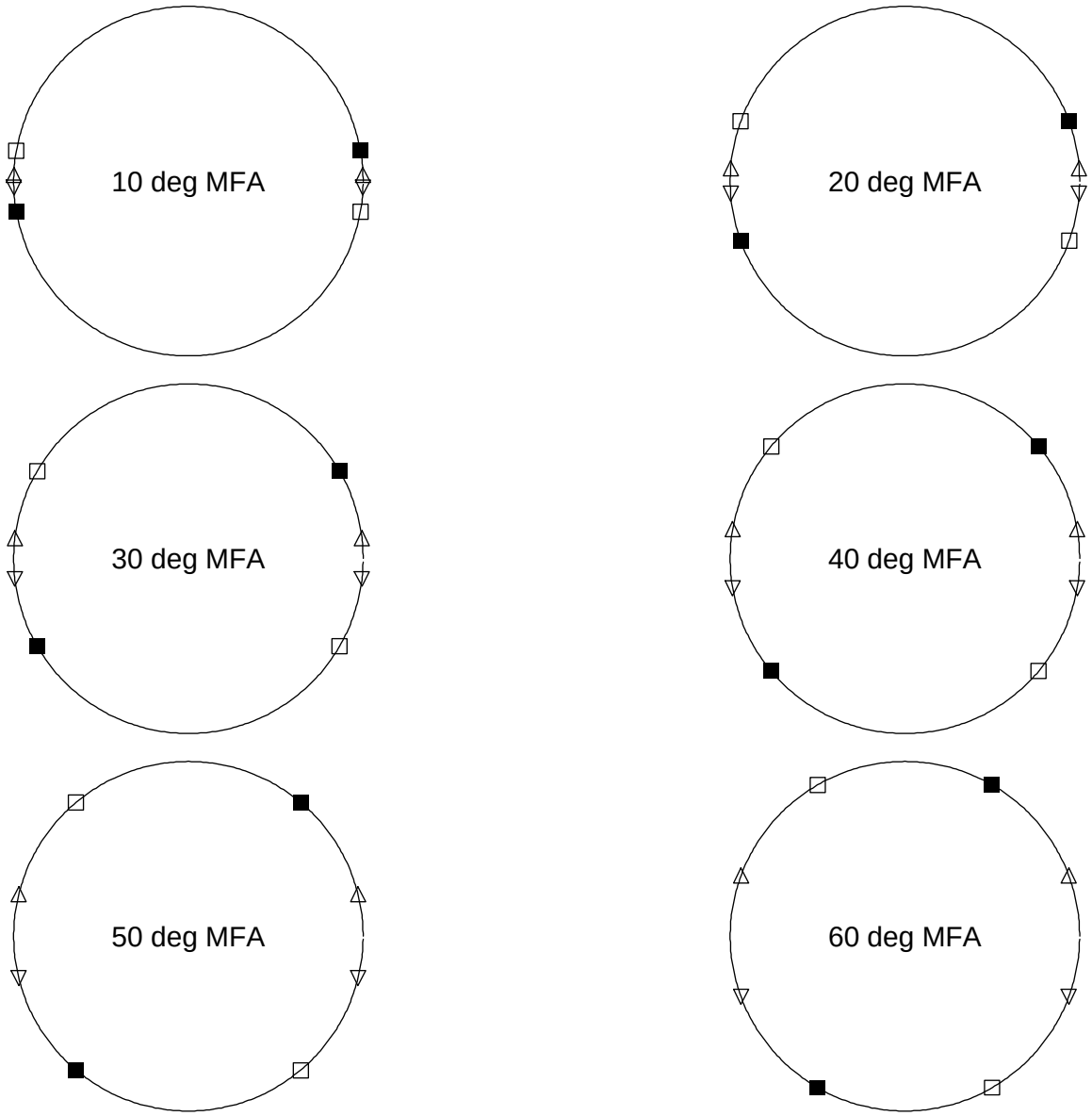

Figure 6: Locations of high intensity X-ray spots on the back plane for a wood cell tilt of 0 degrees and **wood cell rotation = 0 degrees**

□ — spots due to the **front** (before tilt and rotation) face
■ — spots due to the **back** face
△ — spots due to the **right** face
▽ — spots due to the **left** face

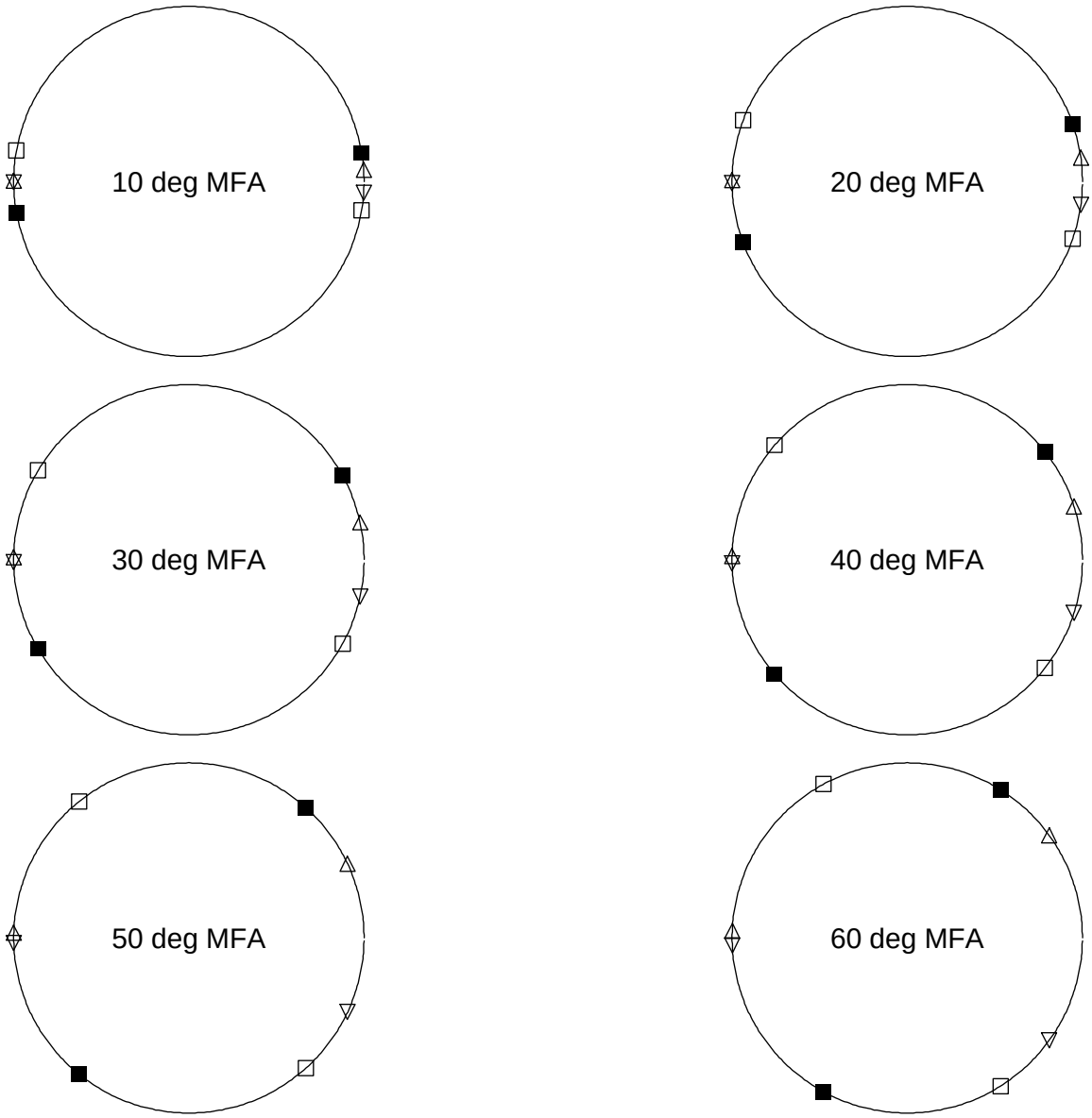

Figure 7: Locations of high intensity X-ray spots on the back plane for a wood cell tilt of 0 degrees and **wood cell rotation = 10 degrees**

□ — spots due to the **front** (before tilt and rotation) face
■ — spots due to the **back** face
△ — spots due to the **right** face
▽ — spots due to the **left** face

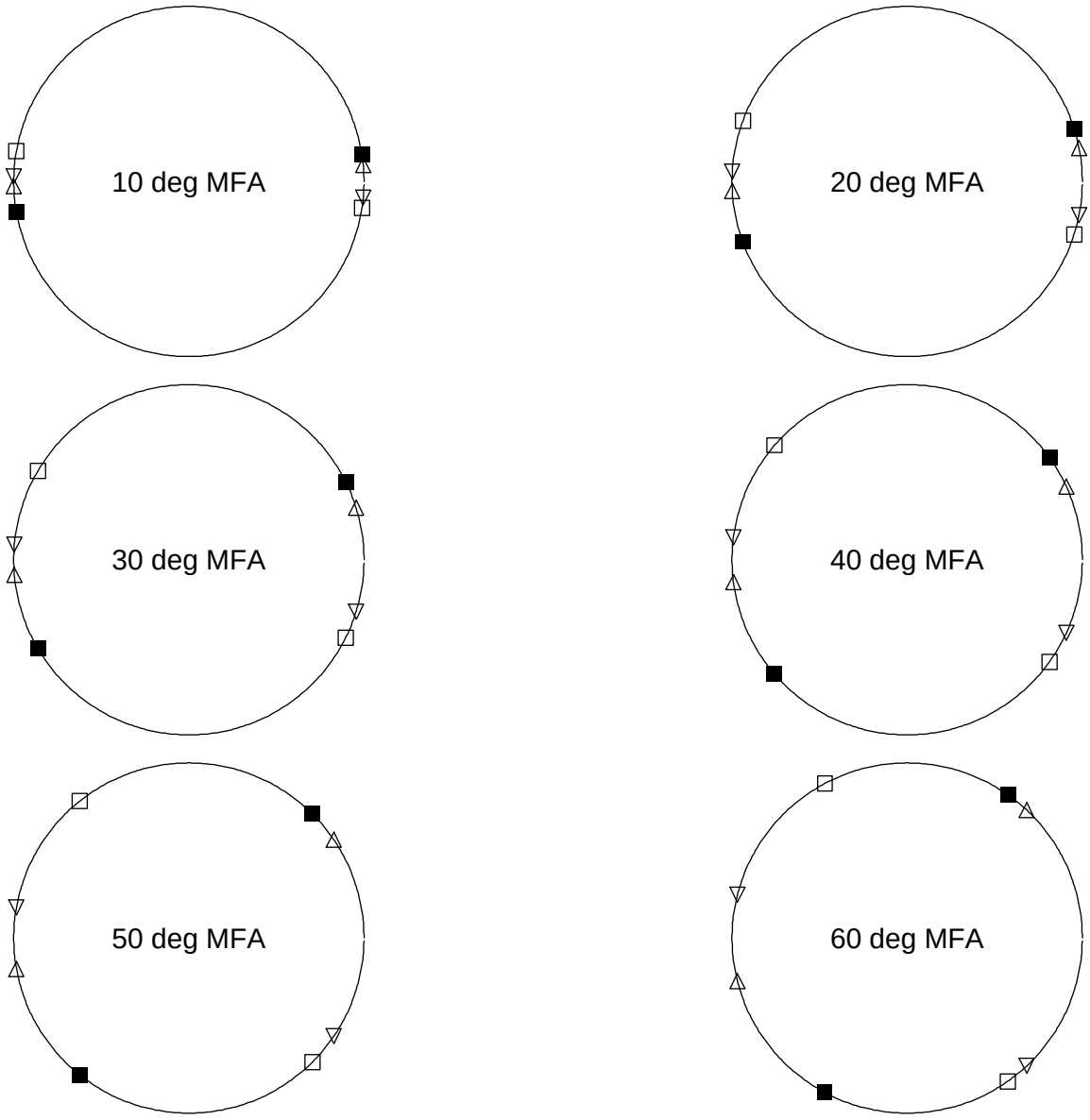

Figure 8: Locations of high intensity X-ray spots on the back plane for a wood cell tilt of 0 degrees and **wood cell rotation = 20 degrees**

□ — spots due to the **front** (before tilt and rotation) face
■ — spots due to the **back** face
△ — spots due to the **right** face
▽ — spots due to the **left** face

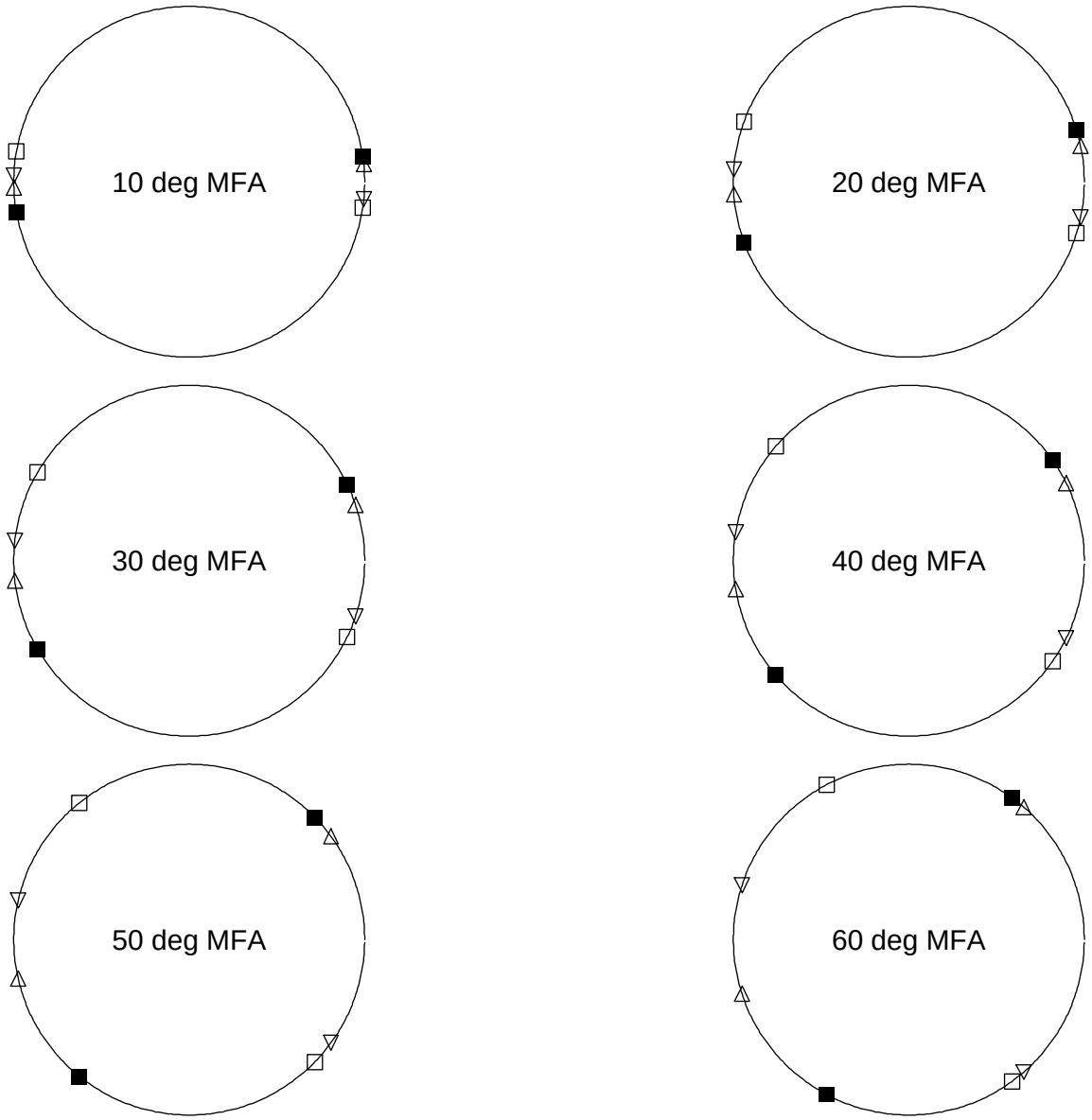

Figure 9: Locations of high intensity X-ray spots on the back plane for a wood cell tilt of 0 degrees and **wood cell rotation = 22.5 degrees**

□ — spots due to the **front** (before tilt and rotation) face
■ — spots due to the **back** face
△ — spots due to the **right** face
▽ — spots due to the **left** face

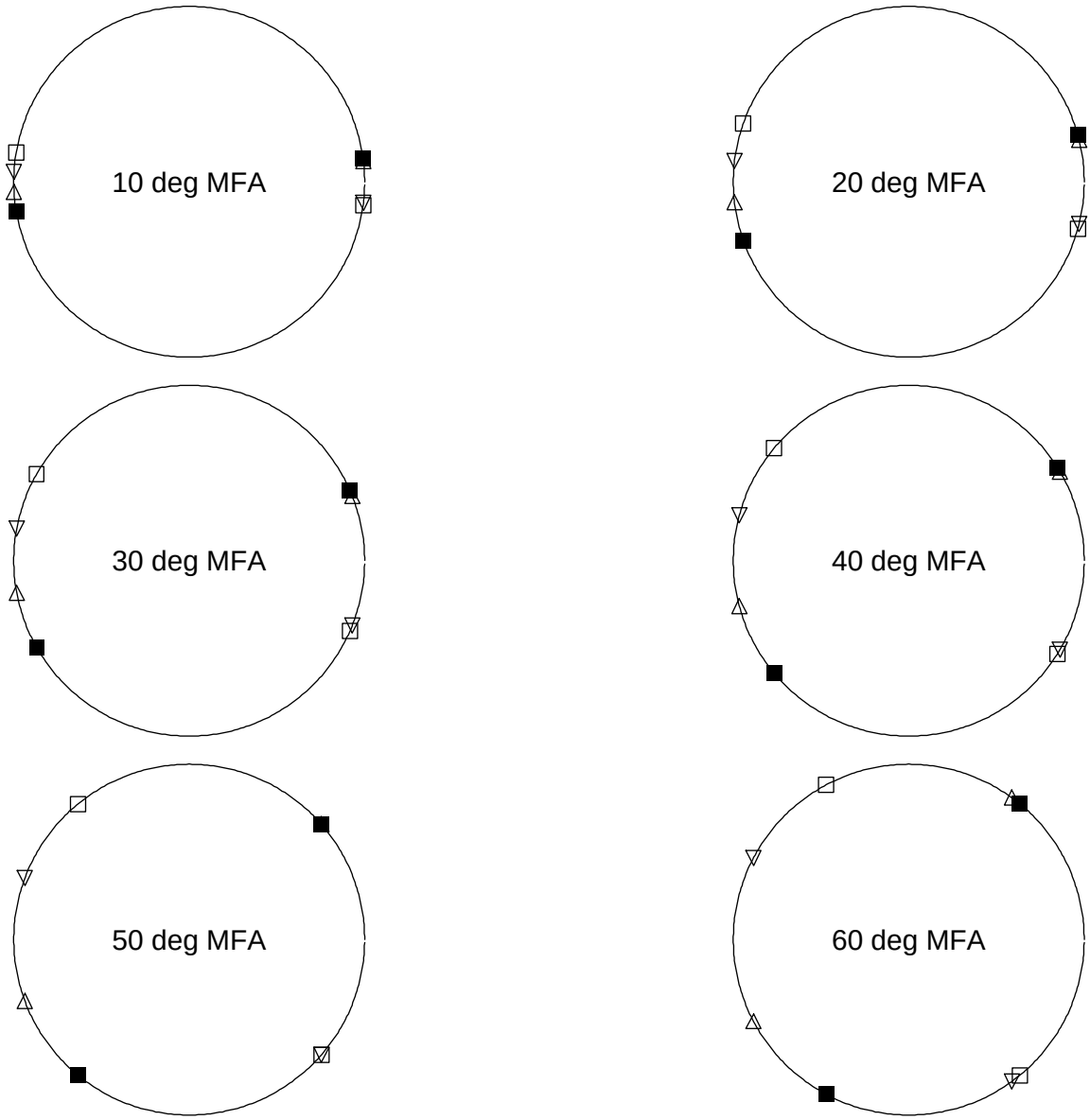

Figure 10: Locations of high intensity X-ray spots on the back plane for a wood cell tilt of 0 degrees and **wood cell rotation = 30 degrees**

□ — spots due to the **front** (before tilt and rotation) face
■ — spots due to the **back** face
△ — spots due to the **right** face
▽ — spots due to the **left** face

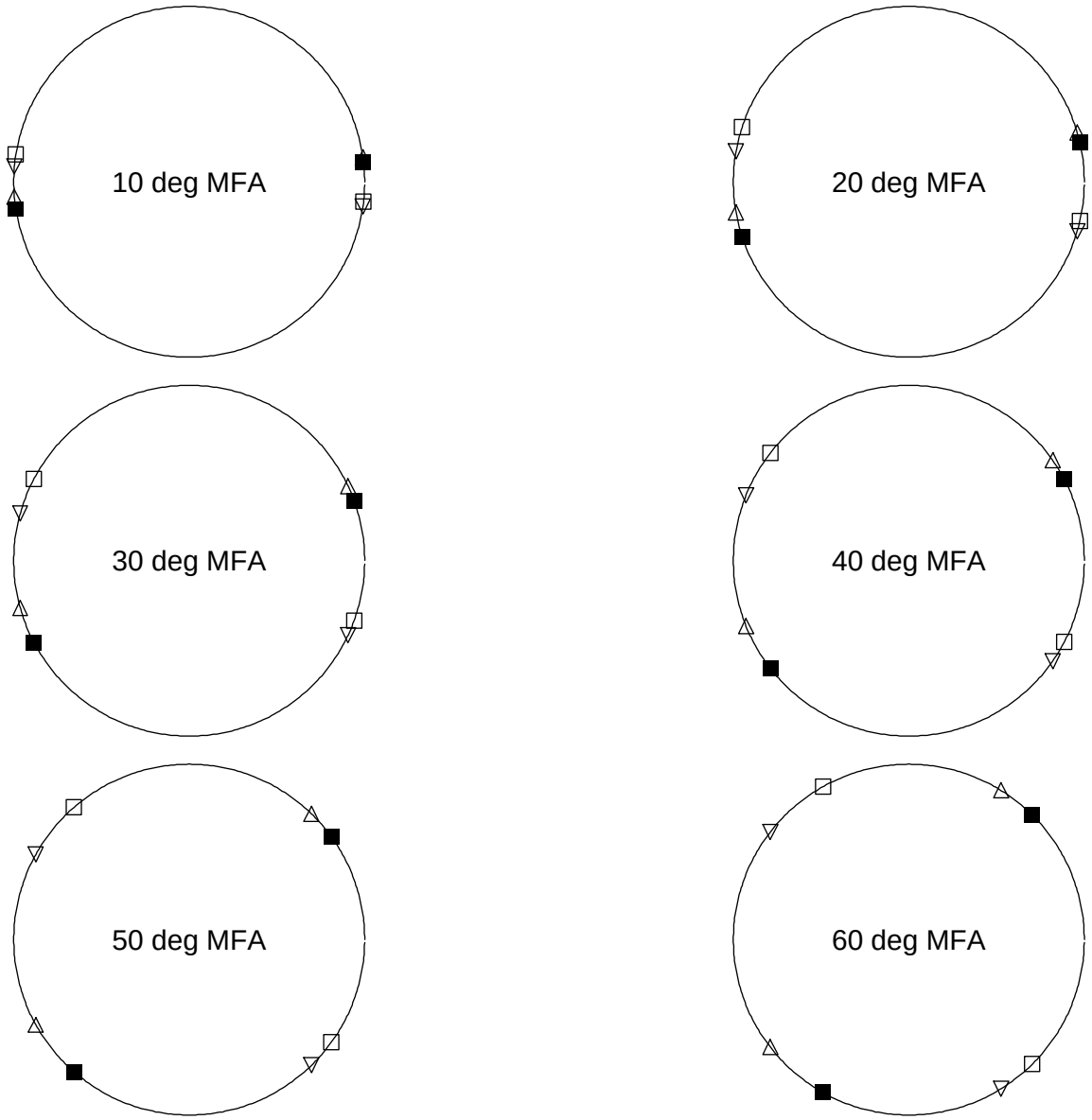

Figure 11: Locations of high intensity X-ray spots on the back plane for a wood cell tilt of 0 degrees and **wood cell rotation = 40 degrees**

□ — spots due to the **front** (before tilt and rotation) face
■ — spots due to the **back** face
△ — spots due to the **right** face
▽ — spots due to the **left** face

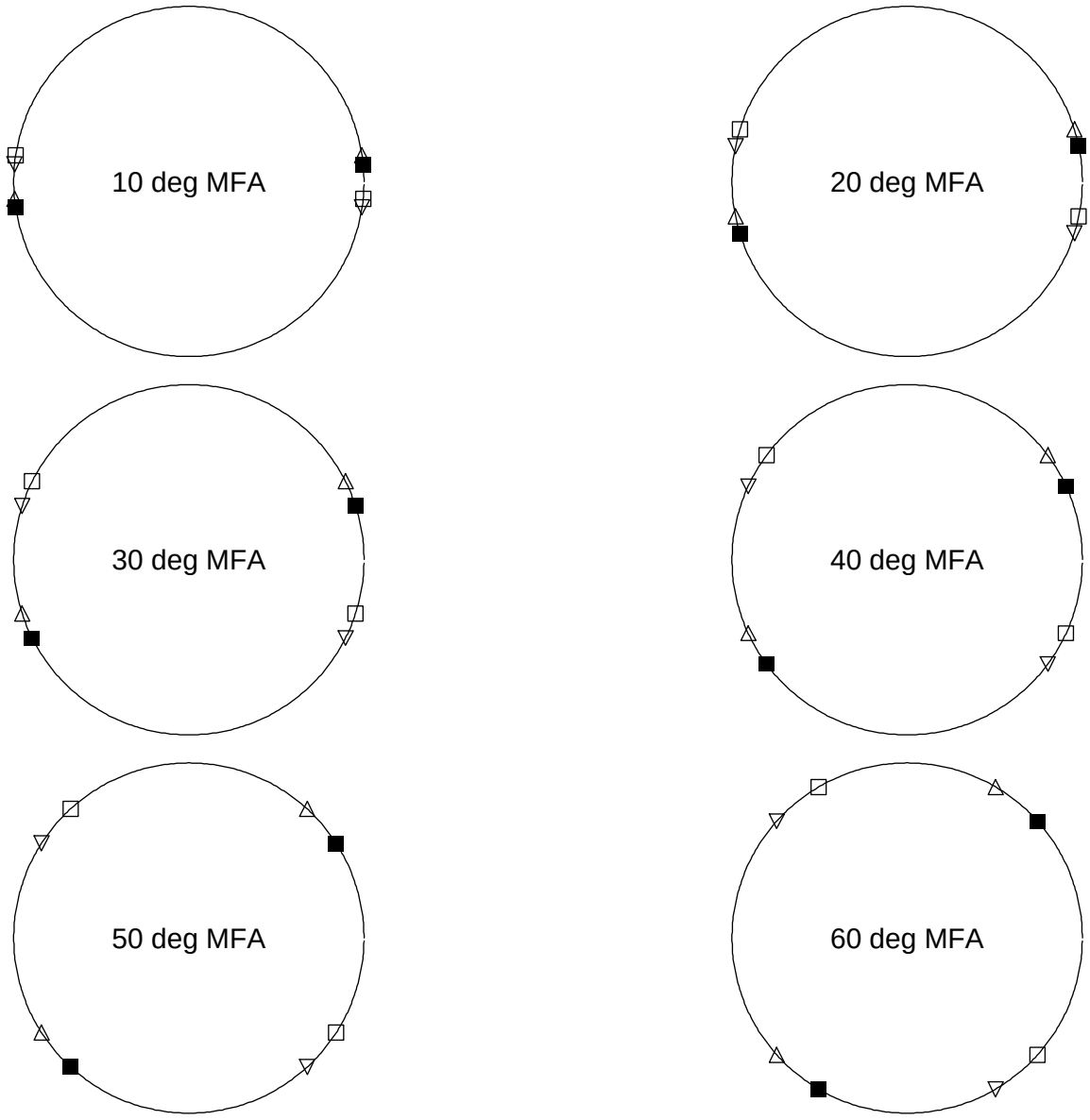

Figure 12: Locations of high intensity X-ray spots on the back plane for a wood cell tilt of 0 degrees and **wood cell rotation = 45 degrees**

□ — spots due to the **front** (before tilt and rotation) face
■ — spots due to the **back** face
△ — spots due to the **right** face
▽ — spots due to the **left** face

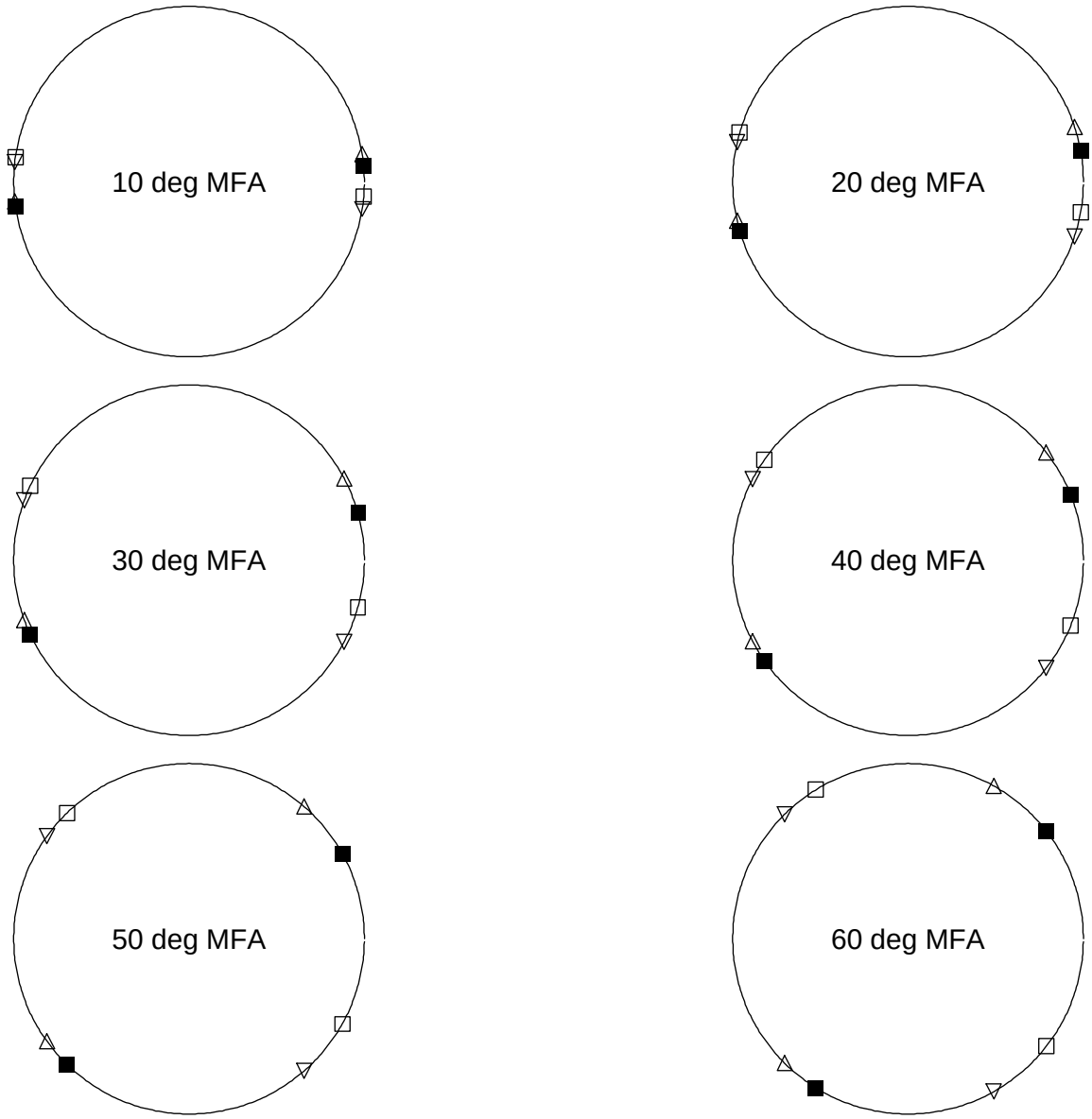

Figure 13: Locations of high intensity X-ray spots on the back plane for a wood cell tilt of 0 degrees and **wood cell rotation = 50 degrees**

□ — spots due to the **front** (before tilt and rotation) face
■ — spots due to the **back** face
△ — spots due to the **right** face
▽ — spots due to the **left** face

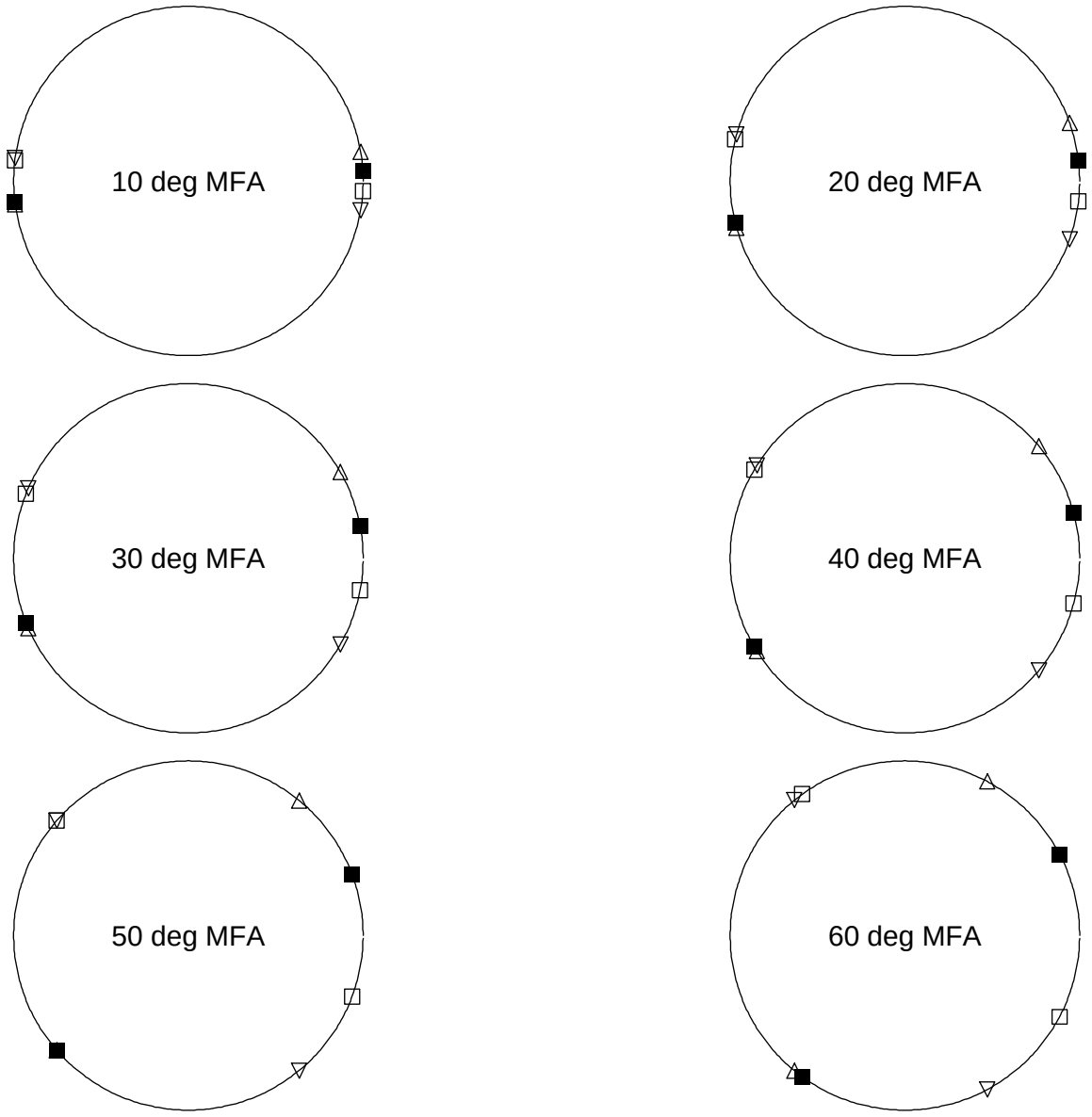

Figure 14: Locations of high intensity X-ray spots on the back plane for a wood cell tilt of 0 degrees and **wood cell rotation = 60 degrees**

□ — spots due to the **front** (before tilt and rotation) face
■ — spots due to the **back** face
△ — spots due to the **right** face
▽ — spots due to the **left** face

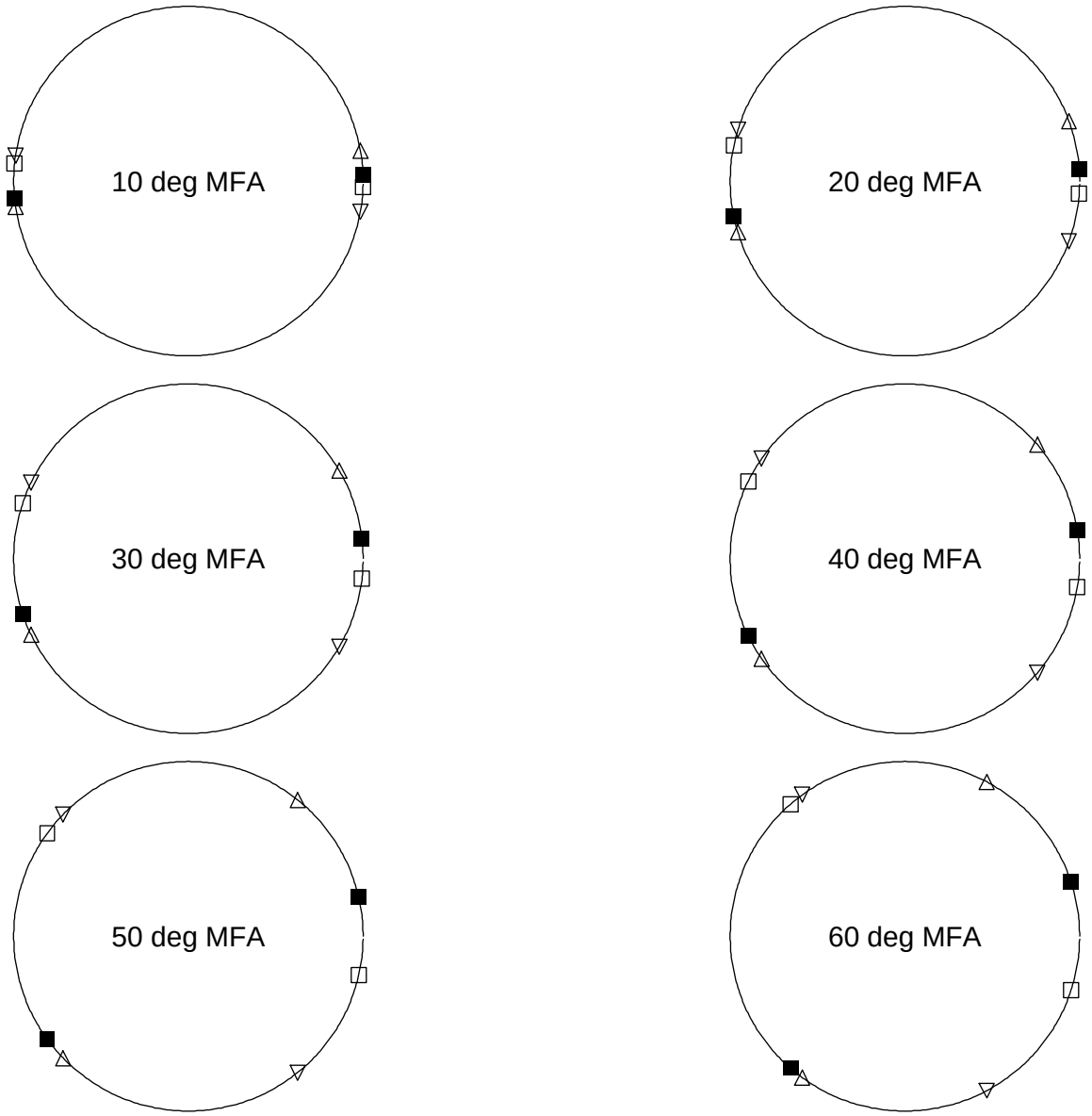

Figure 15: Locations of high intensity X-ray spots on the back plane for a wood cell tilt of 0 degrees and **wood cell rotation = 67.5 degrees**

□ — spots due to the **front** (before tilt and rotation) face
■ — spots due to the **back** face
△ — spots due to the **right** face
▽ — spots due to the **left** face

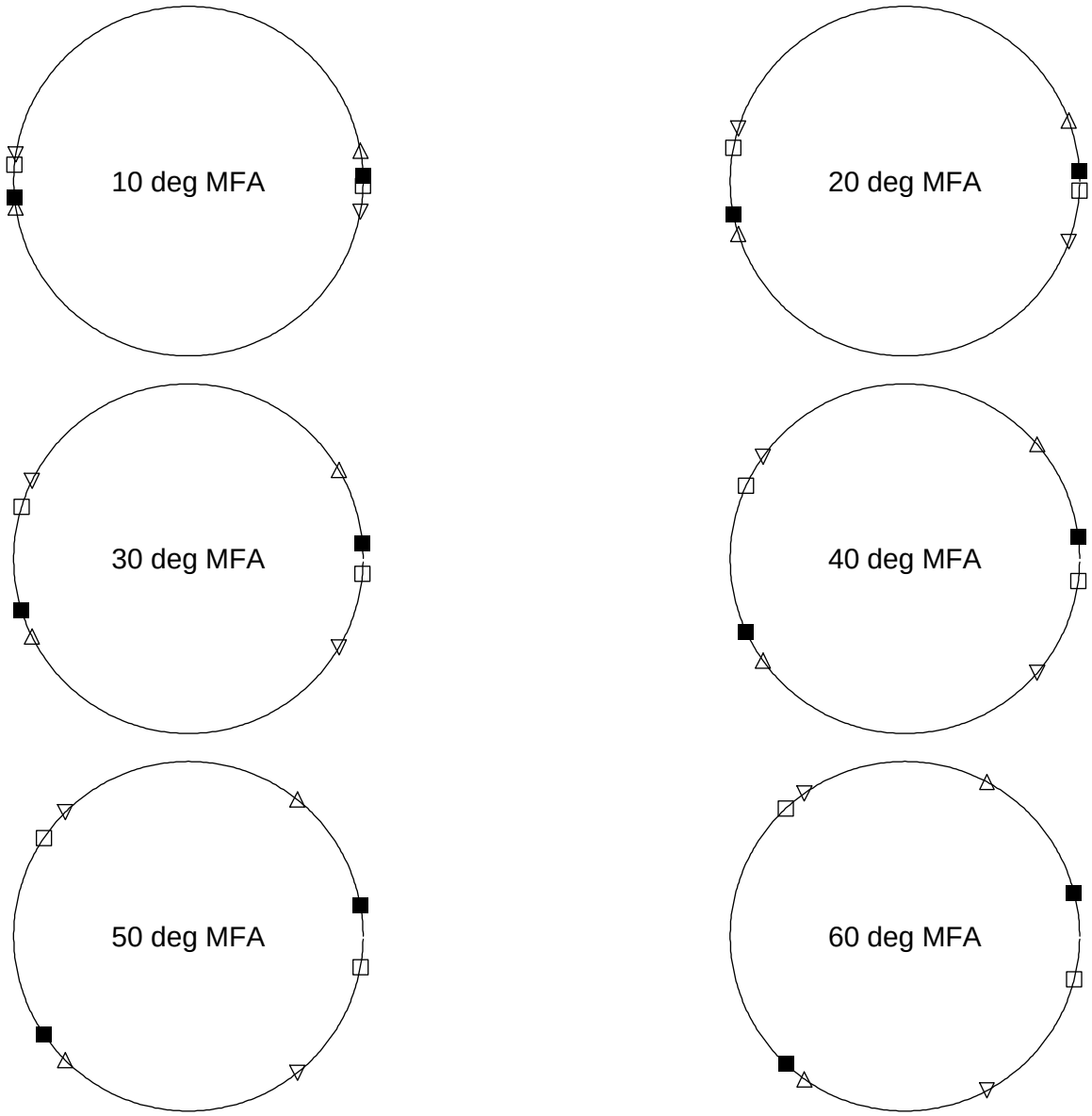

Figure 16: Locations of high intensity X-ray spots on the back plane for a wood cell tilt of 0 degrees and **wood cell rotation = 70 degrees**

□ — spots due to the **front** (before tilt and rotation) face
■ — spots due to the **back** face
△ — spots due to the **right** face
▽ — spots due to the **left** face

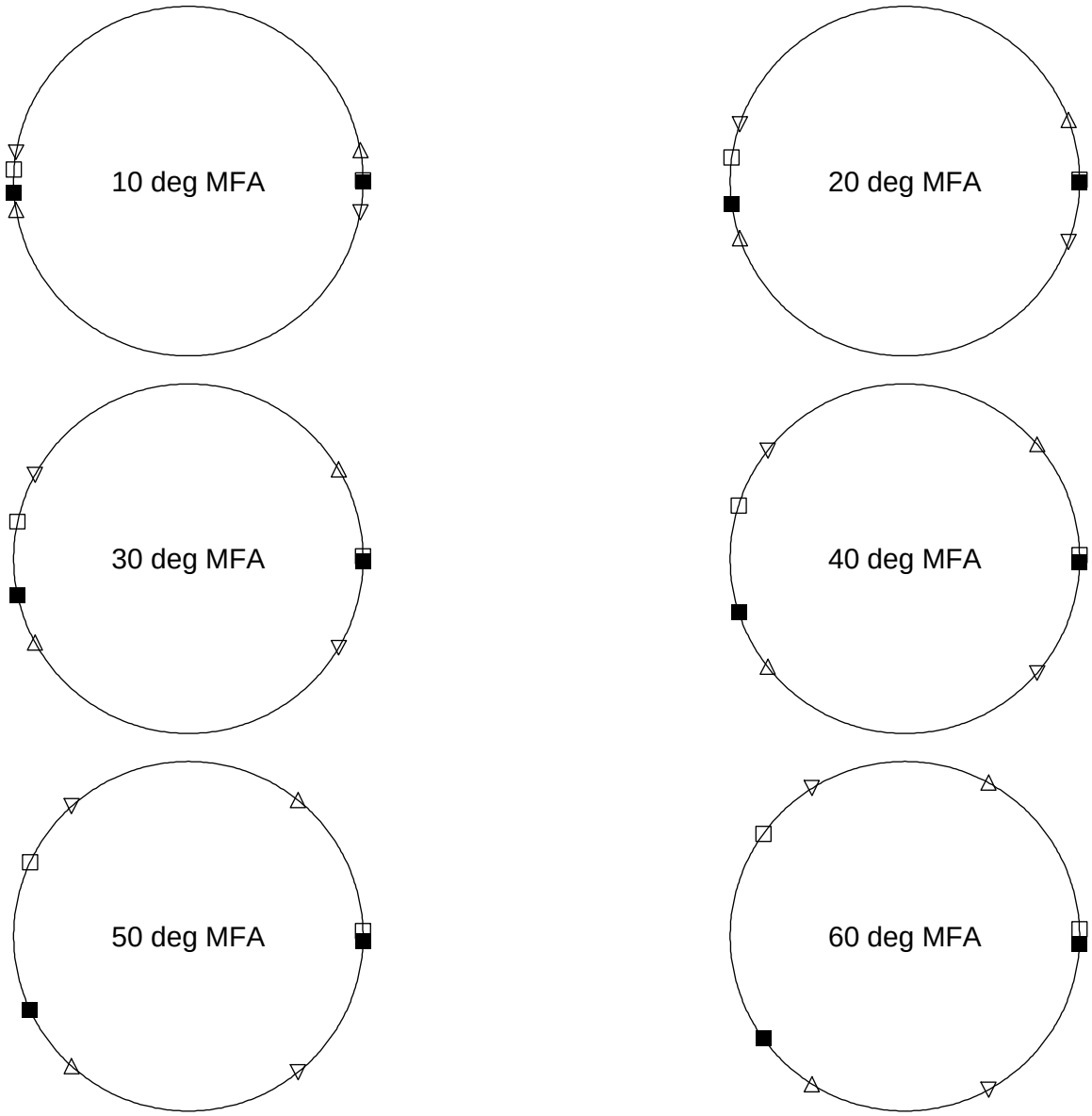

Figure 17: Locations of high intensity X-ray spots on the back plane for a wood cell tilt of 0 degrees and **wood cell rotation = 80 degrees**

□ — spots due to the **front** (before tilt and rotation) face
■ — spots due to the **back** face
△ — spots due to the **right** face
▽ — spots due to the **left** face

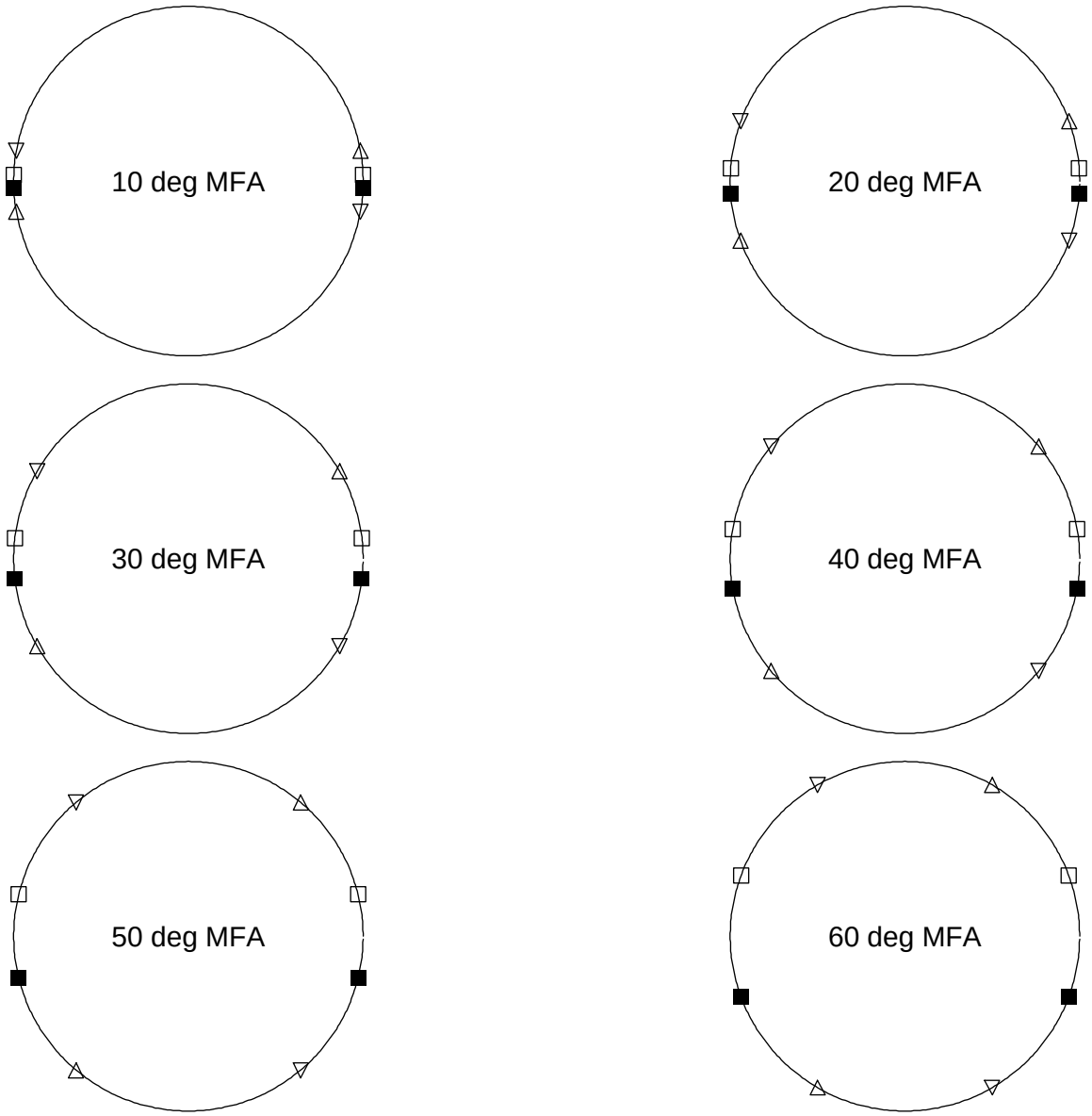

Figure 18: Locations of high intensity X-ray spots on the back plane for a wood cell tilt of 0 degrees and **wood cell rotation = 90 degrees**

□ — spots due to the **front** (before tilt and rotation) face
■ — spots due to the **back** face
△ — spots due to the **right** face
▽ — spots due to the **left** face

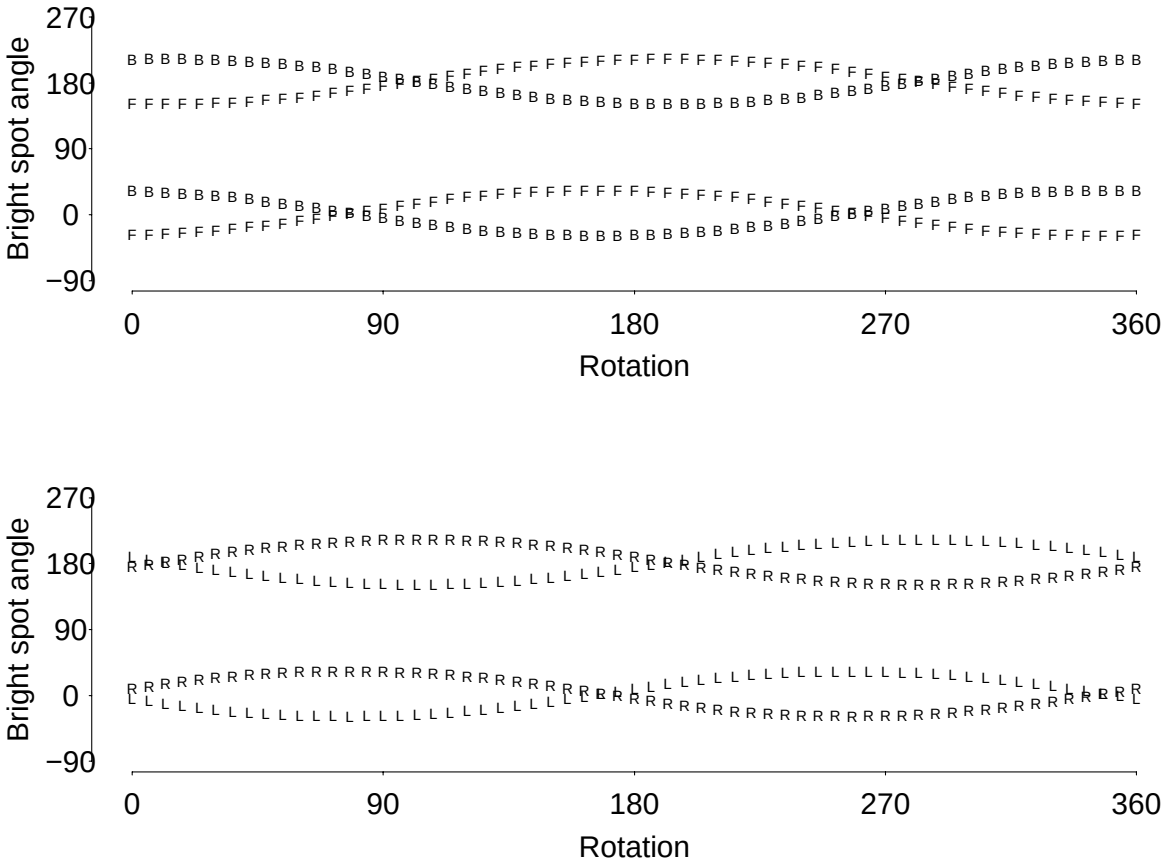

Figure 19: Bright spot angles (counterclockwise from the east in Figure 5) versus cell rotation for an MFA of 30 degrees and a tilt of 0 degrees. F – spot due to the front face, B – spot due to the back face, R – spot due to the right face, L – spot due to the left face.

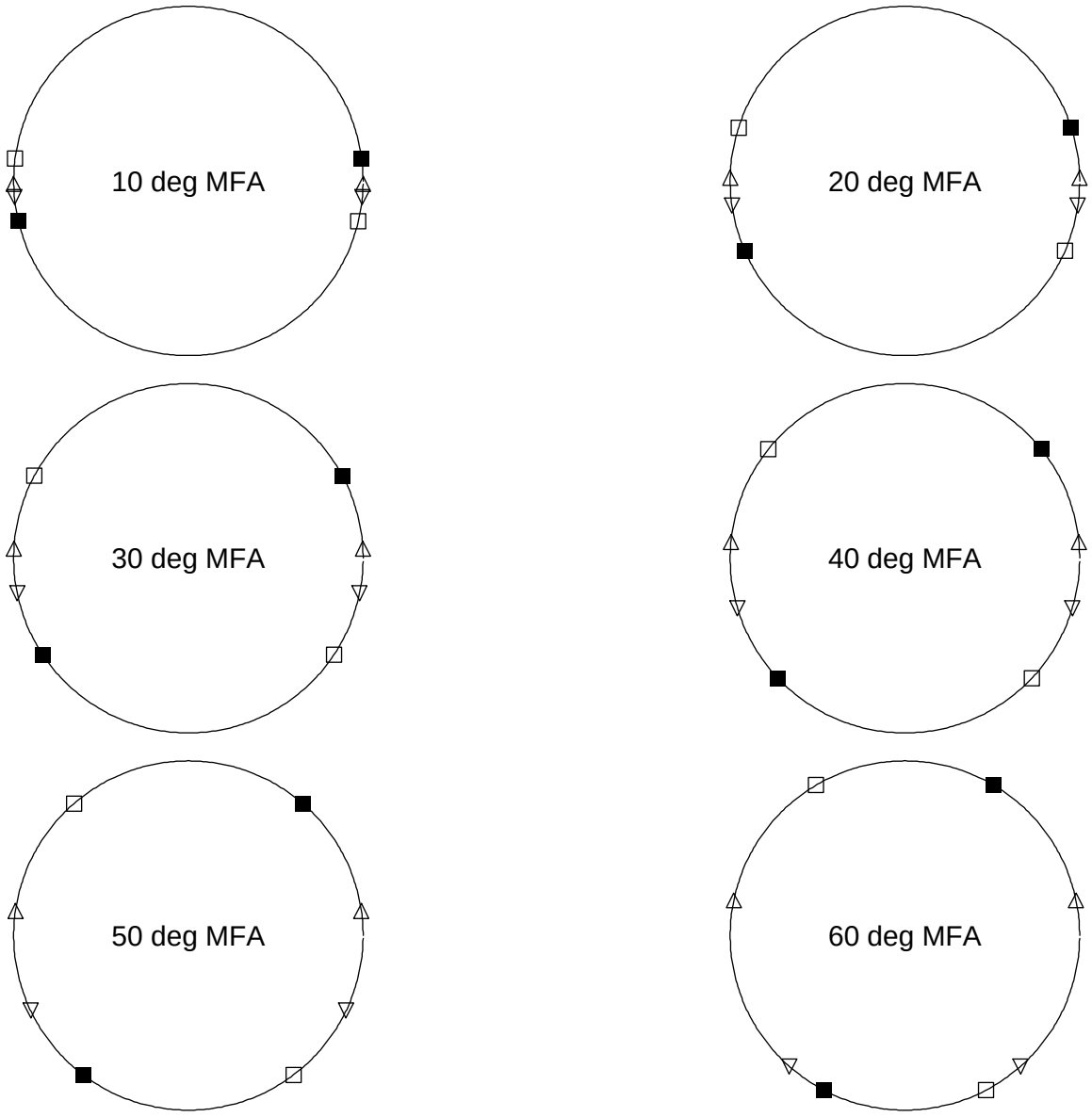

Figure 20: Locations of high intensity X-ray spots on the back plane for a wood cell tilt of 15 degrees and **wood cell rotation = 0 degrees**

□ — spots due to the **front** (before tilt and rotation) face
■ — spots due to the **back** face
△ — spots due to the **right** face
▽ — spots due to the **left** face

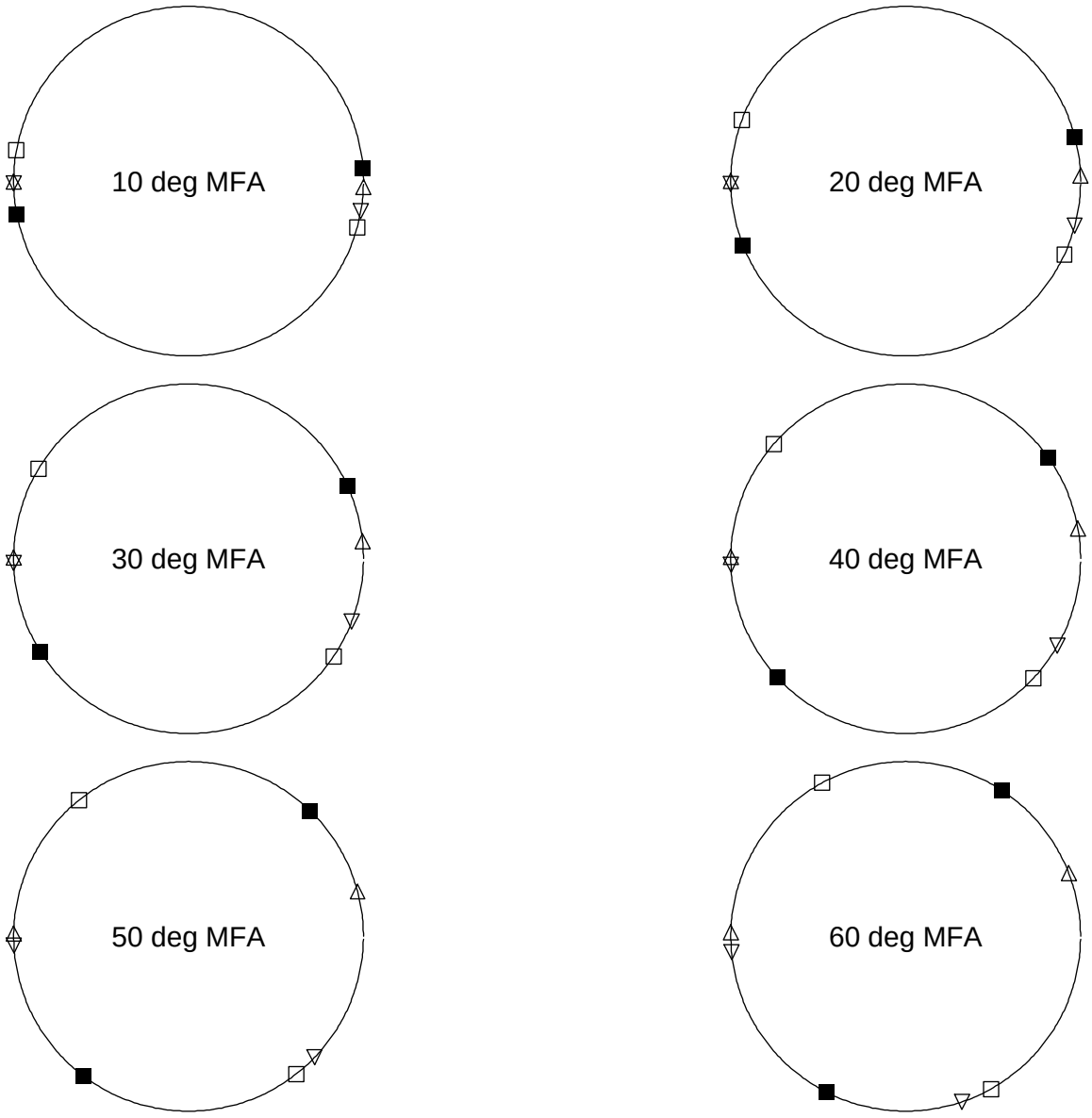

Figure 21: Locations of high intensity X-ray spots on the back plane for a wood cell tilt of 15 degrees and **wood cell rotation = 10 degrees**

□ — spots due to the **front** (before tilt and rotation) face
■ — spots due to the **back** face
△ — spots due to the **right** face
▽ — spots due to the **left** face

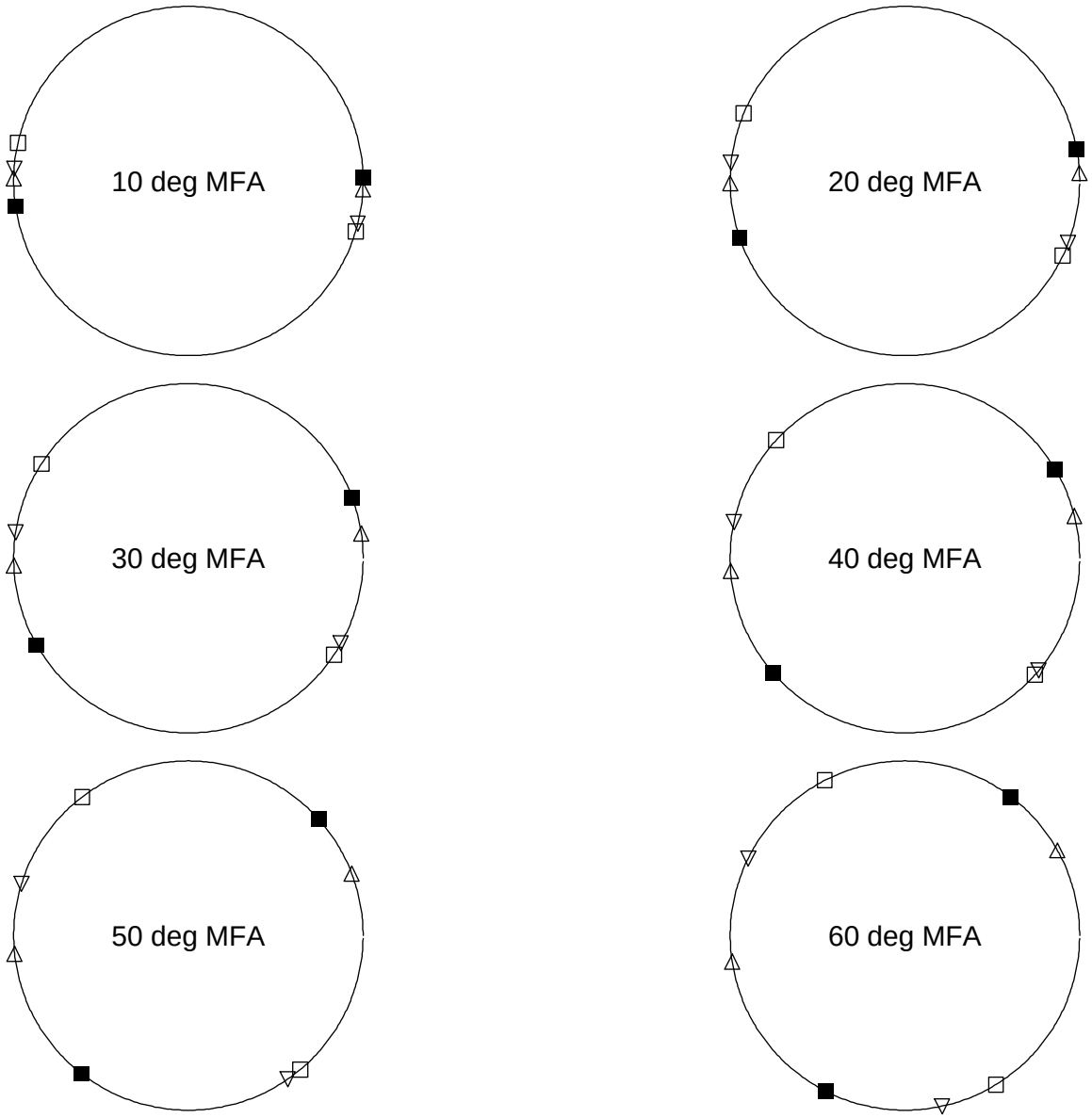

Figure 22: Locations of high intensity X-ray spots on the back plane for a wood cell tilt of 15 degrees and **wood cell rotation = 20 degrees**

□ — spots due to the **front** (before tilt and rotation) face
■ — spots due to the **back** face
△ — spots due to the **right** face
▽ — spots due to the **left** face

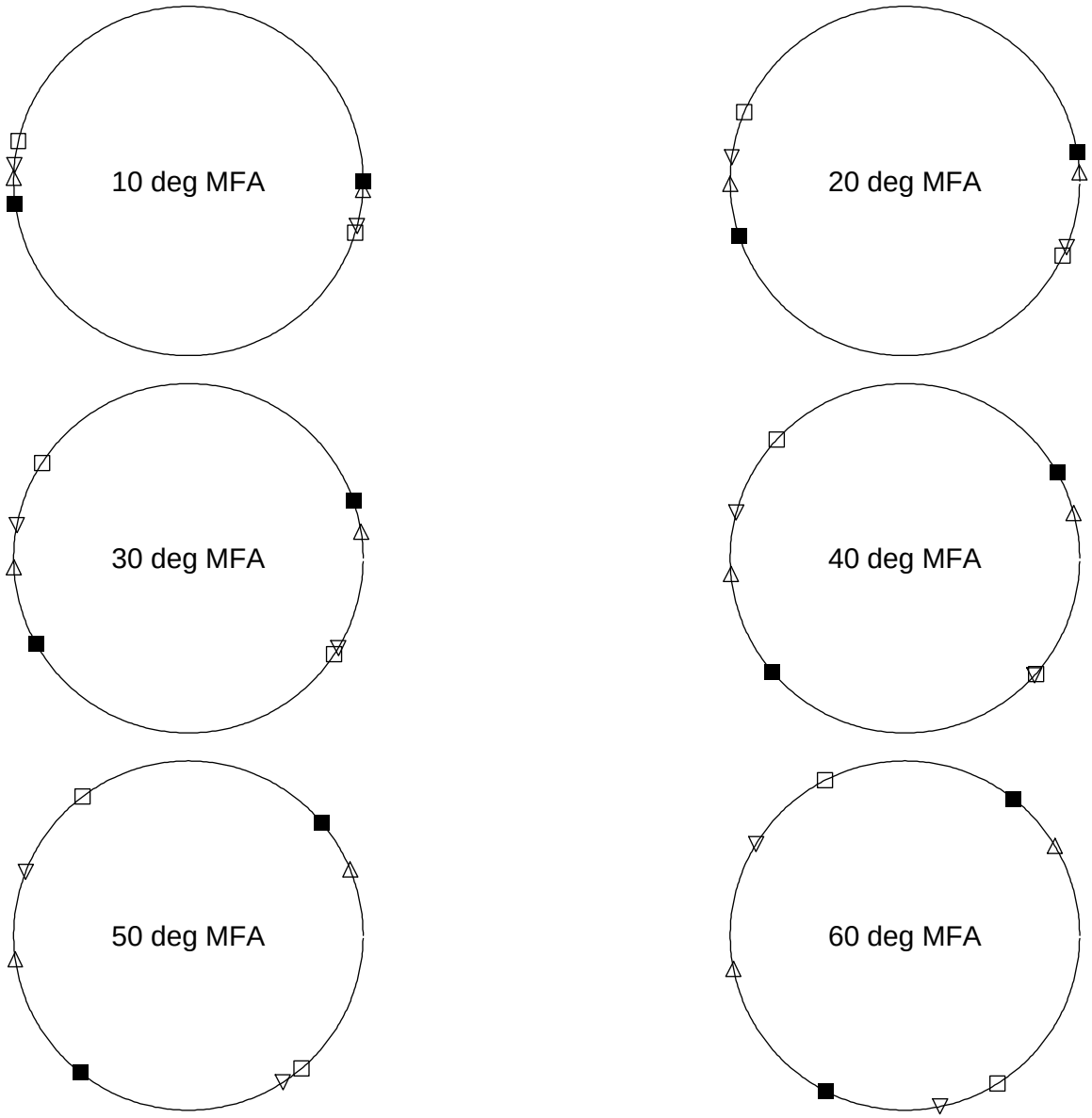

Figure 23: Locations of high intensity X-ray spots on the back plane for a wood cell tilt of 15 degrees and **wood cell rotation = 22.5 degrees**

□ — spots due to the **front** (before tilt and rotation) face
■ — spots due to the **back** face
△ — spots due to the **right** face
▽ — spots due to the **left** face

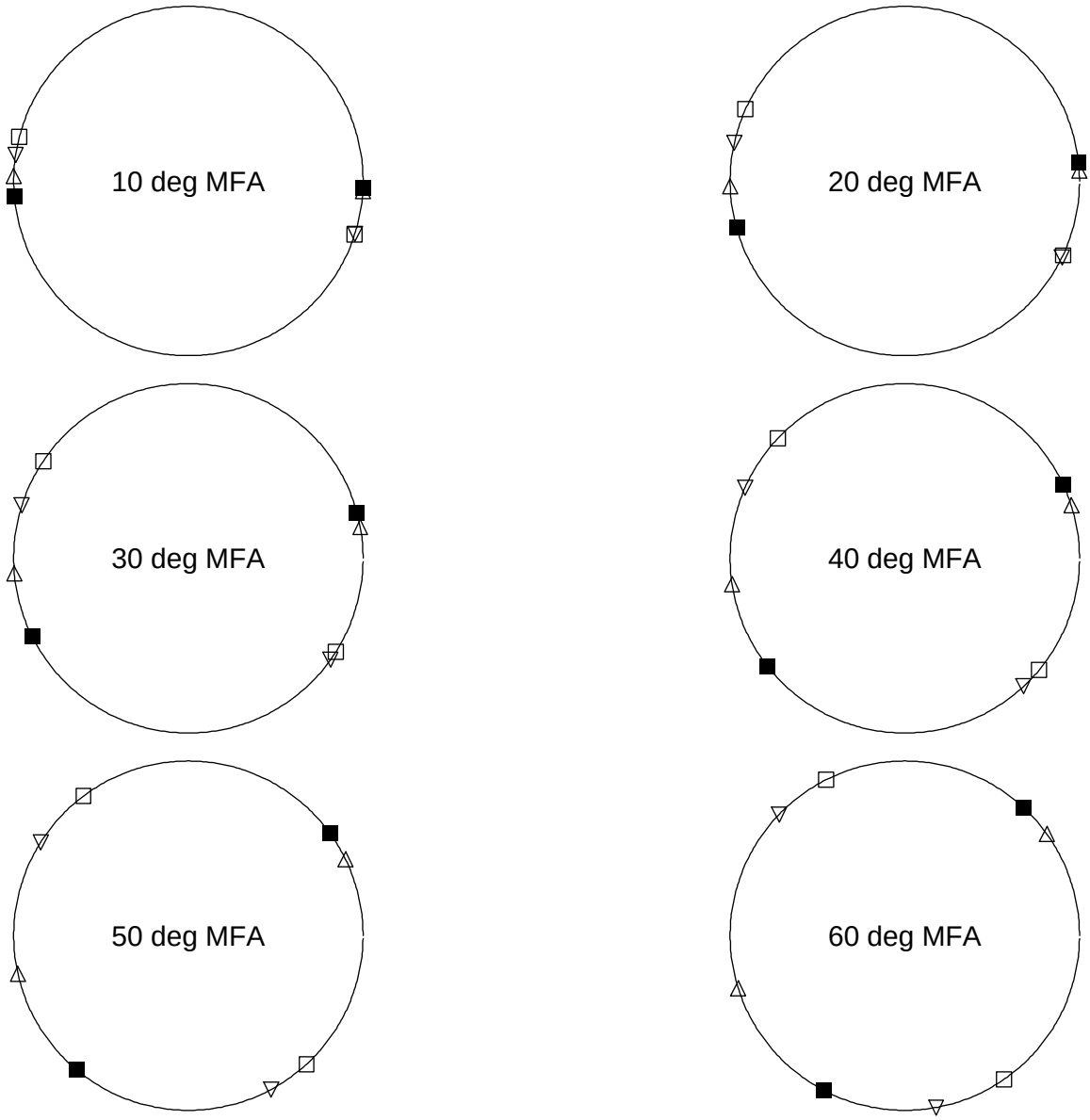

Figure 24: Locations of high intensity X-ray spots on the back plane for a wood cell tilt of 15 degrees and **wood cell rotation = 30 degrees**

□ — spots due to the **front** (before tilt and rotation) face
■ — spots due to the **back** face
△ — spots due to the **right** face
▽ — spots due to the **left** face

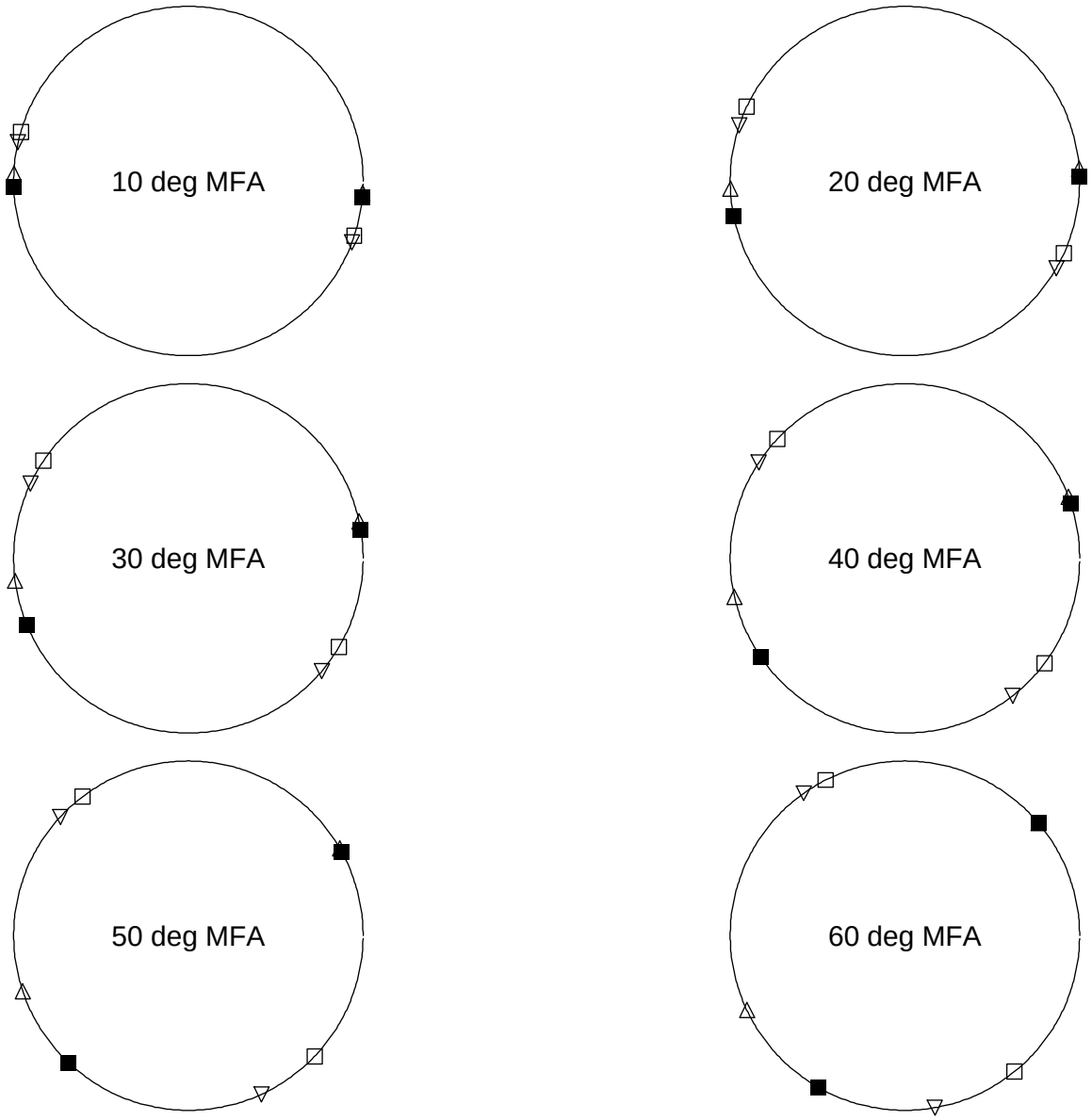

Figure 25: Locations of high intensity X-ray spots on the back plane for a wood cell tilt of 15 degrees and **wood cell rotation = 40 degrees**

□ — spots due to the **front** (before tilt and rotation) face
■ — spots due to the **back** face
△ — spots due to the **right** face
▽ — spots due to the **left** face

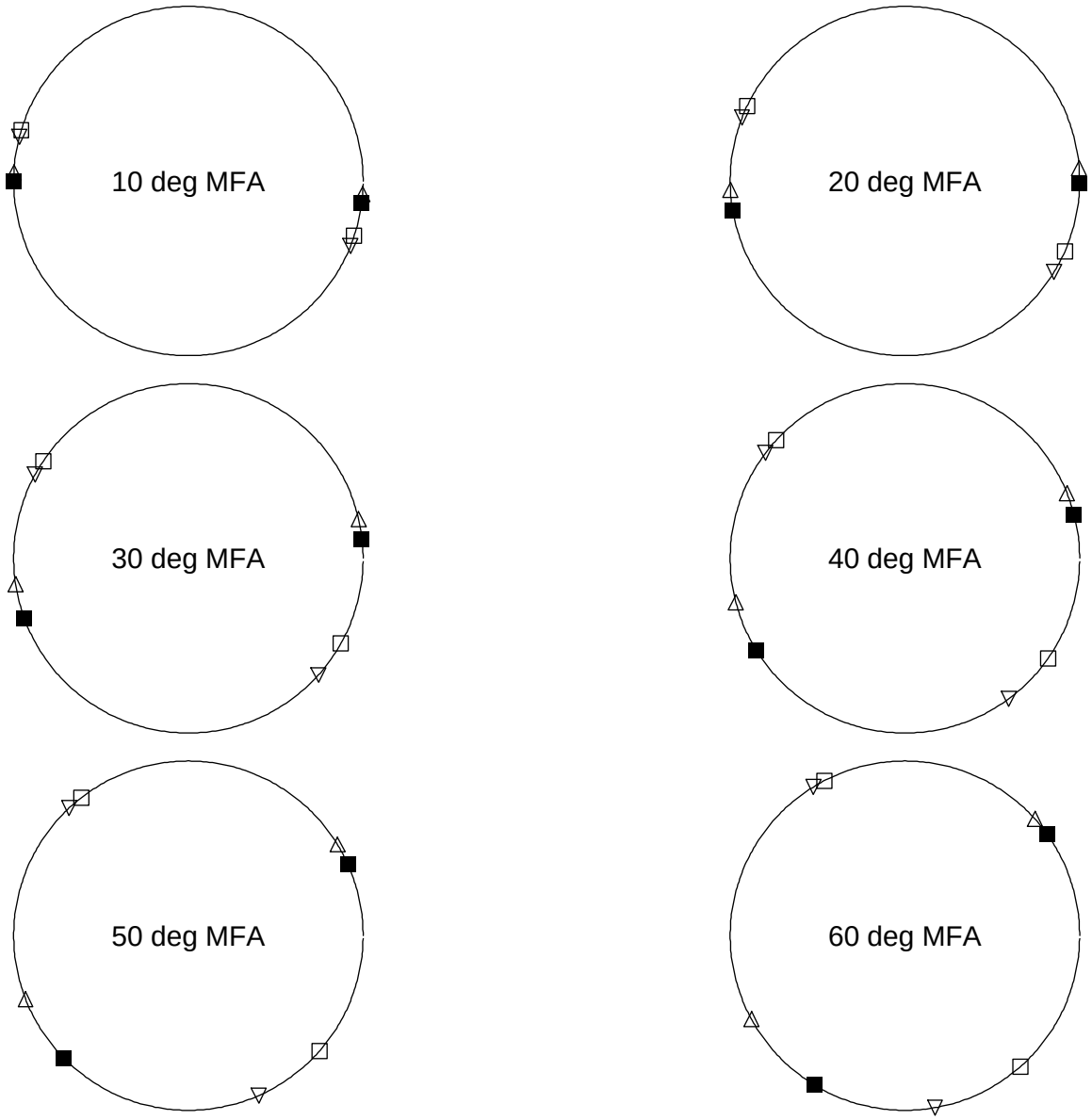

Figure 26: Locations of high intensity X-ray spots on the back plane for a wood cell tilt of 15 degrees and **wood cell rotation = 45 degrees**

□ — spots due to the **front** (before tilt and rotation) face
■ — spots due to the **back** face
△ — spots due to the **right** face
▽ — spots due to the **left** face

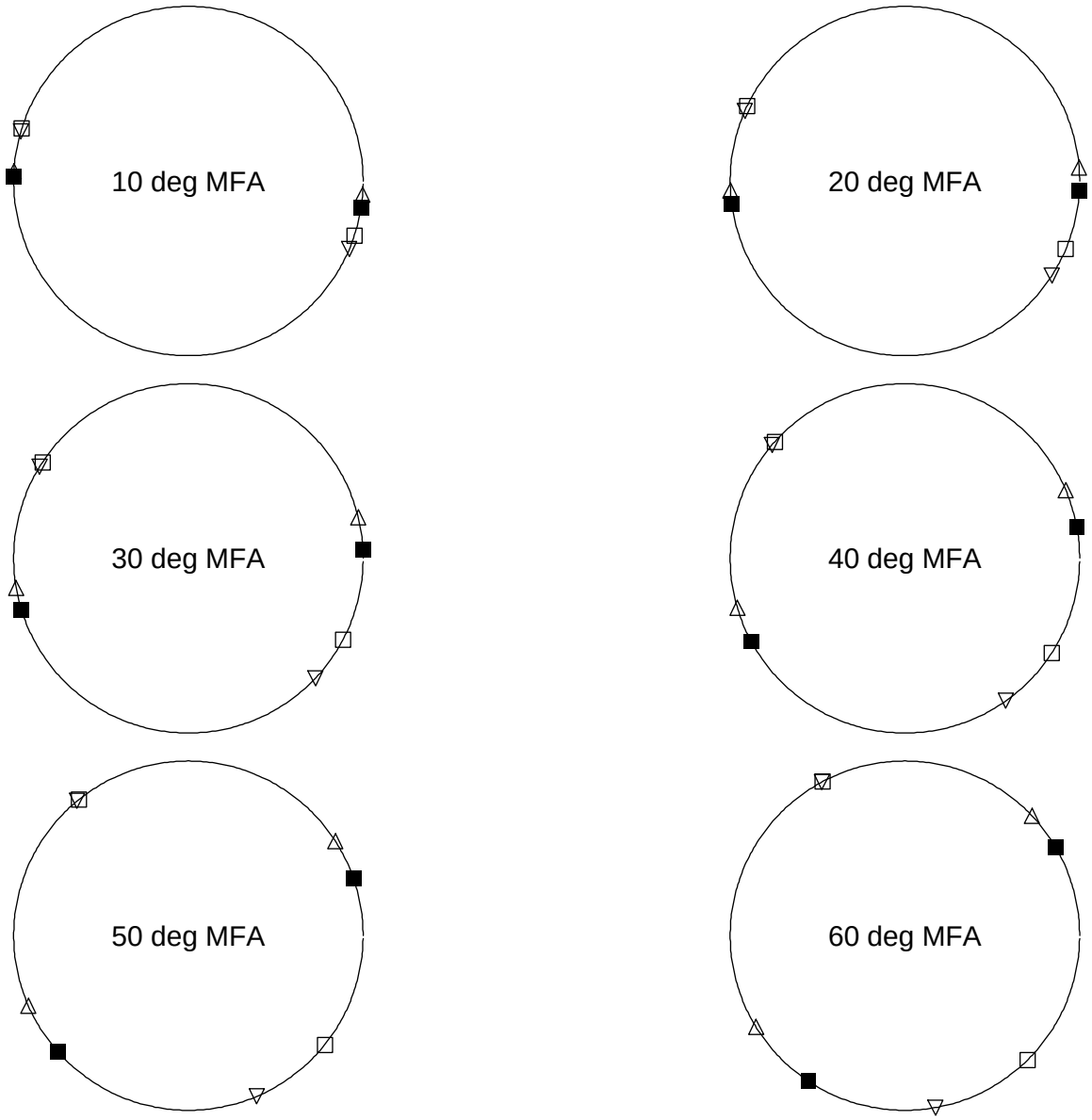

Figure 27: Locations of high intensity X-ray spots on the back plane for a wood cell tilt of 15 degrees and **wood cell rotation = 50 degrees**

□ — spots due to the **front** (before tilt and rotation) face
■ — spots due to the **back** face
△ — spots due to the **right** face
▽ — spots due to the **left** face

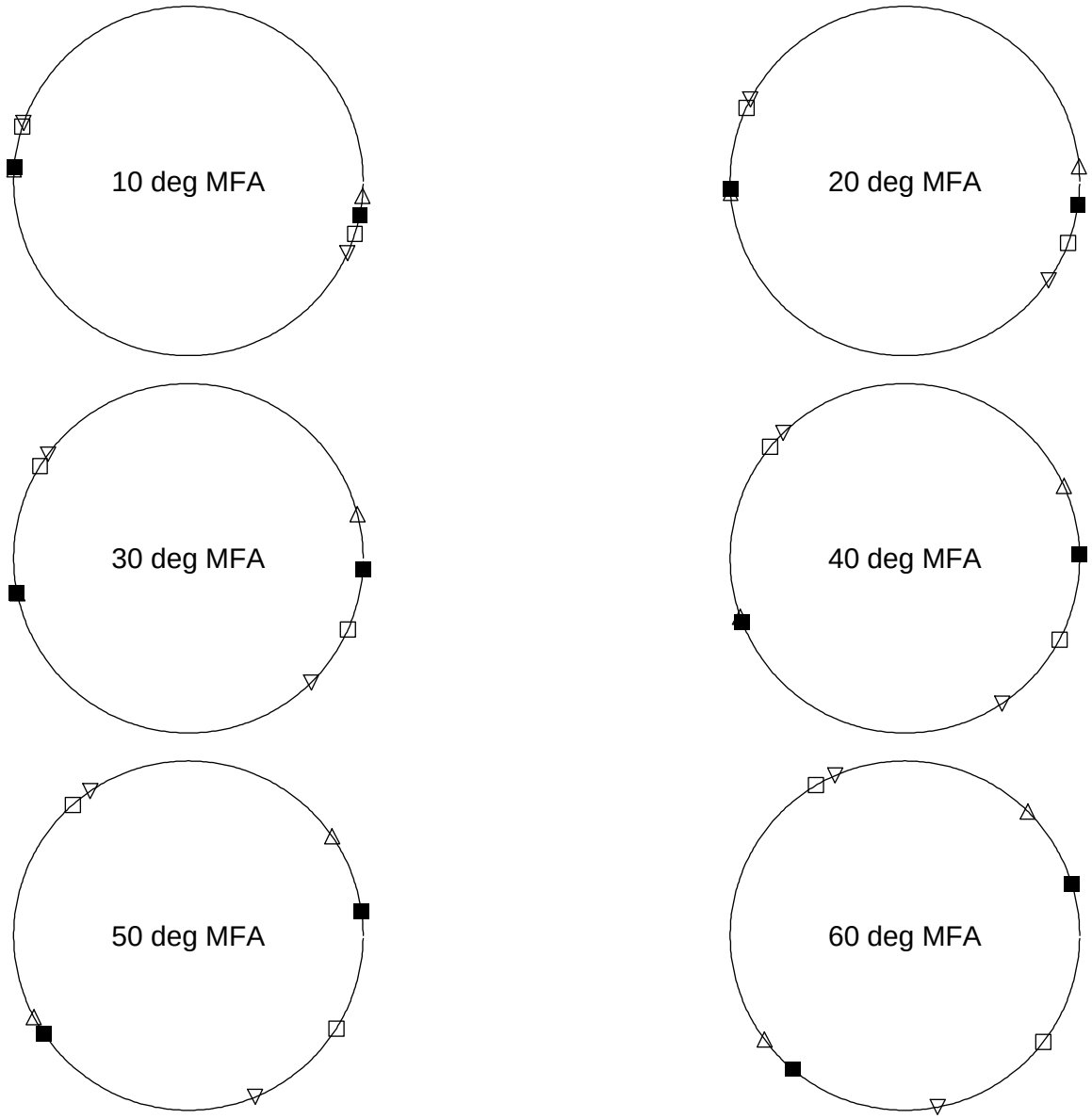

Figure 28: Locations of high intensity X-ray spots on the back plane for a wood cell tilt of 15 degrees and **wood cell rotation = 60 degrees**

□ — spots due to the **front** (before tilt and rotation) face
■ — spots due to the **back** face
△ — spots due to the **right** face
▽ — spots due to the **left** face

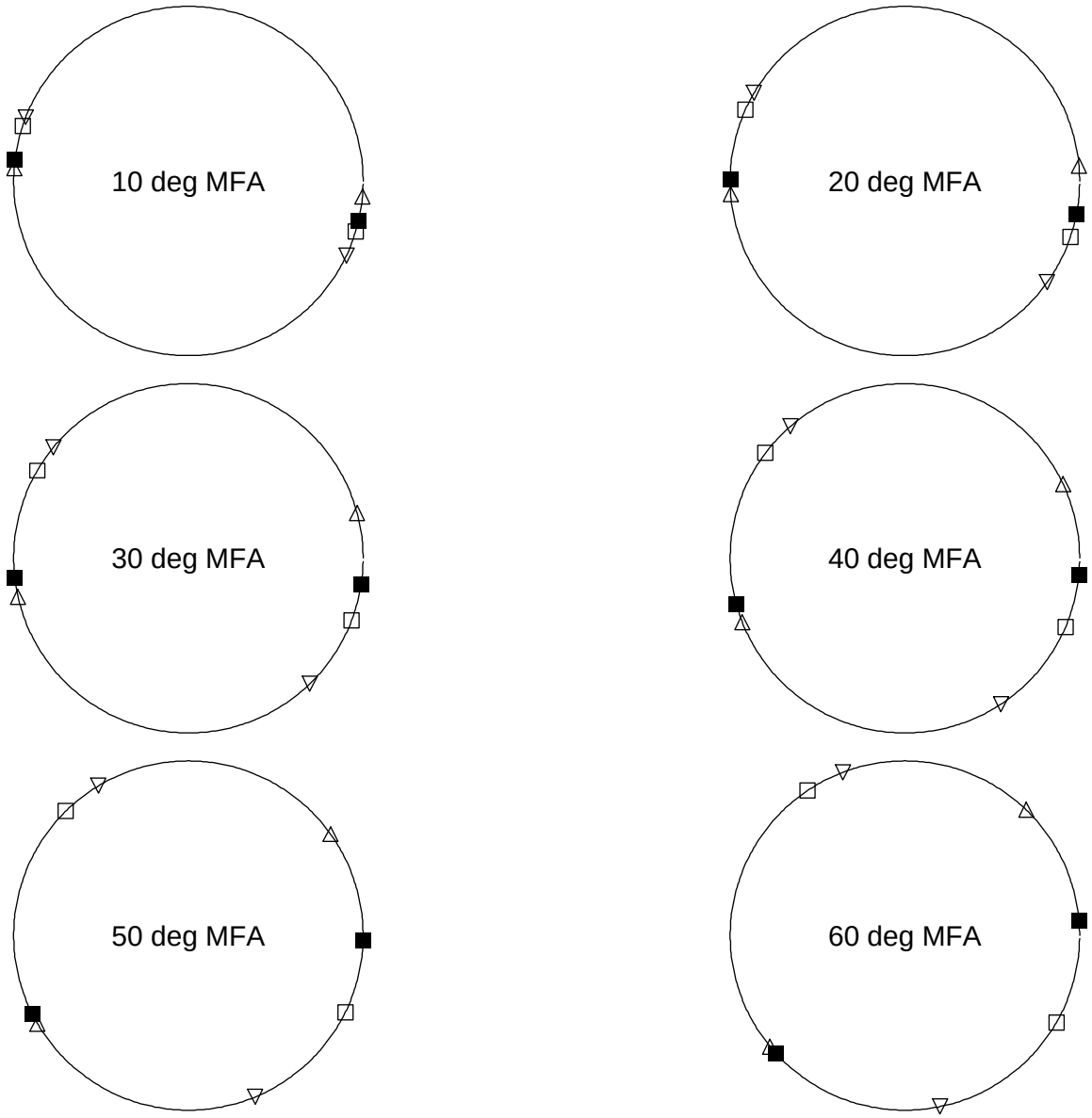

Figure 29: Locations of high intensity X-ray spots on the back plane for a wood cell tilt of 15 degrees and **wood cell rotation = 67.5 degrees**

□ — spots due to the **front** (before tilt and rotation) face
■ — spots due to the **back** face
△ — spots due to the **right** face
▽ — spots due to the **left** face

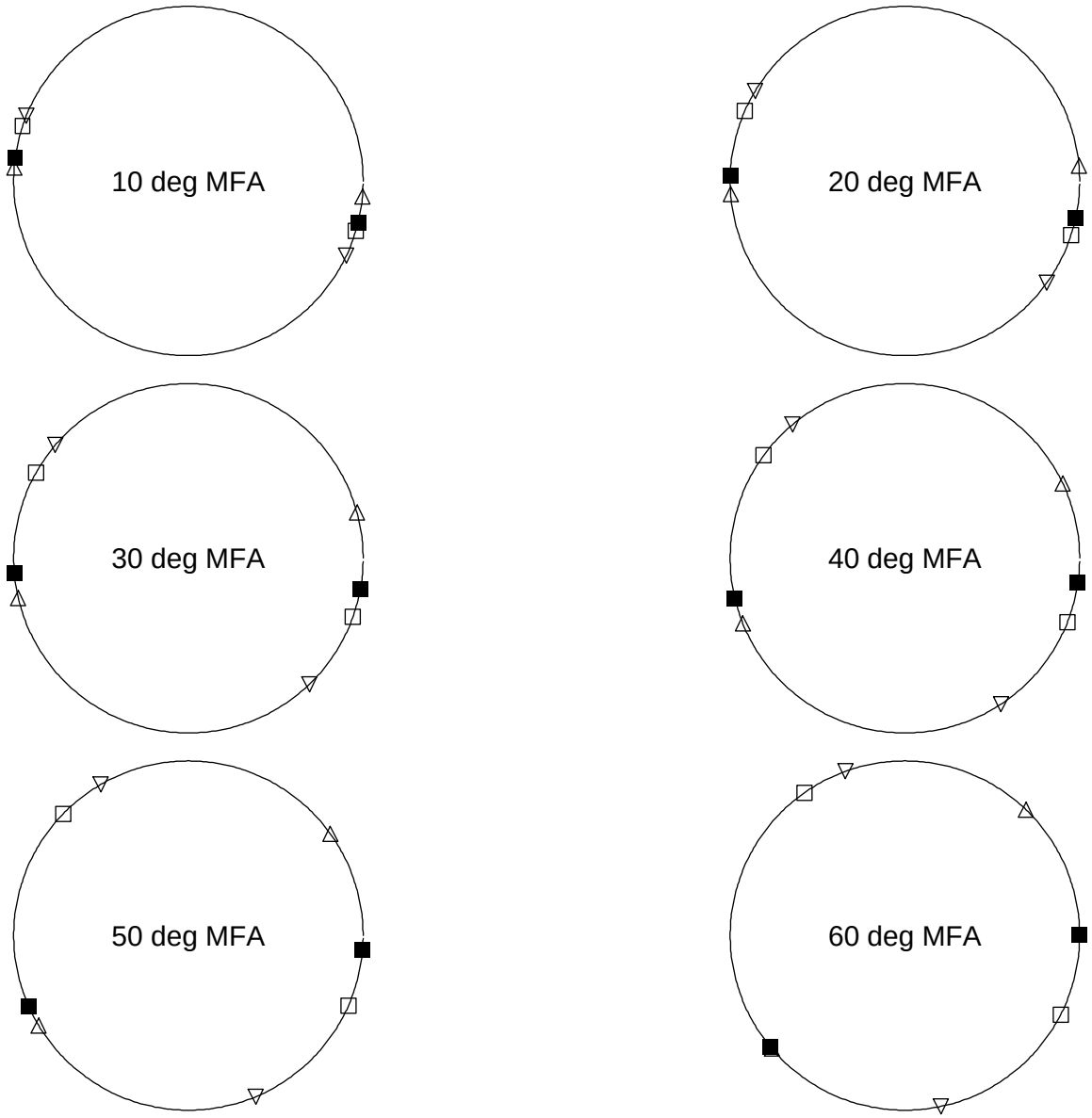

Figure 30: Locations of high intensity X-ray spots on the back plane for a wood cell tilt of 15 degrees and **wood cell rotation = 70 degrees**

□ — spots due to the **front** (before tilt and rotation) face
■ — spots due to the **back** face
△ — spots due to the **right** face
▽ — spots due to the **left** face

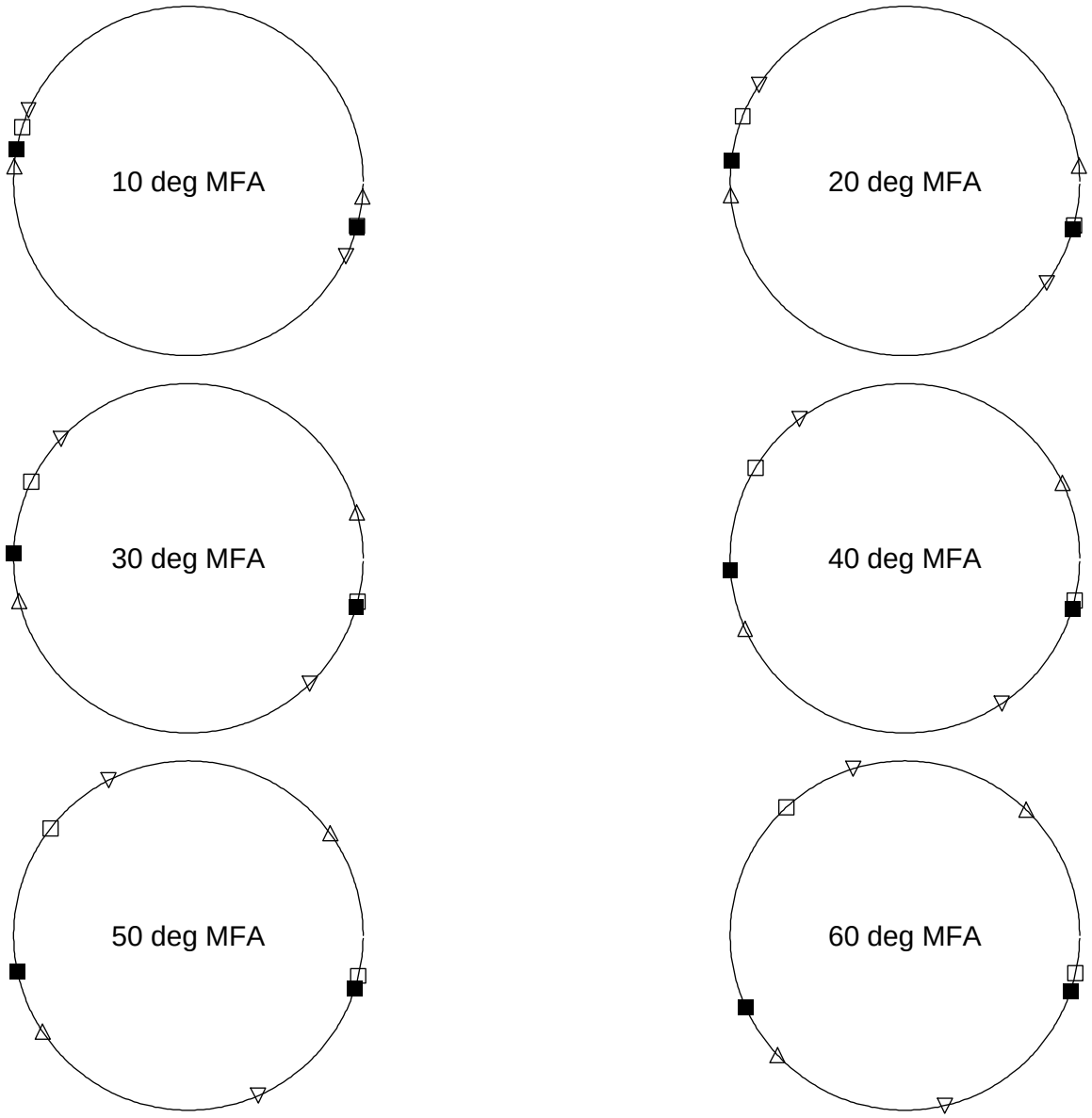

Figure 31: Locations of high intensity X-ray spots on the back plane for a wood cell tilt of 15 degrees and **wood cell rotation = 80 degrees**

□ — spots due to the **front** (before tilt and rotation) face
■ — spots due to the **back** face
△ — spots due to the **right** face
▽ — spots due to the **left** face

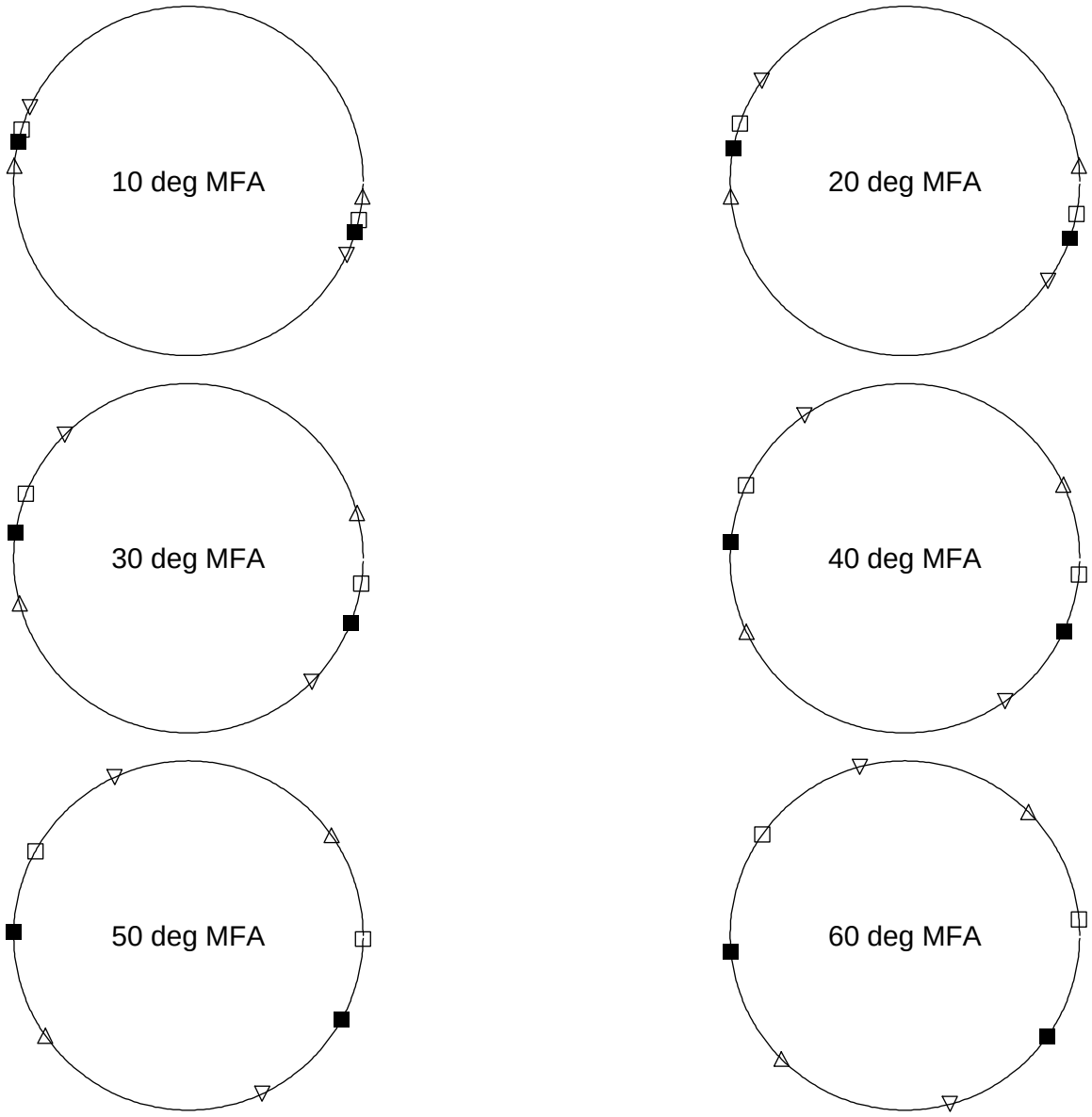

Figure 32: Locations of high intensity X-ray spots on the back plane for a wood cell tilt of 15 degrees and **wood cell rotation = 90 degrees**

□ — spots due to the **front** (before tilt and rotation) face
■ — spots due to the **back** face
△ — spots due to the **right** face
▽ — spots due to the **left** face

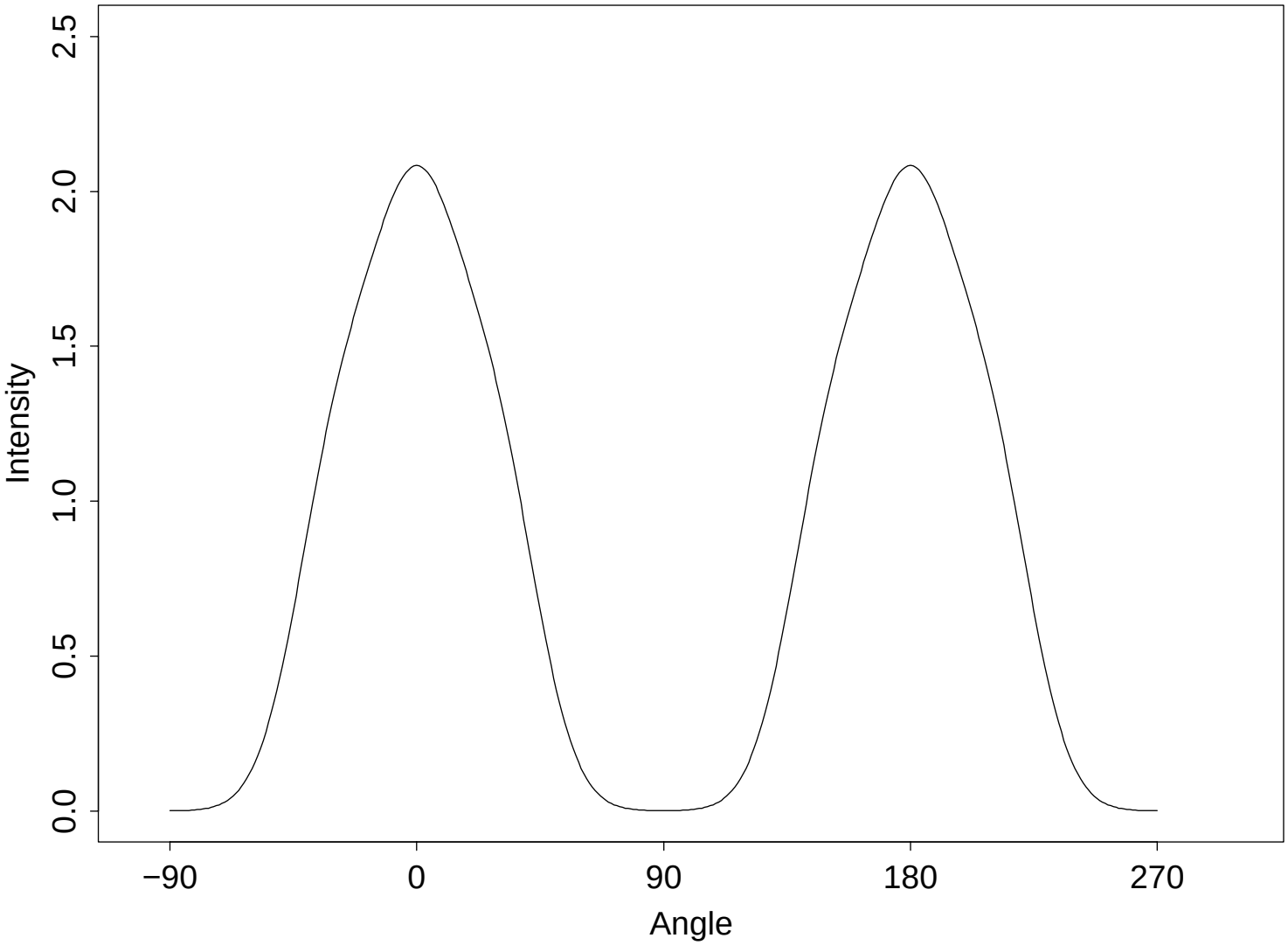

Figure 33: Calculated intensity profile for wood cell tilt = 0 degrees, rotation = 0 degrees, microfibril angle = 30 degrees, broadening factor $\sigma = 15$ degrees. The angle is in degrees counterclockwise from the east (see Figure 5).

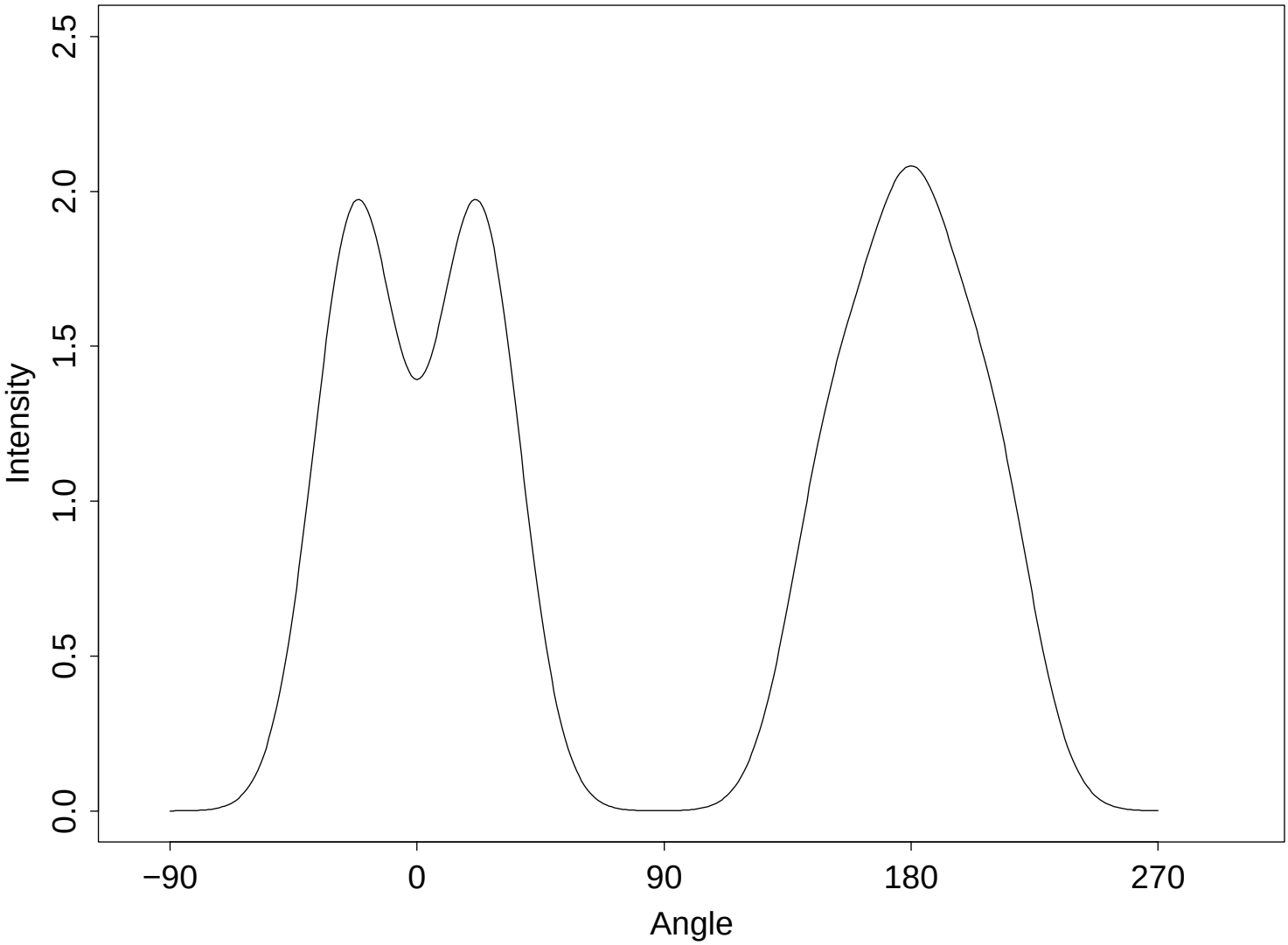

Figure 34: Calculated intensity profile for wood cell tilt = 0 degrees, rotation = 22.5 degrees, microfibril angle = 30 degrees, broadening factor σ = 15 degrees. The angle is in degrees counterclockwise from the east (see Figure 5).

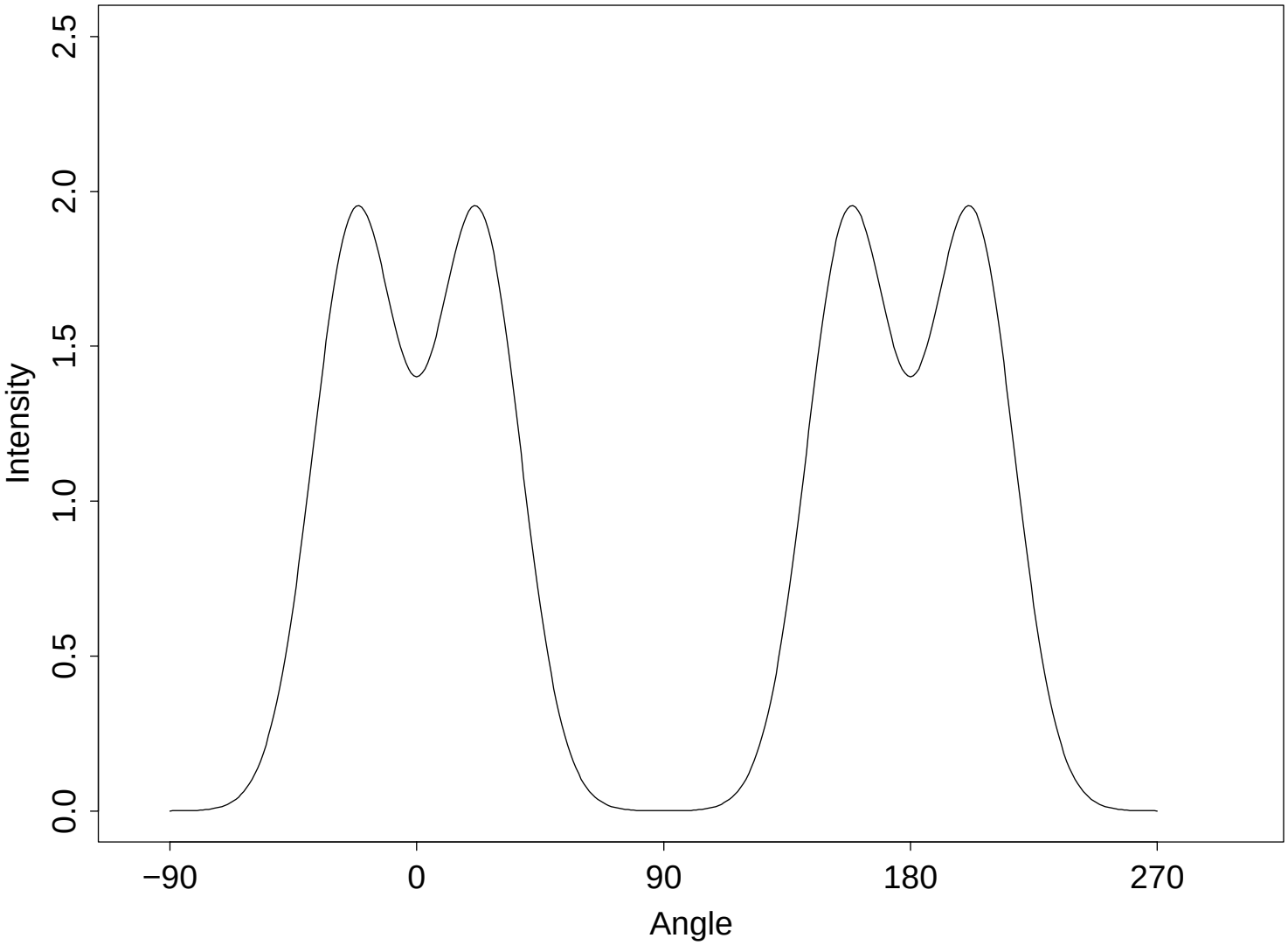

Figure 35: Calculated intensity profile for wood cell tilt = 0 degrees, rotation = 45 degrees, microfibril angle = 30 degrees, broadening factor σ = 15 degrees. The angle is in degrees counterclockwise from the east (see Figure 5).

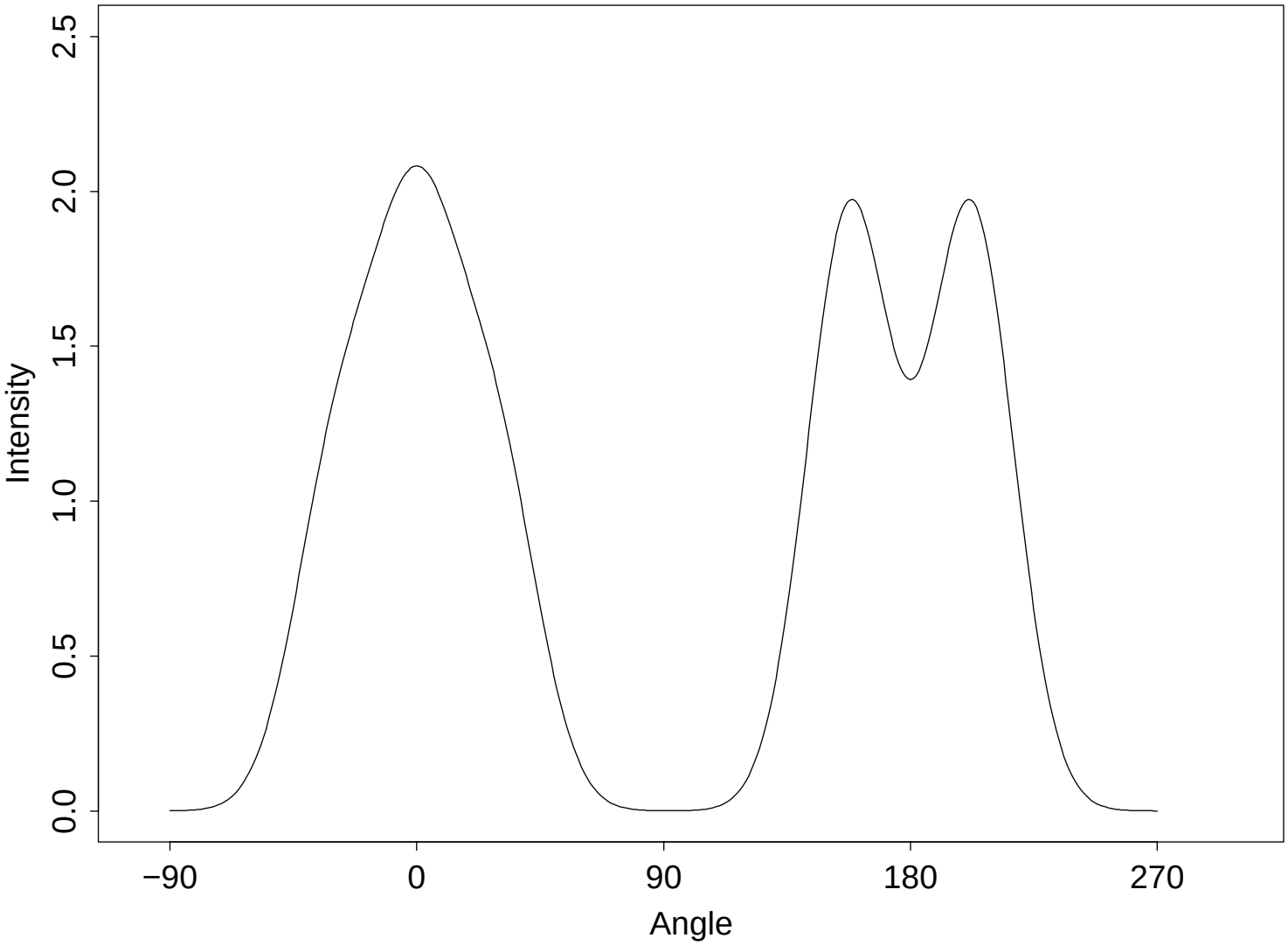

Figure 36: Calculated intensity profile for wood cell tilt = 0 degrees, rotation = 67.5 (or -22.5) degrees, microfibril angle = 30 degrees, broadening factor $\sigma = 15$ degrees. The angle is in degrees counterclockwise from the east (see Figure 5).

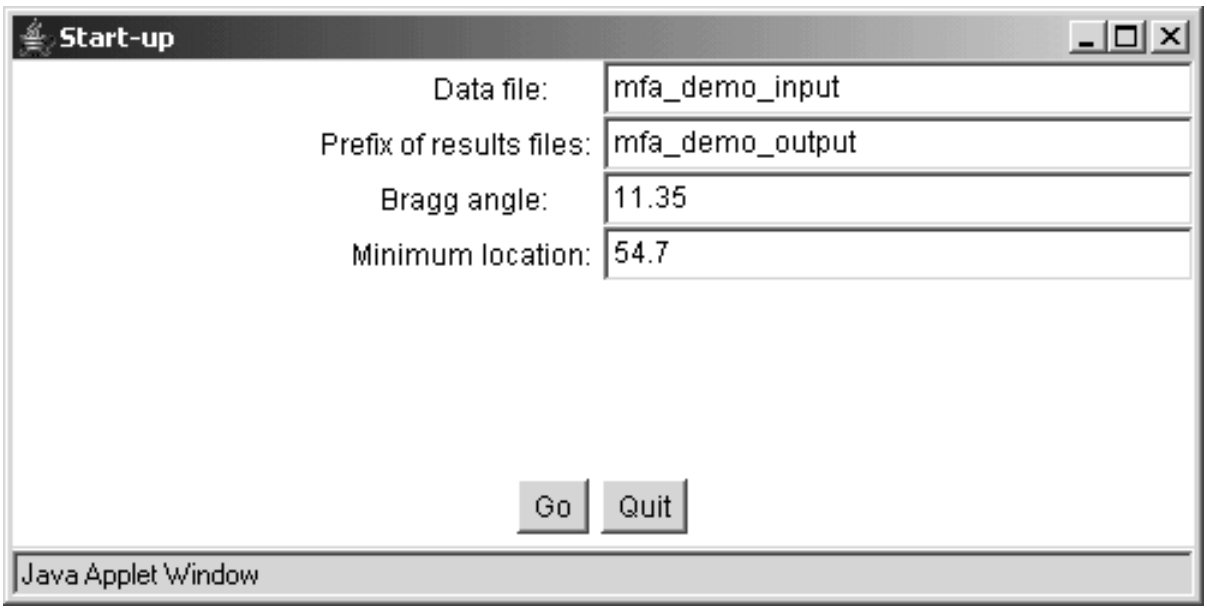

Figure 37: Start-up window for the applet

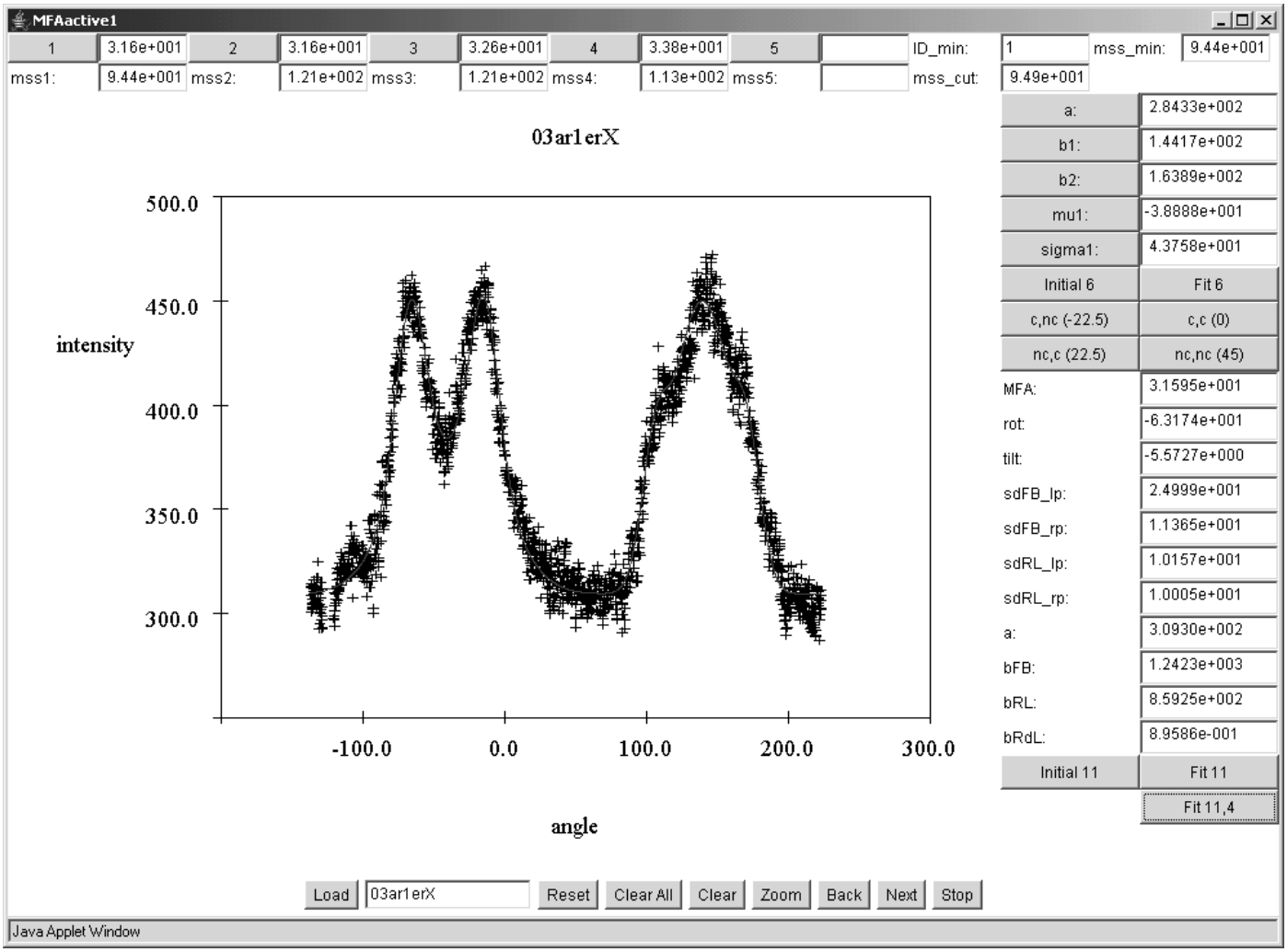

Figure 38: Main window for the applet

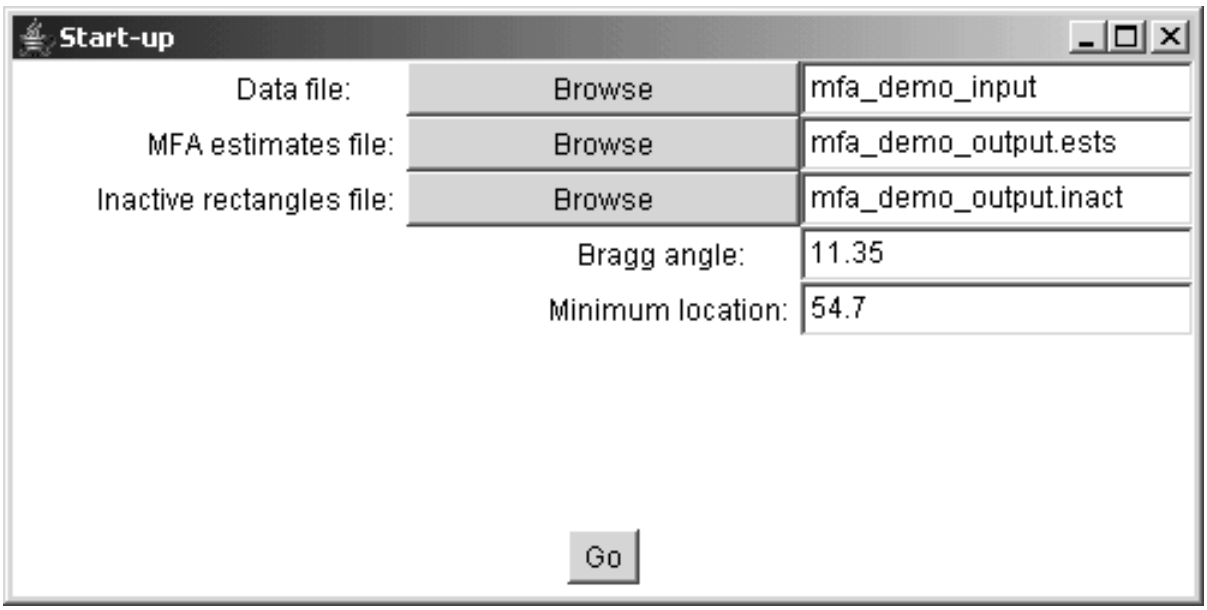

Figure 39: Start-up window for the application

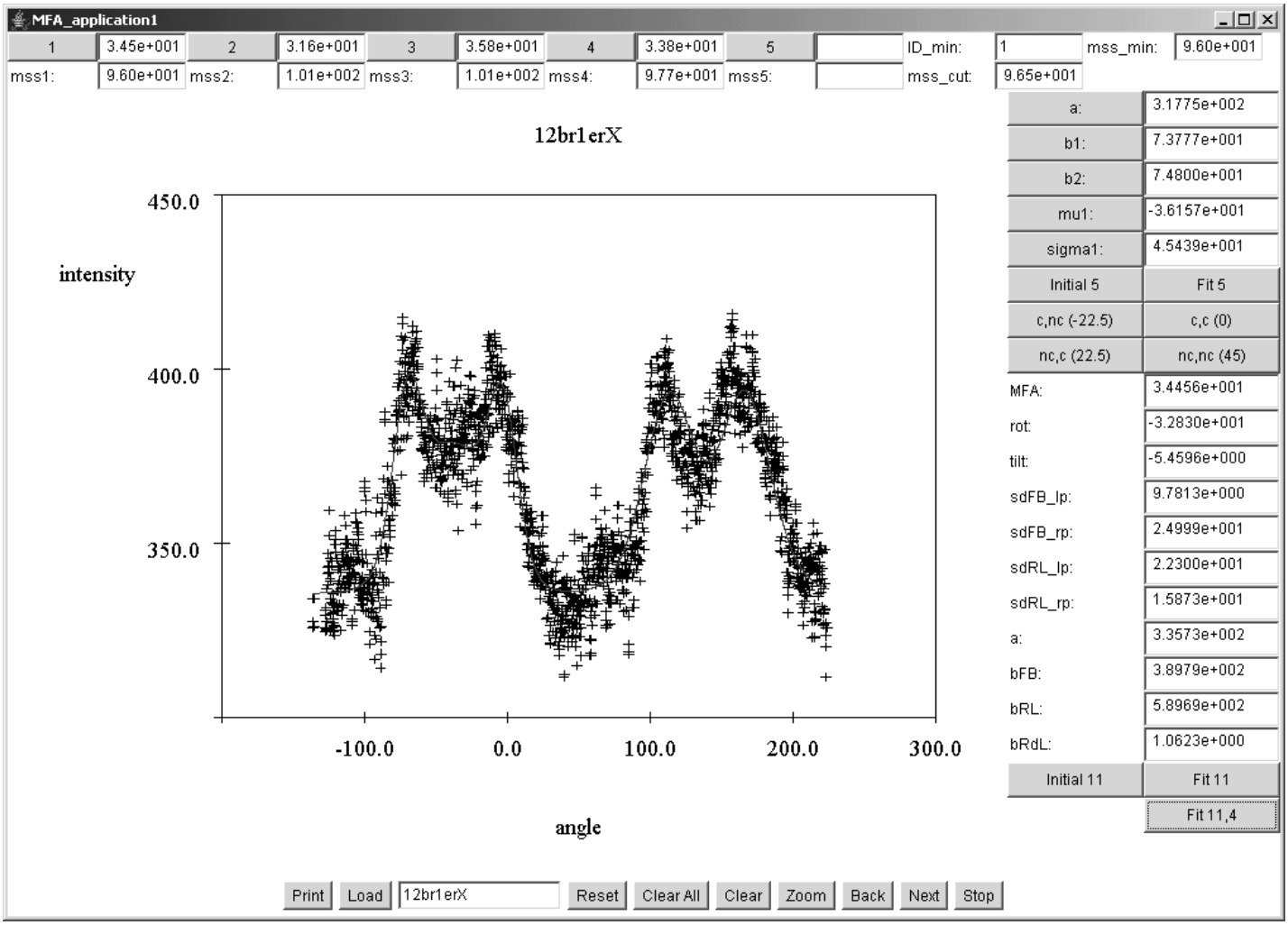

Figure 40: Main window for the application

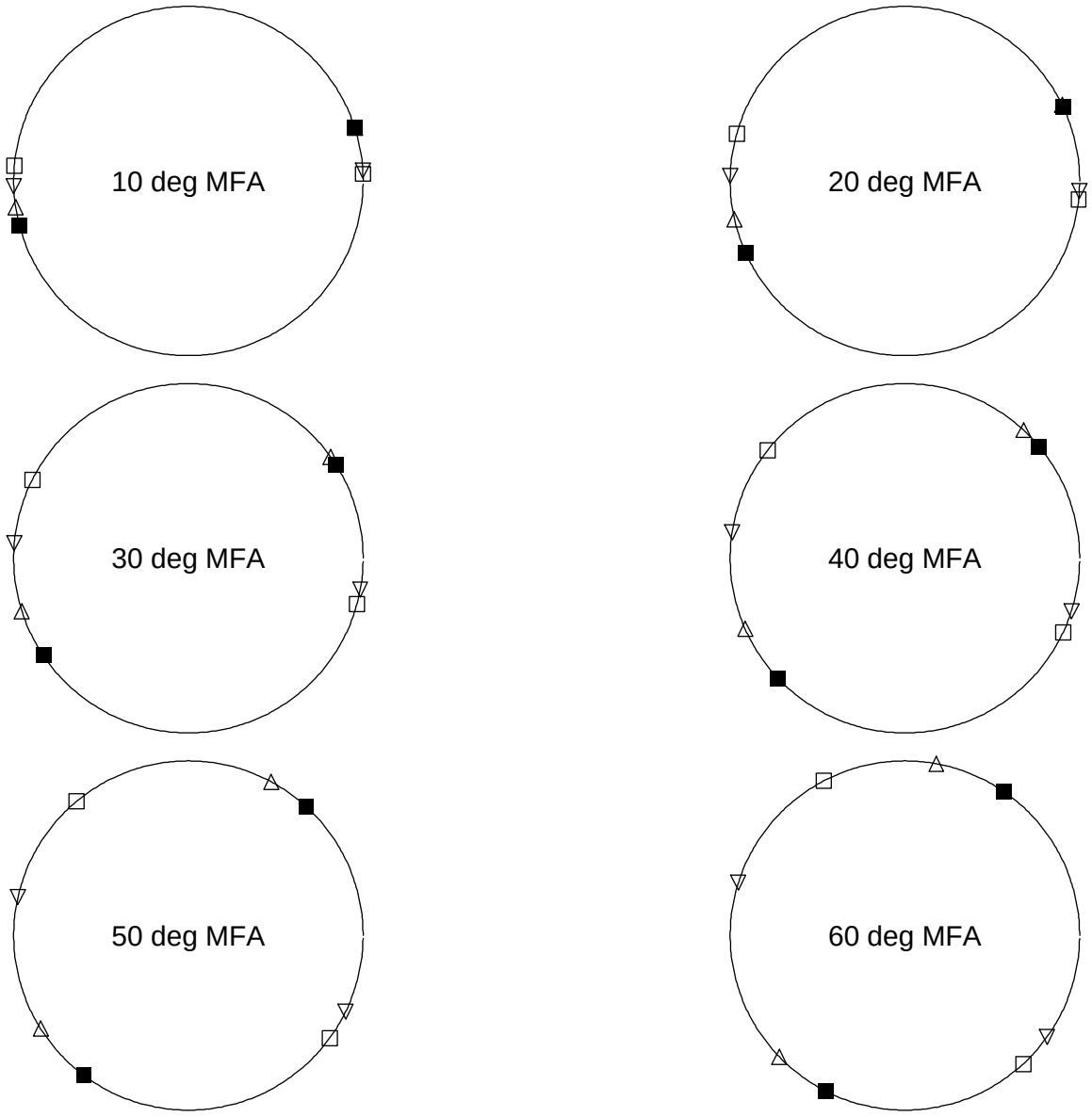

Figure 41: Locations of high intensity X-ray spots on the back plane for a wood cell tilt of -15 degrees and **wood cell rotation = 30 degrees**

□ — spots due to the **front** (before tilt and rotation) face
■ — spots due to the **back** face
△ — spots due to the **right** face
▽ — spots due to the **left** face

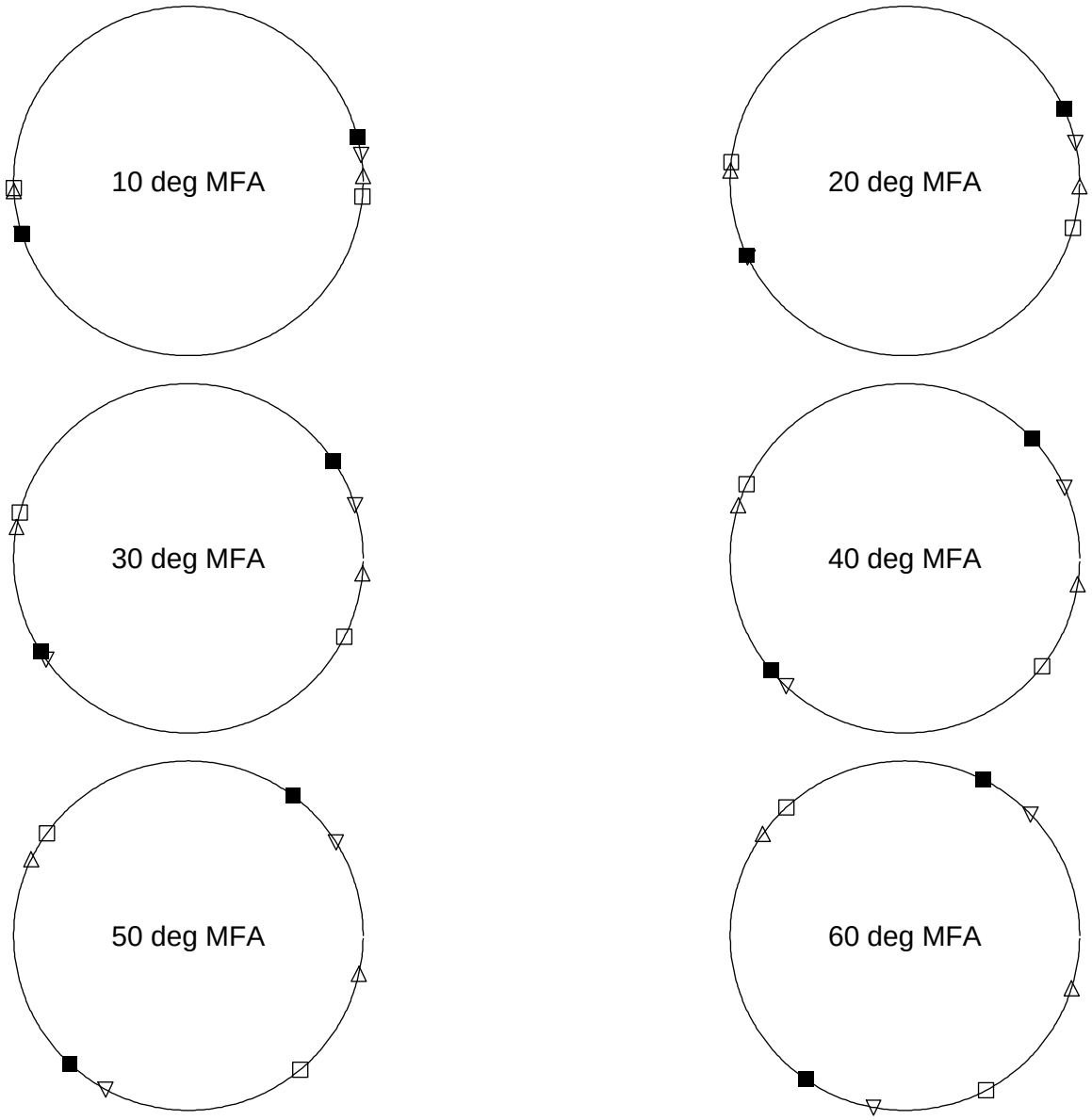

Figure 42: Locations of high intensity X-ray spots on the back plane for a wood cell tilt of 15 degrees and **wood cell rotation = -30 degrees**

□ — spots due to the **front** (before tilt and rotation) face
■ — spots due to the **back** face
△ — spots due to the **right** face
▽ — spots due to the **left** face

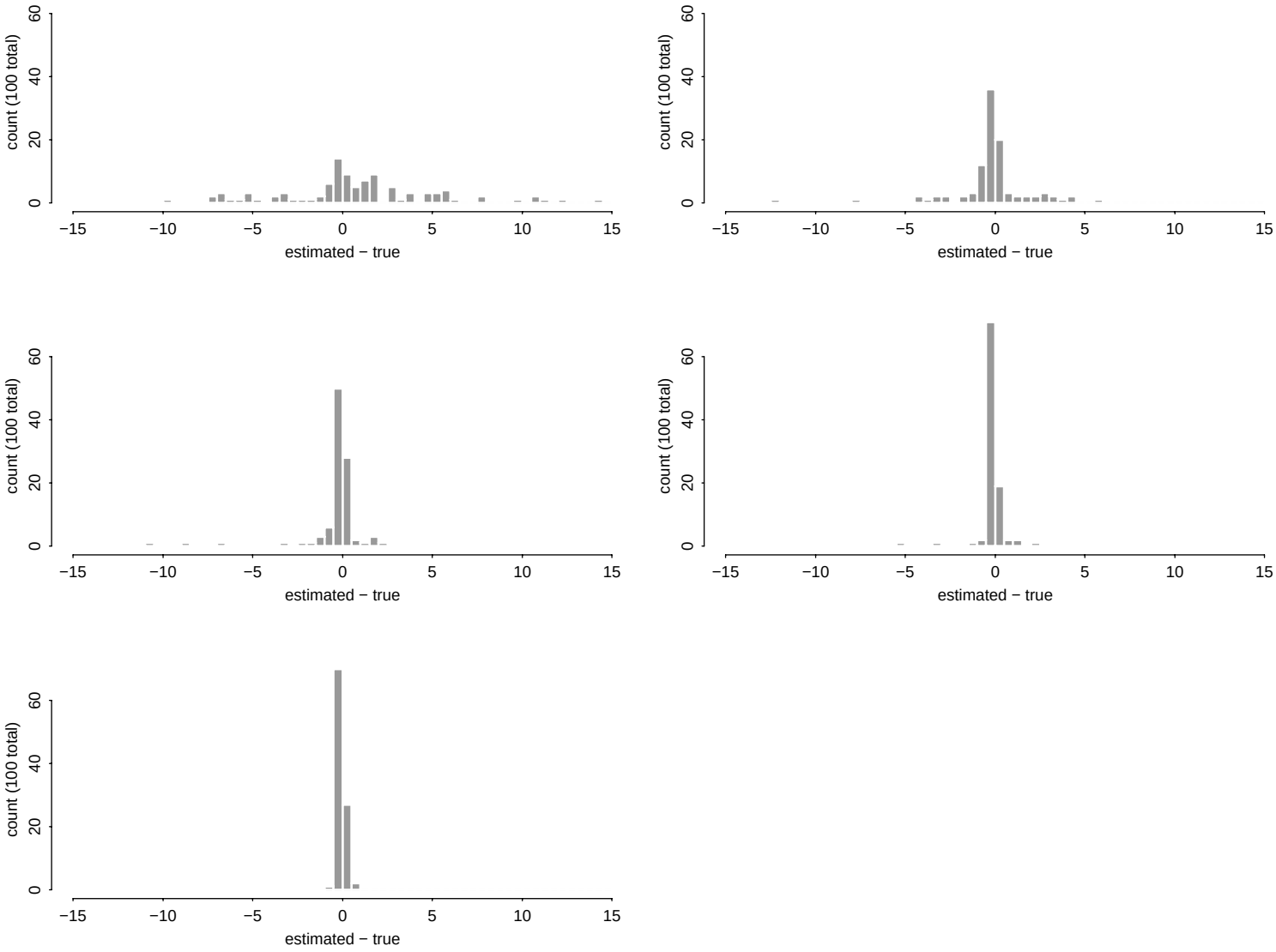

Figure 43: Histograms of estimated MFA minus true MFA values. Upper left — true values between 2 and 10 degrees. Upper right — true values between 10 and 20 degrees. Center left — true values between 20 and 30 degrees. Center right — true values between 30 and 40 degrees. Bottom left — true values between 40 and 55 degrees.

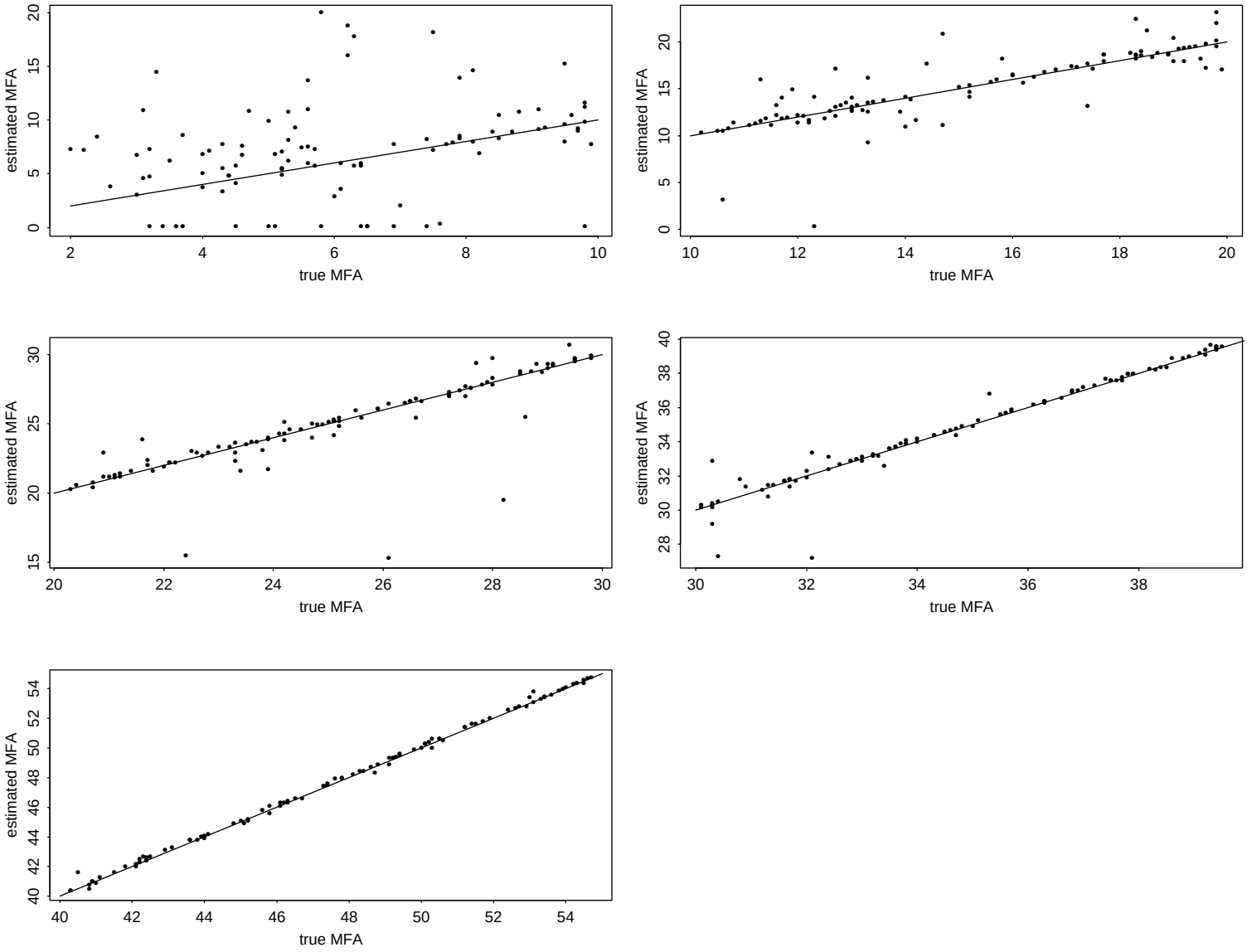

Figure 44: Estimated MFA versus true MFA. The line is the y = x line. Upper left — true values between 2 and 10 degrees. Upper right — true values between 10 and 20 degrees. Center left — true values between 20 and 30 degrees. Center right — true values between 30 and 40 degrees. Bottom left — true values between 40 and 55 degrees.

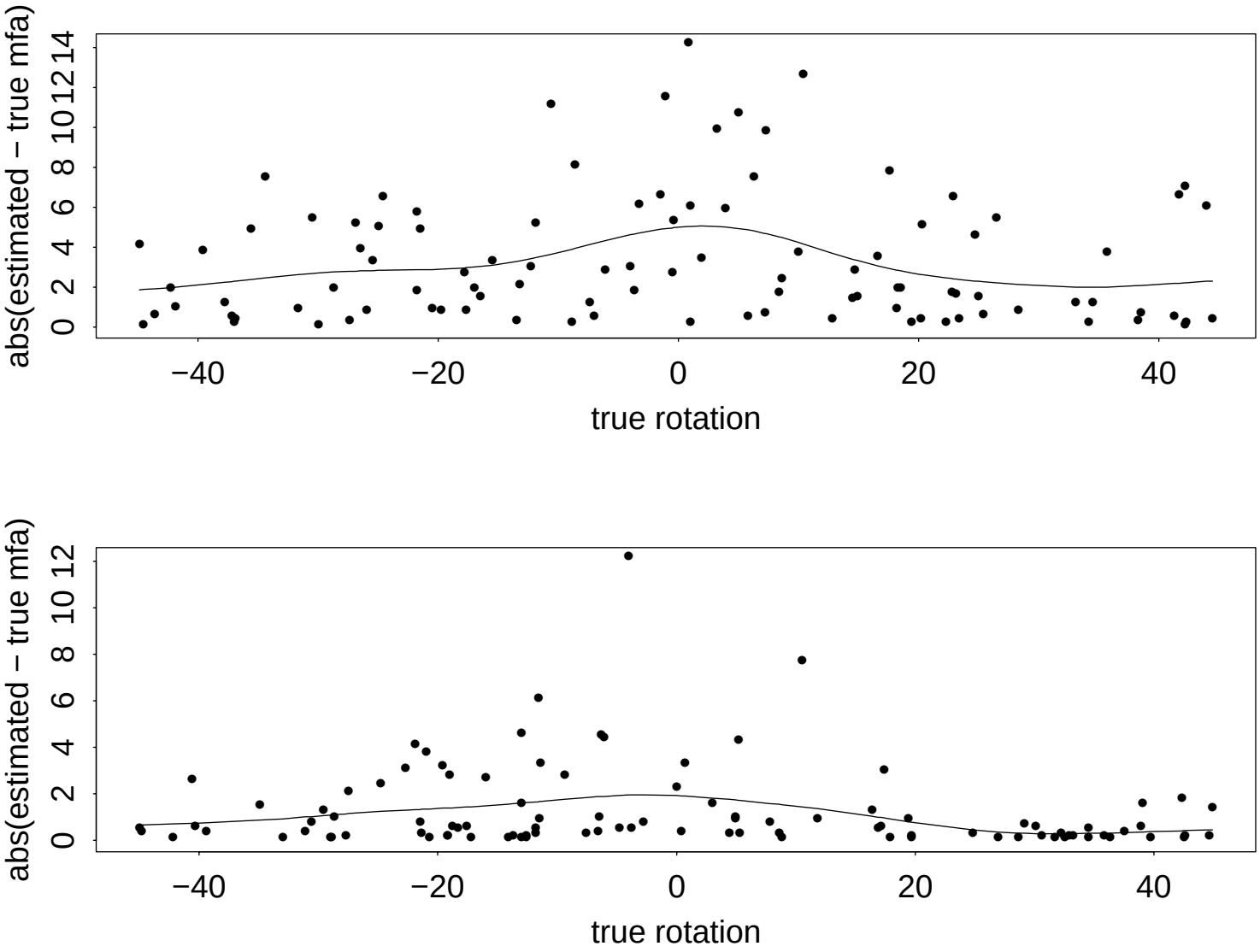

Figure 45: abs(estimated MFA - true MFA) versus cell rotation. The lines are Gaussian kernel smooths of the data. The bandwidth of the kernel was 20 degrees. Top — true values between 2 and 10 degrees. Bottom — true values between 10 and 20 degrees.